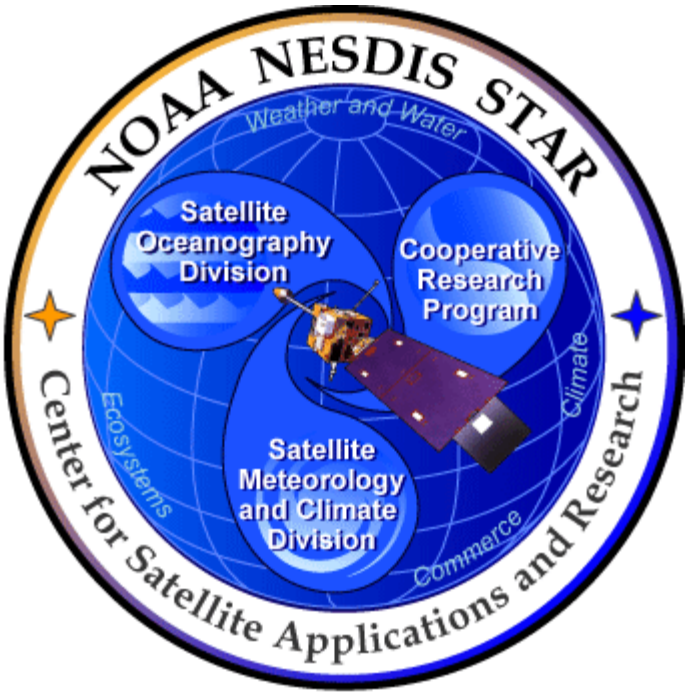

NOAA NESDIS
CENTER for SATELLITE APPLICATIONS and RESEARCH

ALGORITHM THEORETICAL BASIS DOCUMENT

ABI Enterprise Processing System Aerosol Detection Product

Pubu Ciren and Shobha Kondragunta

NOAA/NESDIS/STAR

Version 1.0
October 01, 2020

TABLE OF CONTENTS

LIST OF TABLES

LIST OF FIGURES

LIST OF ACRONYMS

Acronym/ Abbreviation	Definition
AAA	Aerosol, Air Quality, and Atmospheric Chemistry
ABI	Advanced Baseline Imager
ADP	Aerosol Detection Product
AHI	Advanced Himawari Imager
AIT	Aerosol Integration Team
AOD	Aerosol Optical Depth
ATBD	Algorithm Theoretical Basis Document
ATIP	Algorithm and Test Implementation Plan
AVHRR	Advanced Very High Resolution Radiometer
AWG	Algorithm Working Group
BT	Brightness Temperature
BTD	Brightness Temperature Difference
CALIOP	Cloud-Aerosol Lidar with Orthogonal Polarization
CALIPSO	Cloud-Aerosol Lidar and Infrared Pathfinder Satellite Observation
CONUS	Continental United States
CRTM	Community Radiative Transfer Model
DQF	Data Quality Flag
ECM	Enterprise Cloud Mask
EPS	Enterprise Processing System
FMW	Fine Mode Weight
FPM	Focal Plane Module
F&PS	Functional and Performance Specification Document
GOES	Geostationary Operational Environmental Satellite
HIRS	Hyperspectral Infrared Sounder
HMS	Hazard Mapping System
IMS	Interactive Multisensor Snow and Ice Mapping System
IR	Infrared
LHP	Loop Heat Pipe
LZA	Local Zenith Angle
MeanR	Mean of reflectance (in a box of 3 x 3 pixels)
MODIS	Moderate Resolution Imaging Spectroradiometer
MRD	Mission Requirements Document
NDVI	Normalized Difference Vegetation Index
NOAA	National Oceanic and Atmospheric Administration
R	Reflectance
RGB	True Color Imagery (Red-Green-Blue)
RTM	Radiative Transfer Model
SST	Sea Surface Temperature
StdR	Standard Deviation of Reflectance (in a box of 3 x 3 pixels)
SZA	Solar Zenith Angle
TOA	Top of the Atmosphere
VIIRS	Visible Infrared Imaging Radiometer Suite
VZA	(Satellite) View Zenith Angle
UW	University of Wisconsin

ABSTRACT

This document describes the Enterprise System Processing (EPS) algorithm for the Aerosol Detection Product (ADP) (including smoke/dust) over land and water from the multispectral reflectance/brightness temperature measurements observed by the Advanced Baseline Imager (ABI) onboard the GOES-R series satellites. This document includes descriptions of the theoretical basis, physics of the problem, validation of the product, and assumptions and limitations.

Episodic smoke and dust events impact human health and the economy. Therefore, qualitative information regarding the time, location and geographic extent of these events is required for monitoring and forecasting applications. The EPS ADP will meet this need using an algorithm designed to take advantage of the ABI's various spectral measurements. The ABI's 16 spectral bands make measurements spanning the visible, near-IR, and IR wavelengths, with spatial resolutions of 0.5, 1.0, and 2.0 km, depending on the band.

The ADP algorithm is based on the fact that smoke/dust aerosols exhibit features of spectral dependence and contrast in both the visible and infrared spectra that are different from clouds, the surface, and clear-sky atmosphere. The fundamental principle of the ADP algorithm depends on threshold tests that separate smoke/dust aerosols from cloud and clear-sky regions over water and land.

By using MODIS observations as a proxy, the GOES-R ABI EPS ADP algorithm has been tested for different scenarios such as wildfires, dust storms, and dust transport from Africa. Comparison to true color (RGB) images and other satellite products such as Cloud-Aerosol Lidar and Infrared Pathfinder Satellite Observation/Cloud-Aerosol Lidar with Orthogonal Polarization (CALIPSO/CALIOP) have been performed, along with a sensitivity study of the detection on the accuracy of sensor radiances/brightness temperature. In general, the product requirements can be achieved, including 80% correct detection for dust over water and land, 80% correct detection for smoke over land, and 70% correct detection for smoke over water. Preliminary analysis shows that radiometric or calibration errors at the 5% level can be tolerated.

1 INTRODUCTION

Aerosols perturb the Earth's energy budget by scattering and absorbing radiation and by altering cloud properties and lifetimes. They also exert large influences on weather, air quality, hydrological cycles, and ecosystems. Aerosols released into the atmosphere due to natural and anthropogenic activities lead to deteriorated air quality and affect Earth's climate. It is important to regularly monitor the global aerosol distributions and study how they are changing, especially for those aerosols with large spatial and temporal variability, such as smoke, sand storms, and dust [IPCC, 2007]. Detection of these highly variable aerosols is challenging because of strong interactions with local surface and meteorological conditions.

Because atmospheric aerosols can directly alter solar and Earth radiation in both visible and infrared (IR) spectral regions through scattering and absorption processes, both visible and IR remote sensing techniques have been used for detection of aerosols in the atmosphere [e.g., Tanre and Legrand, 1991; Ackerman 1989, 1997; Kaufman et al., 1997; Verge-Depre et al., 2006]. Visible and IR images can be used for detecting episodic smoke and dust particles due to the fact that these aerosol particles display some spectral variations in visible and IR spectral regions different from those of cloud or clear-sky conditions. In practice, the detection is based on the analysis of reflectance (or radiance) in visible bands or brightness temperature (BT) in IR bands. The magnitude of the difference in reflectance or BTs in selected bands (or channels) can be used to infer the signature of dust and smoke. This is the basic idea of our aerosol detection algorithm, which will be described in detail in this document.

1.1 Purpose of This Document

This EPS ADP Algorithm Theoretical Basis Document (ATBD) provides a high level description and the physical basis for the detection of smoke and dust contaminated pixels from measurements made by the Advanced Baseline Imager (ABI) flown on the GOES-R series of next generation NOAA operational geostationary meteorological satellites. The EPS ADP algorithm provides an initial estimate of the presence or absence of smoke or dust within each ABI pixel.

1.2 Who Should Use This Document

The intended users of this document are those interested in understanding the physical basis of the EPS ADP algorithm and how to use the output of this algorithm to optimize episodic aerosol detection for a particular application. This document also provides information useful to anyone maintaining or modifying the original ABI baseline ADP algorithm.

1.3 Inside Each Section

This document is broken down into the following main sections:

- **System Overview**: Provides relevant details on ABI instrument characteristics and a detailed description of the products generated by the EPS ADP algorithm.

- **Algorithm Description**: Provides a detailed description of the EPS ADP algorithm including the physical basis, required inputs, and derived output. Examples from algorithm processing using proxy input data are provided.

- **Test Data Sets and Outputs**: Provides a description of the test data sets used to characterize the performance of the algorithm and the quality of the output. The precision and accuracy of the output is estimated and an error budget is calculated.
- **Practical Considerations**: Provides an overview of the issues involving numerical computation, programming and procedures, quality assessment and diagnostics, and exception handling.
- **Assumptions and Limitations**: Provides an overview of assumptions on which the algorithm is based and the current limitations of the approach. The plan for overcoming some limitations with further algorithm development is also given.

1.4 Related Documents

Besides the references given throughout, this document is related to the following documents:

(1) GOES-R Mission Requirements Document (MRD)
(2) GOES-R Functional and Performance Specification Document (F&PS)
(3) GOES-R ABI ADP Algorithm and Test Implementation Plan (ATIP)
(4) GOES-R ABI ADP Validation Plan

1.5 Revision History

This is the first version (Version 1.0) of this document, which is based on Version 3.0 of the ABI ADP baseline. This document includes updates on the mitigation of the GOES-17 Focal Plane Module (FPM) temperature anomaly and also a description of how a single EPS algorithm works with observations from multi-satellite platforms including GOES-R. These documents were created by the GOES-R Aerosol, Air Quality, and Atmospheric Chemistry (AAA) ADP team led by Dr. Shobha Kondragunta of NOAA/NESDIS/STAR and including Dr. Pubu Ciren of I.M. System Group, Inc., Maryland. This document accompanies the delivery of Version 1.0 of the EPS ADP algorithm to the GOES-R Algorithm Working Group (AWG) Algorithm Integration Team (AIT).

2 OBSERVING SYSTEM OVERVIEW

This section will describe the products generated by the ABI EPS ADP algorithm including smoke and dust and the requirements it places on the sensor.

2.1 Products Generated

As described in Table 1 ADP measurement accuracy is defined as 80% correct classification for dust over water and land, 80% correct classification for smoke over land, and 70% correct classification for smoke over water. The measurement range is binary (yes/no) detection above a threshold of 0.2 aerosol optical depth (AOD), as stated in GOES-R Ground Segment F&PS (G417-R-FPS-0089 V1.9). AOD of 0.2 defines background atmospheric aerosol and is not computed in the EPS ADP algorithm nor imported from the EPS AOD algorithm.

Table 1. GOES-R mission requirements for Aerosol Detection.

Specification	Requirement
Geographic Coverage (Scan View)	Full disk, CONUS, mesoscale
Vertical Resolution	Total Column
Horizontal Resolution	2 km
Mapping Accuracy	1 km
Measurement Range	Binary detection (yes/no) for AOD > 0.2
Measurement Accuracy	Dust: 80% correct detection over land and water Smoke: 80% correct detection over land, 70% correct detection over land
Refresh Rate/ Coverage Time Option	15 min
Vendor-Allocated Ground Latency	806 s
Measurement Precision	10%
Temporal Coverage Qualifiers	Day
Product Extent Qualifier	Quantitative: LZA ≤ 60 degrees; Qualitative: LZA > 60 degrees
Cloud Cover Conditions Qualifier	Clear conditions down to feature of interest associated with threshold accuracy
Product Statistics Qualifier	Over specified geographic area

The purpose of the ADP algorithm is to identify ABI pixels which are contaminated by either smoke or dust during daytime to facilitate the monitoring of occurrences and development of smoke/dust episodes. However, due to the relatively weak contribution of aerosols compared to reflection from the surface to the satellite measured reflectances/brightness temperatures, the ADP algorithm performs better for heavy smoke /dust episodes (with aerosol optical depth >0.2) over dark surface than over bright surfaces. Smoke detection over semi-arid and arid regions is less accurate due to lower contrast with the background.

The EPS ADP algorithm output is written in netCDF4 format. At the pixel level, there are 6 aerosol type flags (1/0 for yes/no): volcanic ash (passed down from volcanic ash product, currently set as 0 for ABI EPS ADP product), dust, smoke, cloud, none/unknown/clear, and snow/ice. All of the variables output from the EPS ADP algorithm are listed in Table 2. Details about the quality flags are listed in Table 3 and Table 4; note that "missing/bad" data are flagged due to either the GOES-17 FPM temperature anomaly or missing observations. In addition, diagnostic bit-wise flags are also generated, as listed in Tables 5-8.

Table 2. Variables output from the EPS ADP algorithm.

Variable	Type	Description	Dim	Units	Range
ADP_granule_level_quality_flag	Byte	Quality flag for the whole granule	0	1	-128,127
Ash	Byte	Volcanic Ash Flag: 1 = yes, 0 = No	2	1	0,1
AshConfidHighPct	Float	Percent of high confidence ash	0	Percent	0, 100
AshConfidLowPct	Float	Percent of low confidence ash	0	Percent	0, 100
AshConfidMediumPct	Float	Percent of medium confidence ash	0	Percent	0, 100
AshPct	Float	Percent of good ash retrieval	0	Percent	0, 100
QC_Flag (Byte1)	Byte	Quality Flag for Ash, Smoke, Dust and NUC (see Table 3)	2	1	-128,127
PQI1 (Byte2)	Byte	Product Quality Information (see Table 4)	2	1	-128,127
PQI2 (Byte3)	Byte	Product Quality Information (see Table 5)	2	1	-128,127
PQI3 (Byte4)	Byte	Product Quality Information (see Table 6)	2	1	-128,127
PQI4 (Byte5)	Byte	Product Quality Information (see Table 7)	2	1	-128,127
Cloud	Byte	Cloud Flag: 1 = yes, 0 = no	2	1	0,1
SAAI (DAII)	Float	Scaled Absorbing Aerosol Index	2	1	
Dust	Byte	Dust flag: 1 = yes, 0 = no	2	1	0,1
DustConfidHighPct	Float	Percent of high confidence dust	0	Percent	0, 100
DustConfidLowPct	Float	Percent of low confidence dust	0	Percent	0, 100
DustConfidMediumPct	Float	Percent of medium confidence dust	0	Percent	0, 100
DustPct	Float	Percent of good dust retrieval	0	Percent	0, 100
Latitude	Float	Pixel latitude in field latitude	2	° North	-90, 90
Longitude	Float	Pixel longitude in field longitude	2	° East	-180, 180
DSDI (NDAI)	Float	Dust Smoke Discrimination Index	2	1	
NUC	Byte	None, Unknown, Clear_sky Flag: 1 = yes, 0 = no	2	1	0, 1
NUCConfidHighPct	Float	Percent of high confidence NUC	0	Percent	0, 100
NUCConfidLowPct	Float	Percent of low confidence NUC	0	Percent	0, 100
NUCConfidMediumPct	Float	Percent of medium confidence NUC	0	Percent	0, 100
NUCPct	Float	Percent of good NUC retrieval	0	Percent	0, 100
NoAshPct	Float	Percent of ash not determined (bad)	0	Percent	0, 100
NoDustPct	Float	Percent of dust not determined (bad)	0	Percent	0, 100
NoNUCPct	Float	Percent of NUC not determined (bad)	0	Percent	0, 100
NoSmokePct	Float	Percent of smoke not determined (bad)	0	Percent	0, 100

Variable	Type	Description	Dim	Units	Range
NumOfGoodAshRetrieval	Long	Number of Good Ash Retrievals	0	1	
NumOfGoodDustRetrieval	Long	Number of Good Dust Retrievals	0	1	
NumOfGoodNUCRetrieval	Long	Number of Good NUC Retrievals	0	1	
NumOfGoodSmokeRetrieval	Long	Number of Good Smoke Retrievals	0	1	
NumOfQualityFlag	Long	Number of quality flags	0	1	
NumOfSatZenAngLess60	Long	Number of pixels with satellite zenith angle < 60 degree	0	1	
NumOfSolZenAngLess60	Long	Number of pixels with solar zenith angle < 60 degree	0	1	
Smoke	Byte	Smoke Flag: 1 = yes, 0 = no	2	1	0, 1
SmokeCon	Float	Smoke Concentration	2	$\mu g/m^3$	
SmokeConfidHighPct	Float	Percent of high confidence smoke	0	Percent	0, 100
SmokeConfidLowPct	Float	Percent of low confidence smoke	0	Percent	0, 100
SmokeConfidMediumPct	Float	Percent of medium confidence smoke	0	Percent	0, 100
SmokePct	Float	Percent of good smoke retrieval	0	Percent	0, 100
SnowIce	Byte	Snow Ice Flag: 1 = yes, 0 = no	2	1	0, 1
StartColumn	Long	Start column index	0		
StartRow	Long	Start row index	0		
TotalPixel	Long	Total number of pixels where retrievals are attempted	0	1	

Table 3. Definitions of the bit-wise granule level quality flag for the EPS ADP algorithm.

Bit*	Quality Flag Name	Meaning (2-bits)		
		01**	00	11***
0-1	**ADP_granule_level_quality_flag**	**bad**	**good quality**	**bad**

*Start from the least significant bit
**Bad data due to missing observations
***Bad data due to FPM temperature anomaly

Table 4. Definitions of bit-wise quality flags for the EPS ADP "QC_Flag" variable.

Bit*	Quality Flag Name	Meaning (2-bits)			
		01	10	00	11**
0-1	QC_ASH_CONFIDENCE	Low quality	Medium quality	High quality	**Bad/missing**
2-3	QC_SMOKE_CONFIDENCE				
4-5	QC_DUST_CONFIDENCE				
6-7	**QC_NUC_CONFIDENCE**				

*Start from the least significant bit
**Bad data due to FPM temperature anomaly or missing due to missing observations

Table 5. Definitions of bit-wise diagnostic flags for the EPS ADP "PQI1" variable.

Bit*	Diagnostic Flag Name	Meaning			
		1-bit	0 (default)	1	-----
		2-bits	00 (default)	01	11
0	QC_INPUT_LON	1-bit	Valid longitude	Invalid longitude (longitude > 180 or < -180)	-----
1	QC_INPUT_LAT	1-bit	Valid latitude	Invalid latitude (latitude > 90 or < -90)	-----
2-3	QC_INPUT_SOLZEN	2-bits	Valid solar zenith angle (SZA) (0 ≤ SZA ≤ 90)	Invalid SZA (SZA > 90 or < 0)	90 ≥ SZA > 60
4-5	QC_INPUT_SATZEN	2-bits	Valid local zenith angle (VZA) (0 ≤ VZA ≤ 90)	Invalid VZA (VZA > 90 or < 0)	90 ≥ VZA > 60
6-7	QC_INPUT_SNOW/ICE_SOURCE	2-bits	VIIRS snow/ice mask	IMS snow/ice mask	Internal snow/ice mask

*Start from the least significant bit

Table 6. Definitions of bit-wise diagnostic flags for the EPS ADP "PQI2" variable.

Bit*	Diagnostic Flag Name	Meaning (1-bit)	
		0 (default)	1
0	QC_INPUT_SUNGLINT_SOURCE	VIIRS sun glint mask (from Cloud Mask product)	Internal sun glint mask
1	QC_INPUT_SUNGLINT	Outside of sun glint	Within sun glint
2	QC_INPUT_LAND/WATER	Water	Land
3	QC_INPUT_DAY/NIGHT	Day	Night
4	QC_WATER_SMOKE_INPUT	Valid VIIRS inputs	Invalid VIIRS inputs
5	QC_WATER_SMOKE_CLOUD	Cloud-free	Obscured by clouds
6	QC_WATER_SMOKE_SNOW/ICE	Snow/ice free	With snow/ice
7	QC_WATER_SMOKE_TYPE (only for IR/Visible algorithm path)	Thin Smoke	Thick Smoke

*Start from the least significant bit

Table 7. Definitions of bit-wise diagnostic flags for the EPS ADP "PQI3" variable.

Bit*	Diagnostic Flag Name	Meaning (1-bit)	
		0 (default)	1
0	QC_WATER_DUST_INPUT	Valid VIIRS inputs	Invalid VIIRS inputs
1	QC_WATER_DUST_CLOUD	Cloud-free	Obscured by clouds
2	QC_WATER_DUST_SNOW/ICE	Snow/ice free	With snow/ice
3	QC_WATER_DUST_TYPE (only for IR/Visible algorithm path)	Thin dust	Thick dust
4	QC_LAND_SMOKE_INPUT	Invalid VIIRS inputs	Valid VIIRS inputs
5	QC_LAND_SMOKE_CLOUD	Cloud-free	Obscured by clouds
6	QC_LAND_SMOKE_SNOW/ICE	Snow/ice free	With snow/ice
7	QC_LAND_SMOKE_TYPE (only for IR/Visible algorithm path)	Fire	Thick smoke

*Start from the least significant bit

Table 8. Definitions of bit-wise diagnostic flags for the EPS ADP "PQI4" variable.

Bit*	Diagnostic Flag Name	Meaning				
		1-bit	0 (default)	1	-----	-----
		2-bits	00 (default)	10	01	11
0	QC_LAND_DUST_INPUT	1-bit	Valid VIIRS inputs	Invalid VIIRS inputs	-----	-----
1	QC_LAND_DUST_CLOUD	1-bit	Cloud-free	Obscured by clouds	-----	-----
2	QC_LAND_DUST_SNOW/ICE	1-bit	Snow/ice free	With snow/ice	-----	-----
3	QC_LAND_DUST_TYPE (only for IR/Visible algorithm path)	1-bit	Thin dust	Thick dust	-----	-----
4-5	Smoke_Detection_Algorithm_Path	2-bits	Deep-blue	Missing	IR-Visible	Both
6-7	Dust_Detection_Algorithm_Path	2-bits				

*Start from the least significant bit

As shown in Table 2, the EPS ADP algorithm outputs Scaled Absorbing Aerosol Index (SAAI), which is related to the intensity of smoke/dust event, Dust Smoke Discriminating Index (DSDI), and smoke concentration in units of $\mu g/m^3$. These parameters are derived using the deep-blue algorithm path, as described in Section 3. However, the ABI and Advanced Himawari Imager (AHI) on the Himawari satellite series do not have the spectral bands required for the deep-blue algorithm path. As a result, the SAAI, DSDI, and smoke concentration variables are set to default values when the EPS ADP algorithm is applied to the ABI or AHI.

2.2 Instrument Characteristics

The EPS ADP will be produced for each pixel (2 km resolution at nadir) observed by the ABI. Table 9 summarizes the ABI channels used by the EPS ADP algorithm. By definition, the EPS ADP algorithm is able to handle multi-spectral observations from sensors that cover the deep-blue to IR spectral range, such as VIIRS and MODIS, or the visible to IR spectral range, such as AHI and ABI. In the following sections, ABI will be mainly used as an example. The mapping of bands from different satellite sensors to EPS ADP algorithm is given in Table 10.

The backbone of the ADP algorithm in GOES-R ABI is the distinctive spectral and spatial signature of aerosol (smoke/dust). Temporal variability has not been taken advantage of, in the current version of algorithm, but is planned for future versions. Similar to clouds, variability of smoke or dust plume is much larger than the surface over a course of day. Besides the threshold test, by tracking the variability over time, for example, variability over a course of 30 minutes, it is possible to define if a pixel is laden with smoke/dust. However, it must be noted that cloud, smoke and dust may have similar temporal variability. Taking advantage of temporal variability in smoke/dust detection has high requirement on separating clouds from smoke/dust. In addition, as shown in Table 9, different ABI channels have different spatial resolution, ranging from 0.5 km for visible to 2 km for IR channels. In ADP algorithm, the output resolution is 2km. Hence, channels with higher spatial resolution than 2 km have to be aggregated to 2km by sub-sampling/or averaging before applying the ADP algorithm. Like any other threshold-based algorithm, the ADP algorithm requires optimal performance of the instrument. First, the ADP algorithm is designed to work when only a sub-set of the expected channels are available. Missing channels, especially the crucial ones, will impact directly the performance of the algorithm. Second, the ADP algorithm is sensitive to instrument noise and calibration error. Thresholds are required to be adjusted accordingly to the status of instrument operation and performance. Third, calibrated observations are also critical, but since the algorithm does not compare the observed values to those from a forward radiative transfer model, uncertainties in calibration can be ameliorated by modifying thresholds once any calibration issues is identified. The channel specifications are given in the MRD.

Table 9. Channel numbers and wavelengths for the ABI and their use in the EPS ADP algorithm.

ABI Band	Nominal Wavelength Range (µm)	Nominal Central Wavelength (µm)	Spatial Resolution (km)	Use in Algorithm
1	0.45-0.49	0.47	1	Dust and Smoke
2	0.59-0.69	0.64	0.5	Dust and Smoke
3	0.846-0885	0.865	1	Dust and Smoke
4	1.371-1.386	1.378	2	Dust
5	1.58-1.64	1.61	1	Dust and Smoke
6	2.225 - 2.275	2.25	2	Smoke
7	3.80-4.00	3.9		Dust and Smoke
8	5.77-6.6	6.19		-----
9	6.75-7.15	6.95		-----
10	7.24-7.44	7.34		-----
11	8.3-8.7	8.5		-----
12	9.42-9.8	9.61		-----
13	10.1-10.6	10.35		Dust
14	10.8-11.6	11.2		Dust and Smoke
15	11.8-12.8	12.3		Dust
16	13.0-13.6	13.3		-----

Table 10. Mapping of channels for different sensors to channels used in ADP Enterprise Processing System.

Channel in EPS		Use in Algorithm Path	Sensor Bands			
Number	Wavelength (μm)		VIIRS	MODIS	ABI	AHI
1	0.412	Deep-Blue	M1	8	**	**
2	0.445	Deep-Blue	M2	9	**	**
3	0.488	Deep-Blue and IR-Visible	M3	3	1	1
4	0.555	Deep-Blue	M4	4	(2)*	2
5	0.640	Deep-Blue and IR-Visible	M5	1	2	3
6	0.746	Deep-Blue	M6	15	**	**
7	0.865	Deep-Blue and IR-Visible	M7	2	3	4
8	1.24	Deep-Blue	M8	5	(5)*	(5)*
9	1.38	IR-Visible	M9	26	4	(5)*
10	1.61	IR-Visible	M10	6	5	5
11	2.25	Deep-Blue and IR-Visible	M11	7	6	6
12	3.70	IR-Visible	M12	20	(7)*	(7)*
13	4.05	IR-Visible	M13	21	7	7
14	10.35	IR-Visible	(M15)*	(31)*	13	13
15	11.2	IR-Visible	M15	31	14	14
16	12.01	IR-Visible	M16	32	15	15

* Sensor band missing for given wavelength; band in parentheses is substituted.
** Sensor band missing but not required for a given algorithm path, and filled with '-999.9' in order to run EPS ADP algorithm.

3 ALGORITHM DESCRIPTION

3.1 Algorithm Overview

The EPS ADP algorithm has three algorithm paths depending on the wavelength range available from a given sensor: deep-blue path (deep-blue, visible and short-wave IR channels), IR-visible path (visible, short-wave IR and long-wave IR channels), and both paths. Table 10 shows the spectral bands required for each algorithm path. In this document, The IR-visible component of EPS ADP algorithm, which is related to GOES-R ABI ADP, is discussed. The IR-visible path in the EPS ADP algorithm is based on the following heritage algorithms:

- Aerosols (dust) from AVHRR Extended (CLAVR-x) of NESDIS/STAR
- Non-cloud obstruction (including smoke and dust) detection in the MOD/MYD35 MODIS cloud mask developed for MODIS by the University of Wisconsin (UW).

3.2 Processing Outline

The processing outline of the EPS ADP algorithm is summarized in Figure 1, which includes the basic modules as input, output, algorithm path selection and detection over land and water. Note that, EPS ADP algorithm is a one algorithm works on multi-spectral observations. It has uniform input and output. Depending on the availability of spectral coverage, EPS ADP algorithm has three algorithm paths. One is for measurements covering visible and IR wavelengths; the second one is for measurements covering deep-blue and shortwave IR wavelength; and the third one for measurements covering both deep-blue and Visible-IR wavelengths. As for GOES-R ABI, algorithm path 1, i.e., IR-Visible path is chosen. The algorithm is written in C++, and products are outputted in netCDF4 format. For optimizing CPU usage, the ADP algorithm is designed to run on segments of data. Each segment is comprised of multiple scan lines (10 lines).

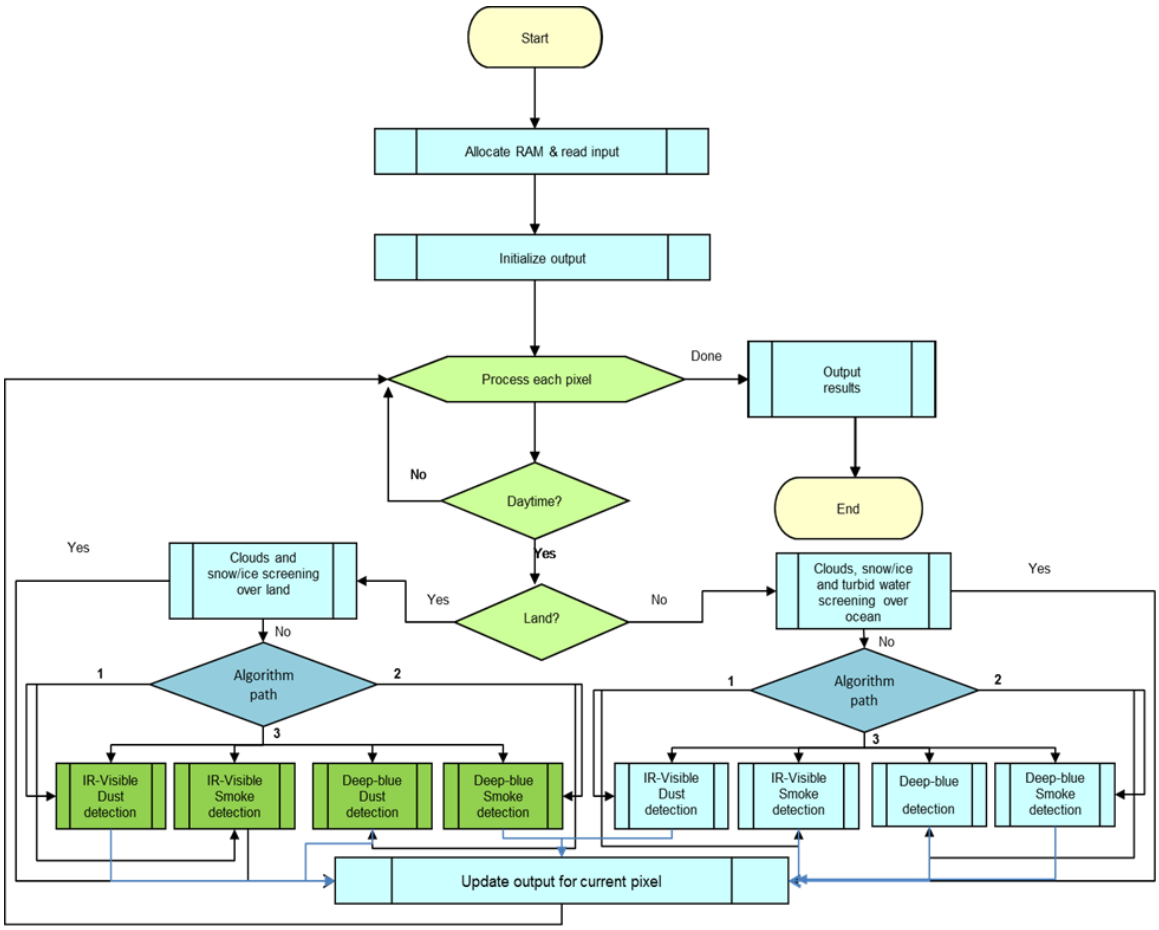

Figure 1. High level flowchart of the EPS ADP algorithm, illustrating the main processing sections.

3.3 Algorithm Input

This section describes the input needed to process the ADP algorithm. The ADP is derived for each pixel, and it requires knowledge of the surrounding pixels. In its current operation, the ADP algorithm is run on segments of 10 scan-lines.

3.3.1 **Primary Sensor Data**

Calibrated/navigated ABI reflectances and brightness temperatures (BTs) on selected channels, geolocation (latitude/longitude) information, and granule level quality flag and ABI sensor quality flags for all used channels are used as the sensor input data for quality controls in the EPS ADP algorithm are listed in Table 11.

Table 11. ABI primary data input to the EPS ADP algorithm.

ABI Primary Input Data	Description	Dimension
Granule Quality flag	Granule Level Quality Flag	none
Focal Plane Temperature	Focal Plane Temperature from GOES-17 to identify anomaly	none
Band 1 reflectance	Calibrated ABI level 1b reflectance at Band 1	grid (xsize, ysize)
Band 2 reflectance	Calibrated ABI level 1b reflectance at Band 2	grid (xsize, ysize)
Band 3 reflectance	Calibrated ABI level 1b reflectance at Band 3	grid (xsize, ysize)
Band 4 reflectance	Calibrated ABI level 1b reflectance at Band 4	grid (xsize, ysize)
Band 5 reflectance	Calibrated ABI level 1b reflectance at Band 5	grid (xsize, ysize)
Band 6 reflectance	Calibrated ABI level 1b reflectance at Band 6	grid (xsize, ysize)
Band 7 brightness temperature	Calibrated ABI level 1b brightness temperature at Band 7	grid (xsize, ysize)
Band 13 brightness temperature	Calibrated ABI level 1b brightness temperature at Band 13	grid (xsize, ysize)
Band 14 brightness temperature	Calibrated ABI level 1b brightness temperature at Band 14	grid (xsize, ysize)
Band 15 brightness temperature	Calibrated ABI level 1b brightness temperature at Band 15	grid (xsize, ysize)
Solar zenith angle	Pixel solar zenith angle	grid (xsize, ysize)
Solar azimuth angle	Pixel solar azimuth angle	grid (xsize, ysize)
Satellite zenith angle	Pixel satellite zenith angle	grid (xsize, ysize)
Satellite azimuth angle	Pixel satellite azimuth angle	grid (xsize, ysize)
Latitude	Pixel latitude	grid (xsize, ysize)
Longitude	Pixel longitude	grid (xsize, ysize)
QC flag for all above Bands	ABI quality control flags with level 1b data	grid (xsize, ysize)

The cloud mask required for the ABI ADP algorithm is designed to primarily come from the ABI cloud product. Bands used to determine the cloud mask are not listed here as that information is part of the cloud mask ATBD.

3.3.2 ABI Product Precedence and Ancillary Data

The dynamic data from ABI Level-1b and Level-2 products required by the EPS ADP algorithm are listed in Table 12. The sun glint mask and the day/night flag are determined internally in the EPS ADP algorithm from viewing and illuminating geometry information. For more information on the relevant ABI level 2 product, consult the corresponding ABI product ATBD.

Table 12. ABI product precedence and ancillary data input to the EPS ADP algorithm.

Type	Name	Source	Dimension
ABI Product Precedence Data	Cloud mask	ABI level 2 cloud product	grid (xsize, ysize)
	Snow/Ice mask	ABI level 2 snow/ice Product	grid(xsize, ysize)
	Sun glint mask	Internally determined but needs information on viewing geometry	grid(xsize, ysize)
	Day/night flag	Internally determined but needs information on viewing geometry	grid(xsize, ysize)
Ancillary Data	Land/Water mask	1 km dataset http://glcf.umiacs.umd.edu/data/landcover	grid(xsize,ysize)

The primary source of the snow/ice mask is the ABI Level-2 Snow/Ice Product. However, if the primary source is missing, the Interactive Multisensor Snow and Ice Mapping System (IMS) (http://nsidc.org/data/g02156.html) snow/ice mask will be the secondary source. In addition, the EPS ADP algorithm has an internal snow/ice test over land and a sea ice test over water, whose function is to eliminate the residuals from external snow/ice mask over land and water, which are applied after the primary/secondary snow/ice mask. Details on the internal snow/ice mask are given in Sections 3.5.2.1. and 3.5.2.3.

The cloud mask is used in the EPS ADP algorithm to eliminate pixels with obvious clouds, such as high clouds or ice clouds, before performing smoke/dust detection. Hence, the cloud mask requirement of the EPS ADP algorithm is more specific than just determining cloudy or clear pixels. A stringent cloud mask has the potential to classify smoke/dust as cloud, while a relaxed cloud mask increases the chance of misidentifying clouds as smoke/dust. The EPS ADP algorithm uses only individual tests, which exist as a diagnostic cloud mask, such as "CloudMaskpacked" in both the Enterprise Cloud Mask (ECM) and baseline cloud mask. The ABI cloud mask product indicates the existence of high clouds, ice clouds, and thin cirrus clouds. In addition, some tests in the cloud mask product, such as cloud shadow and fire hot spot, are used as quality controls for the detected smoke/dust in the ADP. Currently, the EPS ADP algorithm uses the GOES-16 and 17 ABI baseline cloud product as a proxy, including the ABI baseline cloud mask. Based on the definition of individual tests from the ABI baseline cloud mask, Table 13

maps the cloud tests in ABI baseline cloud mask to individual tests in other cloud mask products, such as the ABI EPS cloud mask and MODIS cloud mask.

Table 13. Mapping of diagnostic cloud mask products.

EPS ADP			MODIS Byte (Bit)	ABI Baseline Byte (Bit)	ABI Enterprise Byte (Bit)
Test Name	Description	Location Used			
pCirrus1	CIRREF- Near IR Cirrus Test (1.38 ⍰m) value=3 (confident cloudy)	Smoke over Water Dust over water Smoke over land Dust over land	2 (0) high cloud 1.38 ⍰m	3 (7)	6 (4-5)
pCirrus2	CIRREF- Near IR Cirrus Test (1.38 ⍰m) value=3 (confident cloudy)	Smoke over Water Dust over water Smoke over land Dust over land	1 (7) high cloud 6.7 ⍰m test	2 (5) 4 (1)	6 (4-5)
pCirrus3	Thin Cirrus value=1 (yes)	Smoke over Water Dust over water Smoke over land Dust over land	1 (1) thin cirrus, solar test	3 (7)	2 (3)
pFlag1	PFMFT – Positive FMFT (Split-Window BTD) Test 11um -8.5um test value=3 (confident cloudy)	Smoke over land	2 (2) IR temperature difference test	2 (6)	4 (2-3) 3 (4-5)
pFlag2	ETROP – Emissivity at Tropopause Test value=3 (confident cloudy)	Smoke over land	2 (3) 3.7-11 ⍰m test	3 (8)	3 (2-3)
pShadow	Shadow contaminated Flag	Smoke over water Dust over water Smoke over land Dust over land	1 (2) shadow test	N/A	2 (7)
pFire	Fire contaminated Flag	Smoke over land Dust over land	N/A	N/A	2 (8)

The EPS ADP algorithm is designed to generate internal sun glint mask based on ABI viewing and illuminating angles as second source. The sun glint angle (η) is calculated as following:

$$\cos(\eta) = \cos(\theta_0)\cdot\cos(\theta) + \sin(\theta_0)\cdot\sin(\theta)\cdot\cos(180 - \varphi)$$

Where θ_0 is the solar zenith angle; θ is the satellite zenith angle; and φ is defined as the difference between satellite azimuth angle and solar azimuth angle. An area with the calculated sun glint angle greater than zero and less than 40° is defined as the sun glint area.

A day/night flag is determined internally based upon the solar zenith angle. Day is defined as solar zenith angle of less than or equal to 87°, while night is defined as solar zenith angle greater than 87°.

The only static input required by the EPS ADP algorithm is a global 1 km land/water mask. The global land cover classification collection created by The University of Maryland Department of Geography with Imageries from the Advanced Very High Resolution Radiometer (AVHRR), acquired between 1981 and 1994 [Hansen et al., 1998], is used (http://glcf.umiacs.umd.edu/data/landcover/).

3.4 Mitigation of Impact on ADP from Focal Plane Module (FPM) Temperature anomaly in GOES-17

During post-launch testing of the GOES-17 ABI instrument, an issue with the instrument's cooling system was discovered. The loop heat pipe (LHP) subsystem, which transfers heat from the ABI electronics to the radiator, is not operating at its designed capacity. The consequence of this is that the ABI detectors cannot be maintained at their intended temperatures under certain orbital conditions. Inadequate cooling of the infrared channels leads to partial loss of imagery during some of the overnight hours before and after the vernal and autumnal equinoxes. Infrared signals with long wavelengths can be swamped by infrared light emitted by warm parts of the imager, degrading the signal, resulting in the channels saturate, meaning a useful signal is not available.

As previous described, ADP is daytime product, therefore, the nighttime observations which is heavily affect by this issue do not affect ADP. However, during certain hours in the earlier morning and later afternoon, there may potentially be impacts on ADP, especially on dust detection over both ocean and land, since it relies on the brightness temperature difference between two IR bands. As shown in Figure 2 for some hours in the earlier morning, the brightness temperature difference tends to decrease and for some hours in the late evening, the brightness temperature difference tends to increase. Consequently, both false and missing dust detection anomalies could occur. In addition, ADP is impacted by upstream products that may be degraded by the LHP issue, such as cloud mask and snow/ice mask. ADP smoke detection over land and water will be affected via the internal snow/ice test over land and water, while dust detection over both land and water will be affected via the brightness temperature difference between two IR bands.

The EPS ADP algorithm mitigates the impact of the LHP issue by quality control through three layers. First, the EPS ADP algorithm will read in FPM temperature, and a threshold of 85° is set. In any timestamp, if the FPM temperature is > 85°, then the granule level data quality flag (DQF) for ADP is set a value as 1 to indicate bad quality due to the FPM temperature anomaly. Second, the granule level data DQF from Level-1b will be checked; if the DQF has a value of 4, which means data was produced but the associated FPM temperature exceeded a threshold, the granule level DQF for ADP will be set as 3 to indicate bad quality due to the FPM temperature anomaly. Finally, at the pixel level, for each detection, the data quality will be determined through checking the DQF from Level-1b for the IR channels used in this specific detection. If any one of them has a value of 4, then the DQF for this specific detection in this pixel will be given a value of 3, indicting bad quality due to the FPM temperature anomaly.

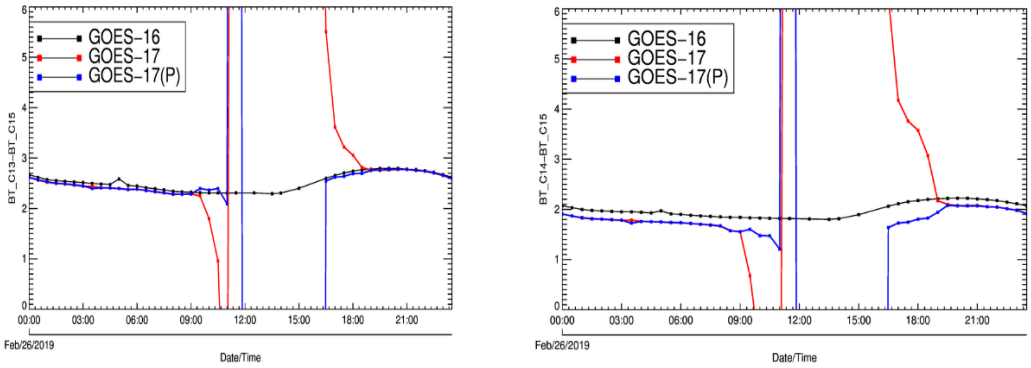

Figure 2. Time series of brightness temperature difference between Band 13 and Band 15 (left) and between Band 14 and 15 (right) on 02/26/2019 over an common area with viewing angle difference < 10° with a GOES-17 FPM temperature varying from 80-103°.

3.5 Theoretical Description

The EPS ADP algorithm attempts to separate cloudy and clear pixels from those with smoke or dust. The detection of smoke or dust relies on the distinctive signature of smoke or dust which is often expressed in terms of spectral variations of the observed brightness temperature or solar reflected energy. The spectral variation of the refractive index plays an important role in the success of these methods. In addition, the scattering and absorption properties of an aerosol also depend on the particle size distribution and the particle shape. Several aerosol remote sensing techniques have been developed using observations from the AVHRR [e.g. Barton et al., 1992]. Similar to dust plumes, volcanic ash plumes often generate negative brightness temperature differences between 11μm (BT_{11}) and 12 μm (BT_{12}). Prata [1989] has demonstrated the detection of volcanic aerosols using two infrared channels, while Ackerman and Strabala [1994] applied observations at 8.6, 11 and 12μm from the Hyper Spectral Infrared Sound (HIRS) instrument to study the Mt. Pinatubo stratospheric aerosol.

Image-based aerosol detection always involves assumptions of the radiometric characteristics of aerosol, clear and cloudy scenes. The surface conditions also influence the separation of aerosol pixels from those with clear-sky or cloud. The ADP algorithm currently uses spectral and spatial tests to identify pixels with smoke or dust in the daytime. Temporal tests are planned for future versions of the algorithm. The algorithm also treats detection differently for water and land.

3.5.1 **Physics of the Problem**

Techniques for the remote sensing of aerosols using solar and thermal measurements from satellites have been developed for several instruments, including AVHRR and MODIS. Fundamentally, these methods are based on the radiative signatures of aerosols. The problem of accurate detection and classification is compounded by the fact that the physical characteristics of aerosols (e.g. particle size distribution, concentration, chemical composition, location in the atmosphere) change as the aerosol layer develops and dissipates. These physical changes are capable of affecting the radiative characteristics of the original aerosol and our capability to detect

them from satellite observations. In addition to being present at the source region, aerosols are transported by winds to other regions of the globe.

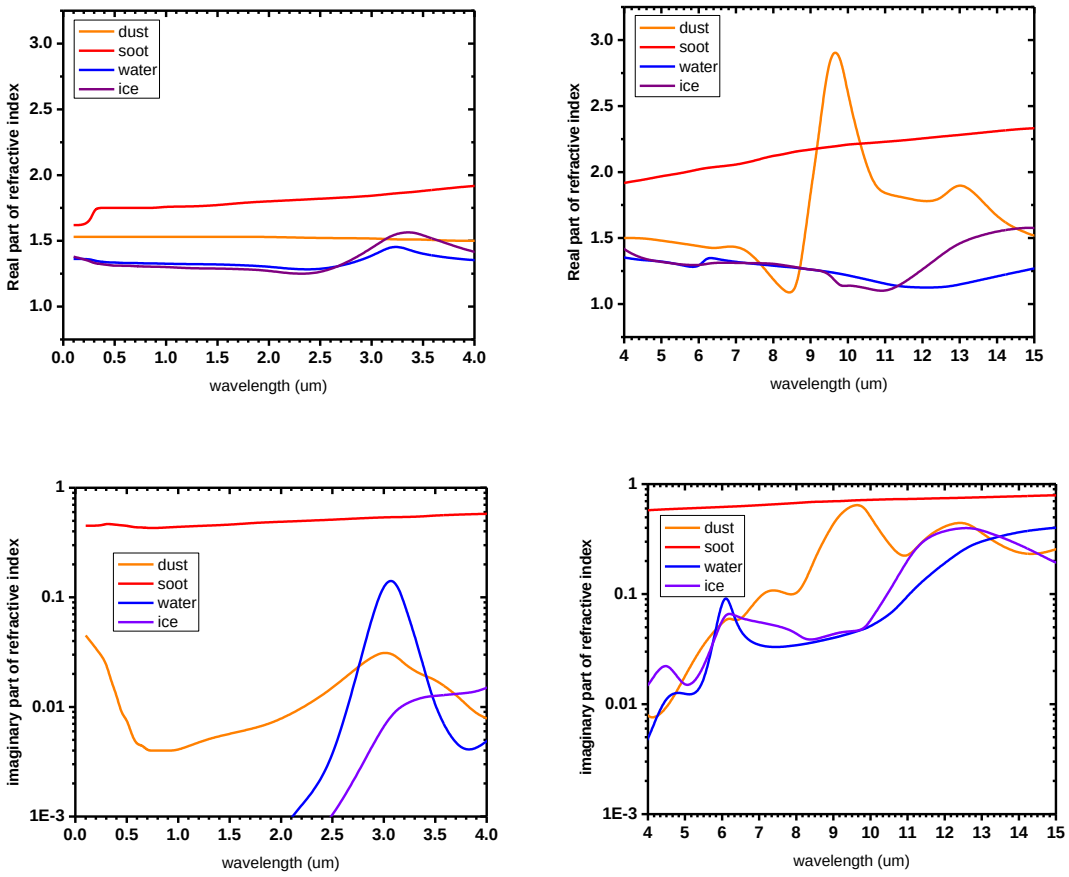

Figure 3: Real and imaginary part of dust, soot, water and ice as a function of wavelength. Plots are based on data obtained from NOAA's Community Radiative Transfer Model (CRTM).

Fundamentally, the radiative signatures of an aerosol layer are determined by the scattering and absorption properties of the aerosol within a layer in the atmosphere. These are:

- Extinction coefficient, σ_{ext} (which integrated over path length gives the optical thickness, τ). This parameter characterizes the attenuation of radiation through an aerosol volume due to aerosol scattering (measured by scattering coefficient σ_{sca}) and absorption (measured by absorption coefficient σ_{abs}) so that $\sigma_{ext} = \sigma_{sca} + \sigma_{abs}$.
- Single scattering albedo, $\omega_{\circ} = \sigma_{sca} / \sigma_{ext}$, which describes how much attenuation of radiation is due to scattering. It ranges between 1 for a non-absorbing medium and 0 for a medium that absorbs and does not scatter energy.
- Phase function, $P(\mu, \mu')$ which describes the direction of the scattered energy. Here μ and μ' are the cosine of solar and local zenith angles, respectively.

There are three important physical properties of a particle that are needed to determine the scattering and absorption properties listed above:

- The index of refraction ($m = m_r - im_i$) of the particle: The index of refraction of the medium is also required, but for air it is 1. Measurements of the index of refraction of a material are very difficult to make [Bohren and Huffman 1983]. The m_r is an indication of the scattering properties while the m_i is an indication of the absorption characteristics of the material. The scattering and absorption properties of an aerosol also depend on the particle size distribution. The index of refraction of smoke and dust is different from ice or water (Figure 3), which suggests that multi-spectral techniques should be useful in separating the aerosol from clouds.
- The shape of the particle: Microscopic analysis reveals that aerosols are irregular in shape. Thus, the assumption of spherical particles is often not accurate but a reasonable approximation. Shape effects may be a particular problem in the vicinity of strong infrared absorption bands for small particles with a uniform size distribution [Bohren and Huffman, 1983]. As no satisfactory method of handling the radiative properties of irregular shaped particles has been developed for general application to remote sensing techniques, the sensitivity studies generally assume spherical shaped particles.
- The size distribution of the particles, n(r): In addition to defining the radiative properties, the n(r) also determines the aerosol mass concentration. Particle size distributions of aerosols are often expressed as a log-normal distribution.

Because of these distinctive wavelength dependent aerosol properties, the spectral threshold based techniques are used to detect dust, smoke, volcanic ash work. The bulk transmittance of many aerosols displays a strong spectral variation in the 8-10 μm and 10-12 μm regions. This is also a spectral region over which the atmosphere is fairly transparent. For these reasons, techniques have been developed which successfully employ satellite radiance measurements at 11 and 12 μ m to detect aerosols. These split window IR techniques have primarily been applied to volcanic aerosols, particularly those from sulfur-rich eruptions [e.g. Prata 1989; Barton et al. 1992] as well as dust outbreaks [Legrand et al., 1992, 2001; Evan et al., 2006]. As demonstrated in Figure 4, dust absorbs more radiation at 12μm than 11μm, which causes the brightness temperature difference between the two to be negative.

There is absorption and emission of water vapor in the 11 and 12 μm channels. Because the weighting function for the 11μm channel peaks lower in the atmosphere than the 12μm channel does, the presence of a dry air mass, often associated with dust events, will tend to reduce the positive $BT_{11\mu m}$-$BT_{12\mu m}$ values associated with clear sky atmospheres. In addition, dust has a larger absorption at 12μm than at 11μm, so that dust plumes generally have a higher emissivity and lower transmissivity in the 12 μm channel [Ackerman, 1997; Dunion and Velden, 2004]. For more elevated dust layers, the increased temperature separation between the dust layer and the surface, and coincident reduction of dry air closer to the peak of the 11μm weighting function makes the split window brightness temperature difference less positive. This difference has also been observed to be affected by the optical thickness of a given dust plume, so that in thick optical depths the $BT_{11\mu m}$-$BT_{12\mu m}$ difference becomes more negative.

Darmenov and Sokolik [2005] further explored the brightness temperature difference technique using MODIS data applied to dust outbreaks from different regions of the globe. In general, $BT_{8\mu m}$-$BT_{11\mu m}$ becomes less negative and $BT_{11\mu m}$-$BT_{12\mu m}$ becomes more negative with increasing dust loading in Figure 4). However, in the ADP algorithm, the 3.9 μm is chosen instead of 8 μm because 3.9 μm has lees water vapor absorption and also to eliminate the false alarm from low level clouds (often towering cumulus).

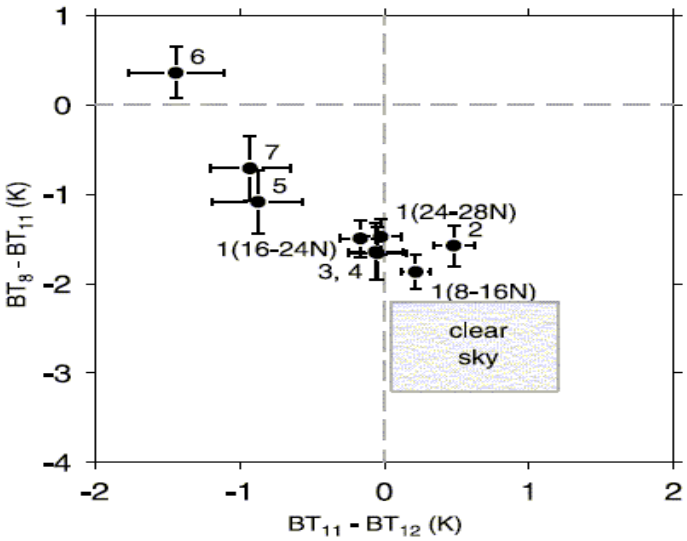

Figure 4. Combined tri-spectral diagram of brightness temperature differences for ''heavy dust'' pixels. From Darmenov and Sokolik [2005].

Dust absorbs at blue wavelengths and appears visually brown in color. Clouds are spectrally neutral and appear white to human eyes. For this reason, the reflectances at 0.86, 0.47 and 0.64μm have been used to identify dust. This is often done in a ratio of one to another or as a normalized difference index. For example, the MODIS aerosol optical depth retrieval algorithm has a condition that ratio of reflectances between 0.47 μm and 0.64 μm should be less than 0.75 for the central pixel in a 3 X 3 box to be identified as dust. Evan et al [2006] use a constraint that the reflectance value of the 0.86μm channel ($\rho_{0.86\mu m}$) divided by the reflectance value of the 0.63μm channel ($\rho_{0.63\mu m}$) is within the range of 0.6–1.0 for the AVHRR (this range is slightly different for MODIS due to differences in the spectral response functions). Again, due to the nonlinear relationship with optical thickness, we chose to square the reflectances prior to applying a test. The physical basis for this test is that the presence of smaller aerosols, like smoke, tends to reduce the values for this ratio, as smaller particles are more efficient at scattering light at 0.63μm. Although dust particles are observed to scatter more light at 0.64μm than at 0.86 μm probably due to their size, they tend to exhibit more uniform scattering across this spectral region [Dubovik et al., 2002]. A ratio type test of $\rho_{0.86\mu m}/\ \rho_{0.64\mu m}$ has been found to be useful in discriminating pixels containing smoke from those with dust. Another test for dust examination over water is the requirement that the ratio of reflectance at 0.47 μm and 0.64 μm is smaller than 1.2. Similar to the dust detection over land, low level clouds (often towering cumulus) can also have a negative split window

brightness temperature difference. Therefore, brightness temperature between 3.9 µm and 11 µm can be used to screen out cloud contaminated pixels.

The RGB image in Figure 5 shows a dust plume with different regions of heavy dust, thin dust, and clear sky clearly identified. For these different regions, the relationship between different visible and IR BTD are plotted in the four panels of Figure 5. Clear sky pixels have low reflectance at both 0.47 and 0.64 um, thin dust has elevated reflectances at these channels, and thick dust pixels have 20% or greater reflectance at these channels. The BTD between 3.9 um and 11 um plotted against the BTD between 11 µm and 12 µm shows a clear separation of thick dust pixels compared to thin dust and clear-sky.

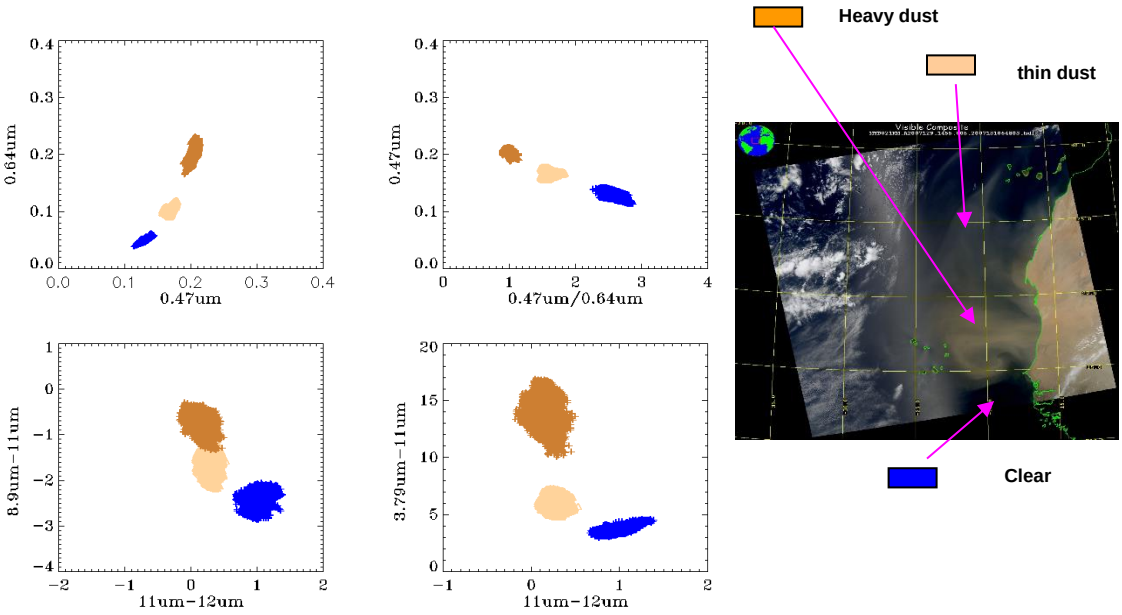

Figure 5. The relationship between various combinations of channels for heavy, thin dust, and clear conditions.

For smoke tests, fire spots are detected by looking at pixels with BTs at 3.9 µm greater than 350K and the BTD between 3.9 µm and 11 µm greater than or equal to 10K. Pixels that pass fire test are assumed to have smoke. For other pixels over land, the smoke tests take advantage of the relationship between surface reflectance at 0.64 µm and that at 2.25 µm, based on the fact that smoke is transparent at shortwave IR channel, such as 2.25 µm. For illustration purpose, a linear relationship observed between MODIS reflectance at 0.64 µm and 2.13µm is given in Figure 6. It is noted that this relationship gets noisy when reflectance at 2.13 µm is greater than 20%, indicating that the relationship may only valid for relatively dark surface, such as the vegetated surface or semi-arid surface. As for ABI, similar liner relationship is developed four different surface types defined by the range of NDVI values, also its intercept and slope is a function of solar zenith. The details on this relationship are given in section 3.5.2.5. When smoke is present in a pixel, there is a larger increase in $\rho_{0.64\mu m}$ than $\rho_{2.13\mu m}$, therefore, if the TOA reflectance at 0.64 µm after correction for the contribution from Rayleigh scattering is greater than the estimated surface reflectance at 0.64 µm based on the relationship, it is assumed that this pixel has the presence of smoke aerosol.

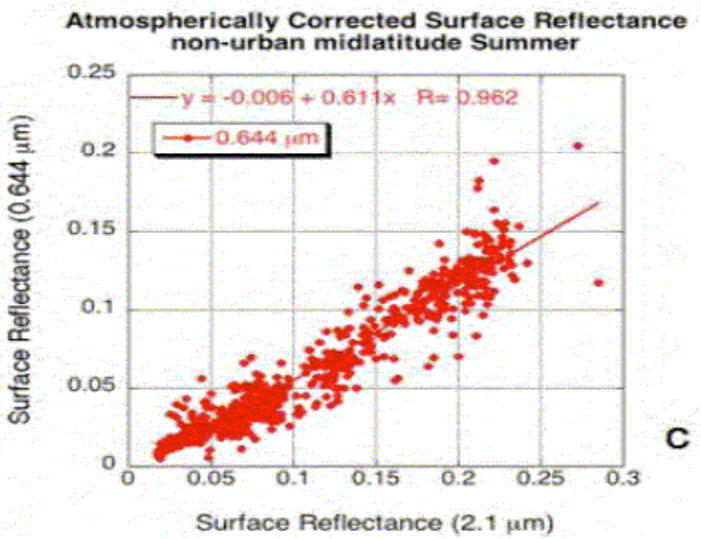

Figure 6. Surface reflectance at 0.64 µm va. surface reflectance at 2.1µm from MODIS. (Reference: Remer et al. 2005).

Most smoke and clouds appear visually as a bright subject, but clouds show a large variability in the 0.64 µm channel compared to smoke over land. Therefore, to further separate smoke from residual clouds, spatial uniformity tests for the 0.64 µm channel can be used. Over water, clear pixels, pixels loaded with thick smoke, and cloudy pixels are more uniform than pixels with partial cloud or thin smoke. By using the standard deviation of reflectance at 0.86 µm, where both aerosol and clouds effects are moderate, pixels which contain thick smoke vs. clouds/thin smoke can be separated. Smoke in visible channels looks brighter than the water surface but darker than a cloud. However, it is very difficult to completely separate them by only using the reflectance test. Therefore, based on the fact that reflection from clouds is spectrally independent, while reflection from smoke has a strong wavelength dependence, spectral contrast tests are combined to separate clouds, smoke, and water surface. First of all, the ratio between 0.47µm to 1.61µm is used, the rationale for choosing these two channels is due to the fact that aerosol effect is larger at 0.47um while water is darker at 1.61um. Secondly, the ratio between 2.25µm to 1.61µm is combined to enhance the separation of smoke from clouds. Thirdly, by constraining $\rho_{0.47\mu m}$ and $\rho_{1.61\mu m}$, thick smoke can be identified. A combination of tests developed using multiple channels for smoke detection over water are shown in Figure 7.

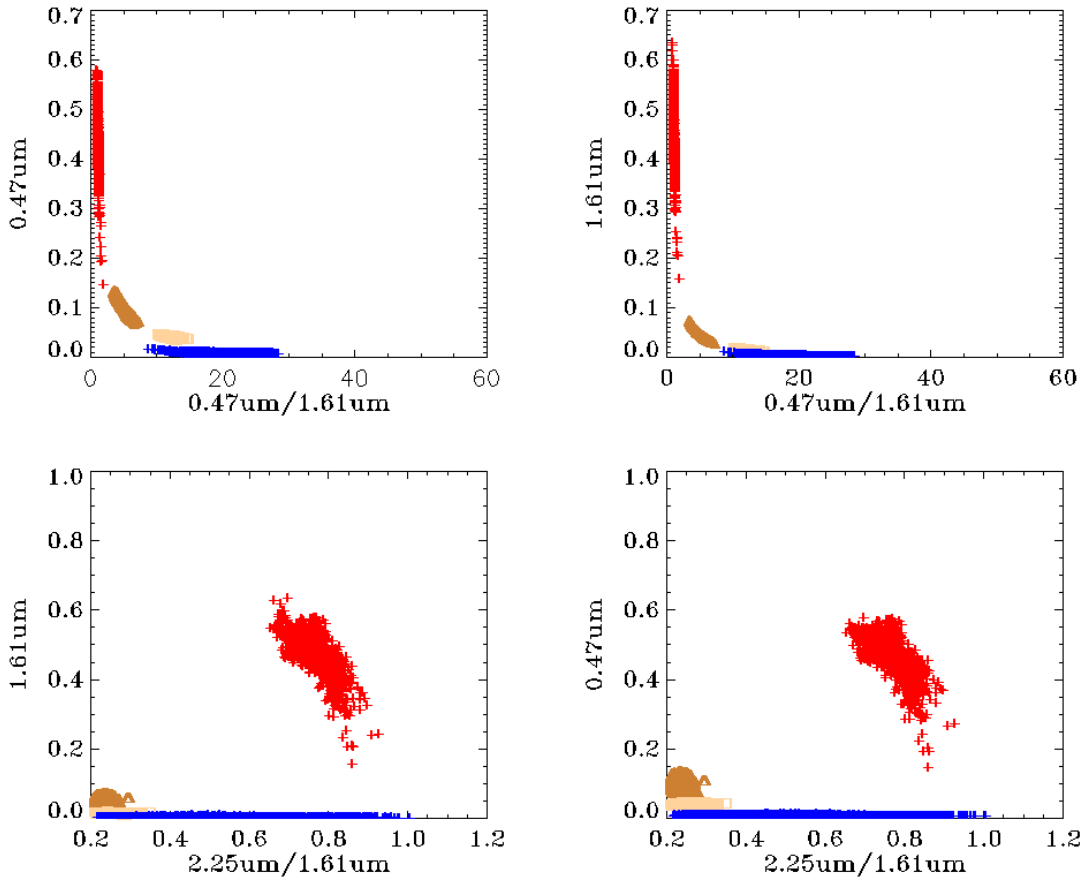

Figure 7. Scatter plots of R_3 vs. $\rho_{0.47\mu m}$, R_3 vs. $\rho_{1.61\mu m}$, R_4 vs. $\rho_{0.47\mu m}$, R_4 vs. $\rho_{1.61\mu m}$ for clear-sky pixels (blue), thick smoke pixels (dark brown), thin smoke (light brown) and cloudy pixels (red). Definitions of R_3 and R_4 are given in section 3.5.2.

3.5.2 **Mathematical Description**

Computation of the binary flag for smoke/dust aerosols in the EPS ADP algorithm is a process of elimination and determination. It has three levels. First, any pixel which contains cloud (high and optically thick clouds) and snow/ice, determined from the input cloud mask and snow/ice mask, is tagged as a cloudy or snow/ice pixel and not processed for smoke detection over land and over water and dust detection over water. For dust detection over land, the cloud mask is not used because of a high tendency for dust to be miss-identified as cloud by the cloud mask. Instead, only the snow/ice mask is used; if the pixel is tagged as snow/ice, it is not processed. Second, pixels contaminated by clouds but not screened by the cloud mask are further identified by a combination of spectral and spatial variability tests, especially for dust detection over land. Third, spectral contrast and variability tests designed for smoke/dust detection determine if a pixel has smoke or dust. Due to the fact that the contrast of smoke/dust to the underlying surface is different for land and water, smoke/dust detection in the EPS ADP algorithm is separated for over land and over water. The following sections describe the various tests

employed in the EPS ADP algorithm. The symbols and formulae used in the various tests in algorithm are defined as follows:

$$Rat_1 = \frac{\rho_{0.64\mu m} - \rho_{0.47\mu m}}{\rho_{0.64\mu m} + \rho_{0.47\mu m}}$$

$$Rat_2 = \frac{(Rat_1)^2}{(\rho_{0.47\mu m})^2}$$

$$NDVI = \frac{\rho_{0.86\mu m} - \rho_{0.64\mu m}}{\rho_{0.86\mu m} + \rho_{0.64\mu m}}$$

$$MNDVI = \frac{(NDVI)^2}{(\rho_{0.64\mu m})^2}$$

$$R_1 = \frac{\rho_{0.47\mu m}}{\rho_{0.64\mu m}}$$

$$R_2 = \frac{\rho_{0.86\mu m}}{\rho_{0.64\mu m}}$$

$$R_3 = \frac{\rho_{0.47\mu m}}{\rho_{1.61\mu m}}$$

$$R_4 = \frac{\rho_{2.25\mu m}}{\rho_{1.61\mu m}}$$

In the formulae listed above, "*Rat*" is ratio, "*NDVI*" is Normalized Difference Vegetation Index, "*MNDVI*" is Modified Normalized Difference Vegetation Index, and "*R*" is the TOA reflectance. Additional variables include "*BT*" for Brightness Temperature, "*BTD*" for Brightness Temperature Difference, and "*StdR*" for Standard Deviation of Reflectence. *StdR* is computed spatially for a pixel centered in a box containing 3 x 3 pixels. For a pixel that is not on the edge of scan, *StdR* is computed from the surrounding 3 by 3 pixels. For pixels on the edge of scan, the standard deviation for the closest pixel is assigned.

3.5.2.1 **Snow/ice test over land**

Before proceeding to any tests over land, the EPS ADP algorithm identifies pixels contaminated by snow/ice. As described earlier, the ABI snow/ice product is the primary source for this test, and if it is unavailable, the snow/ice mask from IMS is used as a secondary source. In addition, a further test is designed to catch any pixels that pass through but have snow/ice.

The specific internal tests as currently implemented are:

1) Good data test
   - $\rho_{0.86\mu m}$, $\rho_{1.61\mu m} > 0$ &
   - $BT_{11\mu m} > 0K$ &
   - ABI quality flags for above channels indicate good data

   If good data test passed then the process precede, otherwise the process is terminated.

2) Snow and Ice tests;

   if $BT_{11\mu m} \leq 285k$ & $(\rho'_{0.86\mu m} - \rho'_{1.61\mu m}) / (\rho'_{0.86\mu m} + \rho'_{1.61\mu m}) > 0.2$

   then snow/ice indicated for this pixel.

   ρ' is the Rayleigh-corrected TOA reflectance

3.5.2.2 **Dust Detection over Land**

Figure 8 is a flow chart of the EPS ADP algorithm to detect the presence of dust over land during daytime (defined as SZA < 87°). The tests are not performed over snow and ice.

The specific tests as currently implemented are:

(1) Test for the presence of snow/ice by using primary snow/ice mask, and if the primary is not available, then using secondary snow/ice mask. However, for dust detection over land, cloud mask is not applied to avoid the frequent miss-identification of dust plume as clouds in cloud mask. Residual cloud contamination is eliminated after detection by the designed test. Any pixel with positive snow/ice mask is not processed. The corresponding snow/ice flag is set as 1.

(2) Test for the quality of the input radiance data

- $\rho_{1.38\mu m} > 0$ &
- $BT_{3.9\mu m}$, $BT_{11\mu m}$, $BT_{12\mu m} > 0K$ &
- ABI quality flags for above channels equal to zero, indicating quality of the data is assured.

If good data test passed then the process precede, otherwise process is terminated and dust quality flag is set as a value of 3, indicating bad data.

(3) Thin Dust detection: BTD and R tests – check for pixels with thin dust and no cirrus clouds

- If $BT_{11\mu m}-BT_{12\mu m} \leq 0.4K$ & $0K \leq BT_{3.9\mu m}- BT_{11\mu m} < 5K$ & $R_{1.38\mu m} < 0.055$ & MNDVI > 0.05 then thin dust (1) is present
- If $BT_{11\mu m}-BT_{12\mu m} \leq 0.4K$ & $BT_{3.9\mu m}- BT_{11\mu m} \geq 5K$ & $0.035 \leq R_{1.38\mu m} < 0.055$ & MNDVI > 0.05 then thin dust (2) is present

(4) Thick dust test

- If $BT_{11\mu m}-BT_{12\mu m} < -0.4K$ & $BT_{3.9\mu m}- BT_{11\mu m} \geq 5K$ & $R_{1.38\mu m} < 0.035$&MNDVI < 0.05 then thick dust is present

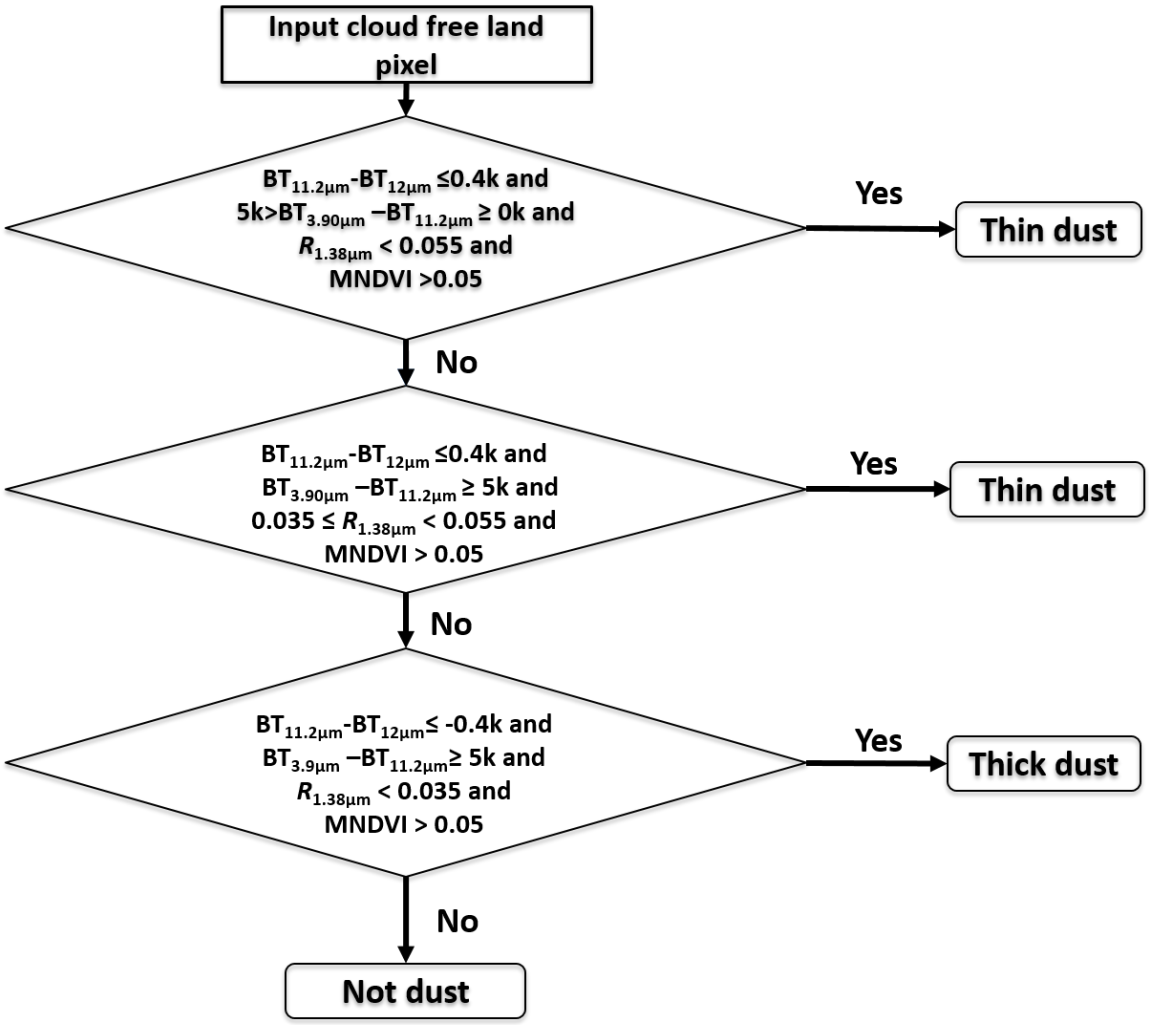

Figure 8. Detailed flow chart of dust detection over land.

3.5.2.3 **Determination of quality and confidence flags**

As shown in Section 2.1, for any pixel that is detected as the presence of dust, its quality is defined by three confidence levels, i.e. low, medium and high. Determination of confidence level relies on how close for a crucial test to the threshold and also solar/viewing angle. In the detection of dust over land, the BTD between $BT_{11\mu m}$ and $BT_{12\mu m}$ is chosen as the crucial test. The confidence level is defined as following:

Crucial Test: $BTD=BT_{11\mu m}-BT_{12\mu m}$

- If $0.3 < BTD \leq 0.4$ or SZA > 60 or VZA > 70, then confidence level = low
- If $0.0 < BTD \leq 0.3$, then confidence level = medium
- If $BTD \leq 0.0$, then confidence level = high

For ADP derived from GOES-17 ABI data, the final pixel level confidence level is set as bad due to the FPM temperature anomaly if DQF for any one of these channels, i.e., Band 7, Band 14, Band 15, has a value of 4.

3.5.2.4 **Example result – dust over land**

The results of applying the dust test over land to Aqua MODIS data on April 15, 2003 at 20:20 UTC and on March 4, 2004 at 19:45 UTC are shown in Figure 9 and Figure 10, respectively. The left hand side of the figure is a RGB true color image of the scene showing the location of blowing dust. The right-hand side of the figure shows the results of the dust test. Pixels flagged as dusty are colored orange. A third example is shown in Figure 11, which shows ADP for a combined smoke and dust event observed by GOES-16 ABI at several UTC timestamps on April 13, 2018.

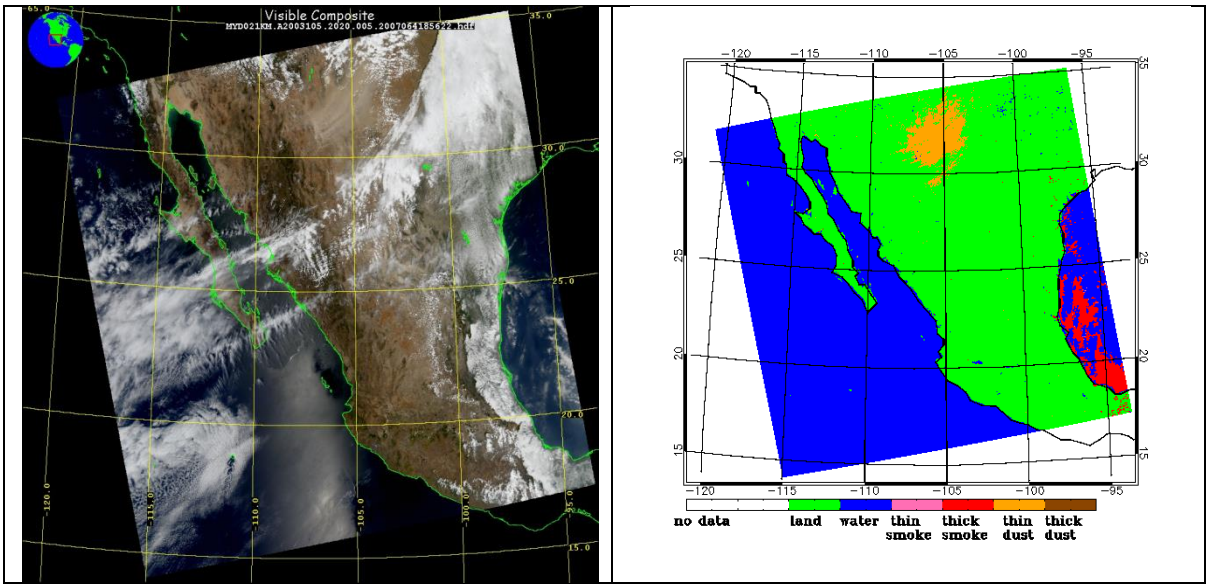

Figure 9. Aqua MODIS true color image on April 15, 2003 at 20:20 UTC (left) and corresponding results of ADP dust test (right).

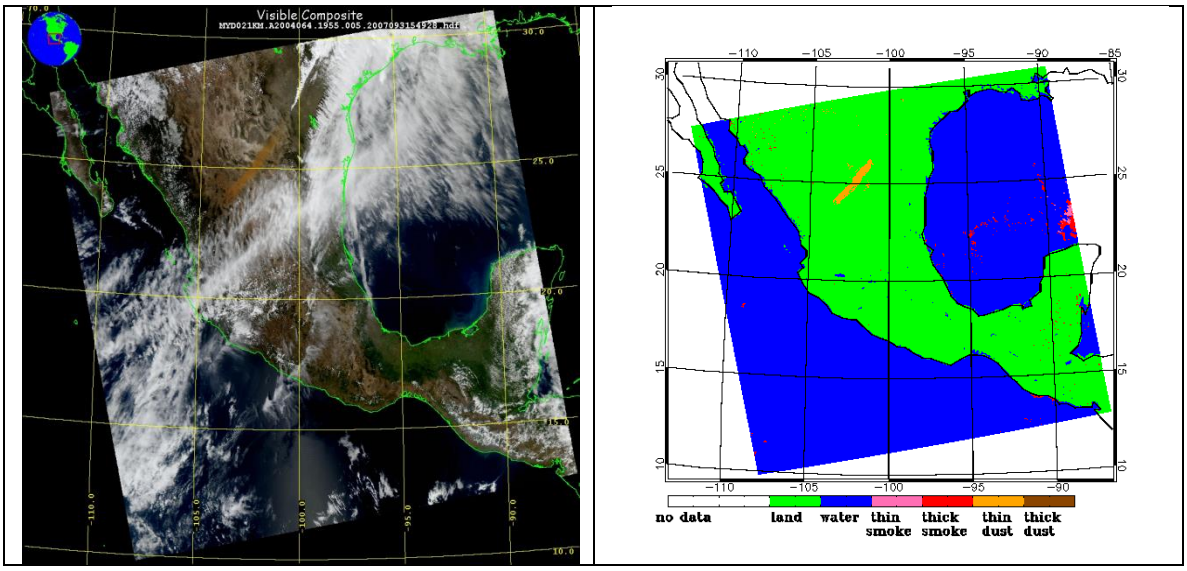

Figure 10. Aqua MODIS true color image on March 4, 2004 at 19:55 UTC (left) and corresponding results of the ADP dust test (right).

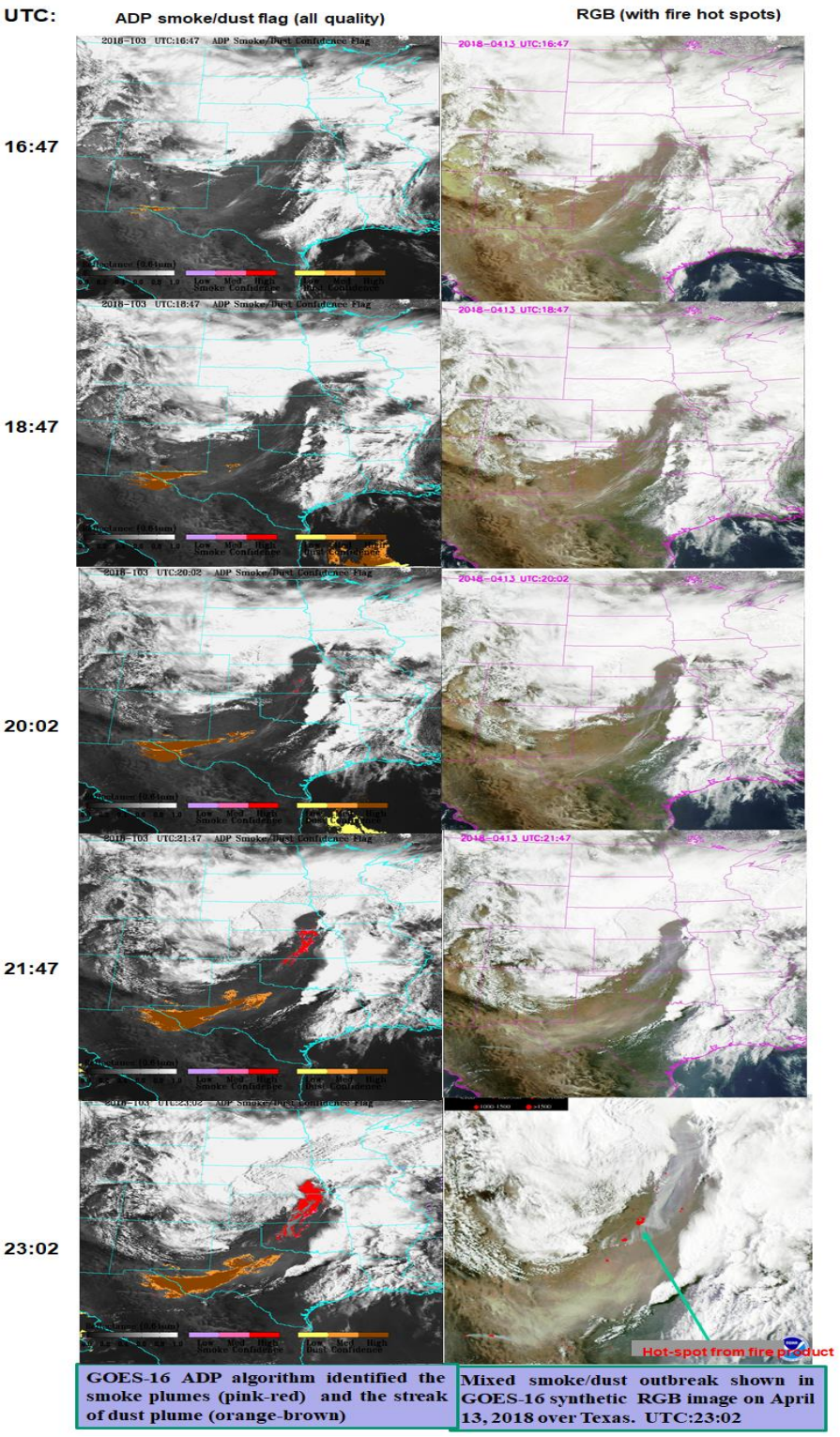

Figure 11. Left: ADP from GOES-16 ABI on April 13, 2018; dust pixels are colored yellow (low confidence), orange (medium confidence) and brown (high confidence), and smoke pixels are colored purple (low confidence), pink (medium confidence) and red (high confidence). Right: GeoColor color imagery with fire hot-spots.

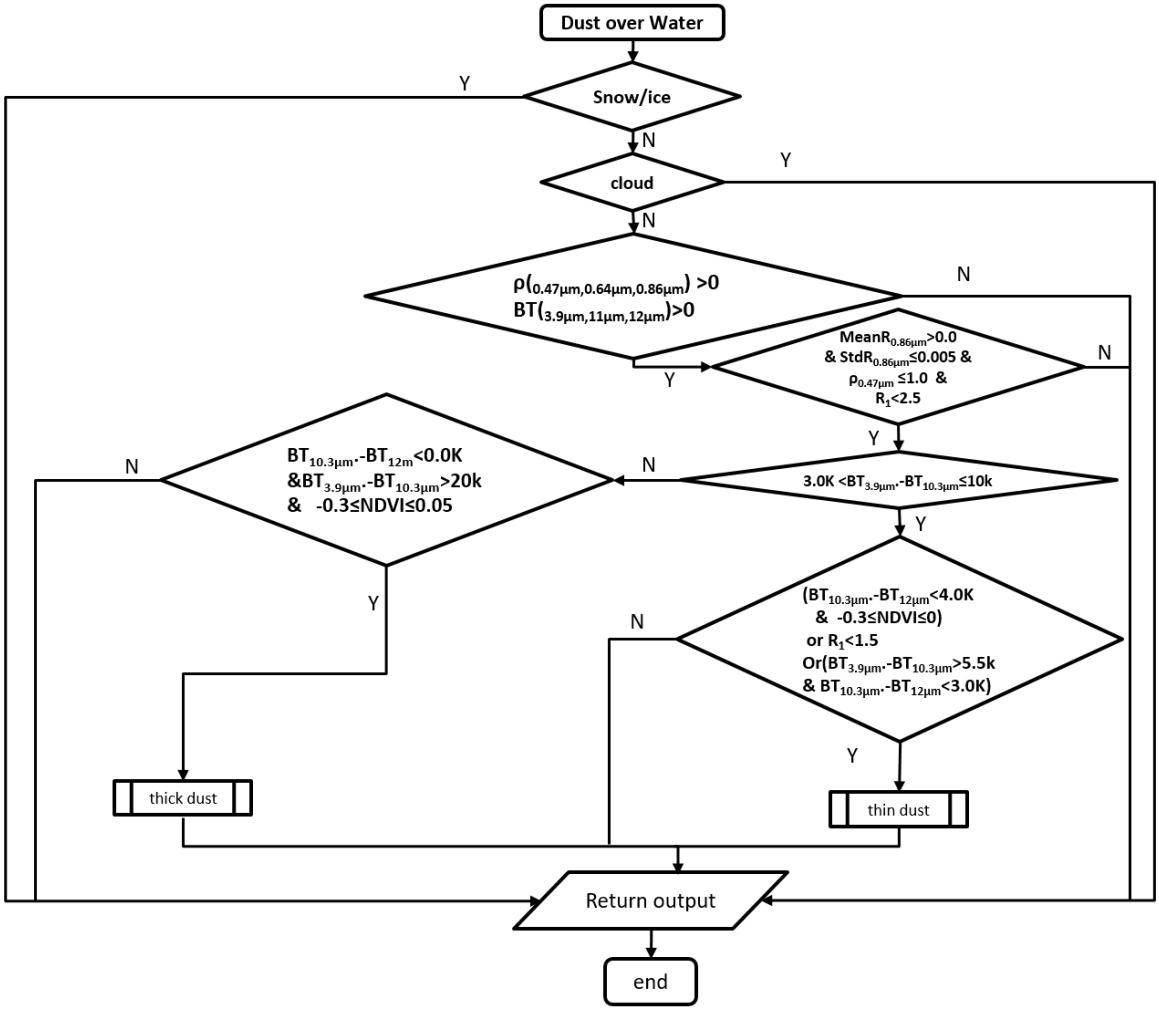

Figure 12: Detailed flow chart of dust detection over water.

3.5.2.5 **Sea ice test over water**

Before proceeding to any tests over water, it is important to identify pixels contaminated by sea ice. As described earlier, ABI snow/ice product is the primary source, and if the primary source is unavailable, snow/ice mask from IMS is used as a second source. However, a further test is designed to catch any pixels that pass through but have sea ice. The specific internal tests as currently implemented are:

1) Good data test
   - $\rho_{0.64\mu m}$, $\rho_{1.61\mu m} > 0$ &
   - $BT_{11\mu m} > 0K$ &
   - ABI quality flags for above channels indicate good data

If good data test passed then the process precede, otherwise process is terminated.

2). Sea Ice tests:
   - If $BT_{11\mu m} \leq 275k$ & $(\rho'_{0.64\mu m} - \rho'_{1.61\mu m})/(\rho'_{0.64\mu m} + \rho'_{1.61\mu m}) > 0.4$ & $\rho'_{0.64\mu m} > 0.1$ & $\rho'_{1.61\mu m} > 0.05$ then sea ice indicated for this pixel.

ρ´ is Rayleigh-corrected TOA reflectance

3.5.2.6 **Dust Detection over Water**

Figure 12 is a detailed flow chart of the algorithm to detect the presence of dust over water during the daytime. The tests are not performed over snow and ice or in the presence of ice clouds.

The specific tests as currently implemented are

1) Test for the presence of snow/ice by using primary snow/ice mask, and if the primary is not available, then using secondary snow/ice mask. After that, internal sea ice test is applied. If the sea ice is presented then detection process is terminated. Test for the presence of clouds relies on diagnostic tests, i.e., "CloudMaskpacked" as in ABI EPS cloud mask and also ABI baseline cloud mask. Pixel is considered to be obscured by clouds if any of these three cloud mask tests in Table 13, i.e. "pCiirus1", "pCirrus2" and "pCirrus3" is true. Any pixel with positive snow/ice/cloud mask is not processed and cloud flag or snow/ice flag is set as 1, correspondingly.

2) Test for the quality of the input radiance data

   - $\rho_{0.47\mu m}$, $\rho_{0.64\mu m}$, $_{0.86\mu m} > 0$ &
   - $BT_{3.9\mu m}$, $BT_{10.3\mu m}$, $BT_{12\mu m} > 0K$
   - ABI quality flags for above channels equal to zero, indicating quality of the data is assured.

If good data test passed then the process precede, otherwise process is terminated and dust quality flag is set as a value of 3, indicating bad data.

3) Uniformity and spectral tests for residual clouds

   - $MeanR_{0.86\mu m} > 0$ and $StdR_{0.86\mu m} \leq 0.005$ &
   - $\rho_{0.47\mu m} \leq 1.0$ &
   - $\rho_{0.47\mu m}/\rho_{0.64\mu m} < 2.5$

   If all above tests passed, then proceed to dust detection. Otherwise, detection is stop here. And, dust flag is set as 0 and cloud flag set as 1.

4) Tests for dust
   - If $3.0K < BT_{3.9\mu m} - BT_{10.3\mu m} \leq 10$ K, then perform thin dust test
   - Otherwise, perform thick dust test

   4.1 thin dust test
   - If $BT_{10.3\mu m} - BT_{12\mu m} < 4.0K$ and $-0.3 \leq NDVI \leq 0$ or $R_{0.47\mu m}/R_{0.64\mu m} < 1.5$ or

$BT_{3.9\mu m}$- $BT_{10.3\mu m}$ > 5.5K and $BT_{10.3\mu m}$- $BT_{12\mu m}$ < 3.0K, then thin dust (1), (2) and (3) is present

4.2 thick dust test

- If $BT_{3.9\mu m}$- $BT_{11\mu m}$ > 20K and $BT_{11\mu m}$-$BT_{12\mu m}$ ≤ 0K and -0.3 ≤ NDVI ≤ 0.05, then thick dust is present

5) Set dust mask flag

There are three separate tests for thin dust over water, each is elaborated above. Any of the tests can pass for the pixel to be flagged as dusty, although some of the tests have multiple conditions that must be passed.

3.5.2.7 **Determination of quality and confidence flags**

For any pixel if it is detected as the presence of dust, its quality is defined by three confidence levels, i.e. low, medium and high. Determination of confidence level relies on how close a crucial test is to the threshold and also the solar/viewing angles. In general, there are three types of tests: (1) value of the test < threshold, (2) value of the test > threshold, and (3) value of the test is within a range of two thresholds. First, a confidence value is assigned to each test. For type 1 test, a confidence value of 0.0, 1.0 and 0.5 is assigned respectively if the actual value is < 1% under the threshold, > 2% under the threshold, and between 1%~2%. For type 2 test, a confidence value of 0.0, 1.0 and 0.5 is assigned respectively if actual value is < 1% above the threshold, > 2% above the threshold, and between 1%~2%. For type 3 test, the range between the lower-threshold and upper-threshold is divided into 5 equal intervals, and a confidence value of 0.0, 1.0 and 0.5 is assigned respectively for the actual value that falls into the outer two intervals, the middle interval, and the remaining two intervals. Secondly, the ensemble confidence value is calculated by averaging the confidence value for all three types of tests. The final confidence level is set by the ensemble confidence value. Details for determination confidence level for dust over water are given as following:

1. Thin dust (1) as shown in section 3.5.2.3

   Test1: 3.0K< $BT_{3.9\mu m}$- $BT_{10.3\mu m}$ ≤ 10K
   Test2: $BT_{3.9\mu m}$- $BT_{10.3\mu m}$ <4.0k
   Test3: -0.3 ≤ NDVI ≤ 0

$$con\_value = \frac{\left[con_{value(Test1)} + con_{value(Test2)} + con_{value(Test3)}\right]}{3.0}$$

   If con_value≤0.33 confidence level=low
   If con_value>0.33 &<0.66 confidence level=medium
   If con_value≥0.66 confidence level=high

2. Thin dust (2) as shown in section 3.5.2.3

Test1: $\rho_{0.47\mu m}/\rho_{0.64\mu m} < 1.5$
Test2: $3.0K < BT_{3.9\mu m} - BT_{10.3\mu m} \leq 10K$

$$con\_value = \frac{\left[con_{value(Test1)} + con_{value(Test2)}\right]}{2.0}$$

If con_value≤0.25 confidence level=low
If 0.25<con_value<0.75 confidence level=medium
If con_value≥0.75 confidence level=high

3. Thin dust (3) as shown in section 3.5.2.3

Test1: $5.5k < BT_{3.9\mu m} - BT_{10.3\mu m} < 10K$
Test2: $BT_{10.3\mu m} - BT_{12\mu m} < 3.0K$

$$con\_value = \frac{\left[con_{value(Test1)} + con_{value(Test2)}\right]}{2.0}$$

If con_value≤0.25 confidence level=low
If con_value>0.25 &<0.75 confidence level=medium
If con_value≥0.75 confidence level=high

4. Thick dust as shown in section 3.5.2.3

Test1: $BT_{3.9\mu m} - BT_{11\mu m} > 20K$
Test2: $BT_{10.3\mu m} - BT_{12\mu m} \leq 0K$
Test3: $-0.3 \leq NDVI \leq 0.05$

$$con\_value = \frac{\left[con_{value(Test1)} + con_{value(Test2)} + con_{value(Test3)}\right]}{3.0}$$

If con_value<=0.33 confidence level=low
If con_value>0.33 &<0.66 confidence level=medium
If con_value>=0.66 confidence level=high

In addition, the confidence level is also determined by the solar/viewing geometry and where the detect dust is within sunglint region, i.e., for a pixel with detected dust, its confidence level is as:

If 0.0≤suglint angle ≤40 or SZA>60 or VZA>70 confidence level=low

For ADP derived from GOES-17 ABI data, the final pixel level confidence level is set as bad due to the FPM temperature anomaly if DQF for any one of these channels, i.e., Band 7, Band 14, Band 15, has a value of 4.

3.5.2.8 **Example result – dust over water**

The results applying the dust test over water to Aqua MODIS data on May 18, 2010 at 12:30 UTC is shown in Figure 13.

The left side of the figure is a RGB true color image, the middle image is MOIDIS AOD (> 0.2), and the right image shows the results of the water and land dust detection algorithm, where orange and brown regions indicate the presence of dust. The MODIS AOD image shows no data over the sun glint region. The RGB image and the ABI dust mask image show qualitative agreement.

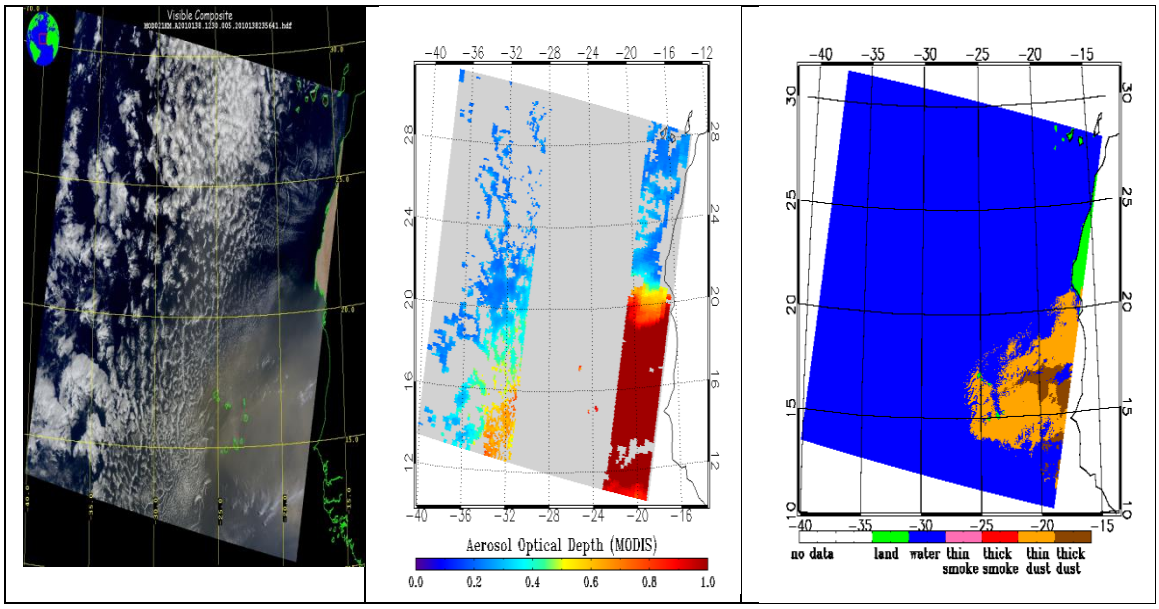

Figure 13. Terra MODIS observations on May 18, 2010 at 12:30 UTC, showing dust from the Sahara desert blowing over the adjacent Atlantic Ocean.

Another example is given in Figure 14, showing is a trans-Atlantic Saharan dust transport event observed by GOES-16 ABI in full disk scan mode. The trans-Atlantic dust shown in the RGB image is also identified in the ADP image. The sun-glint region, where dust is not detected, is shown as a black circle in the ADP image.

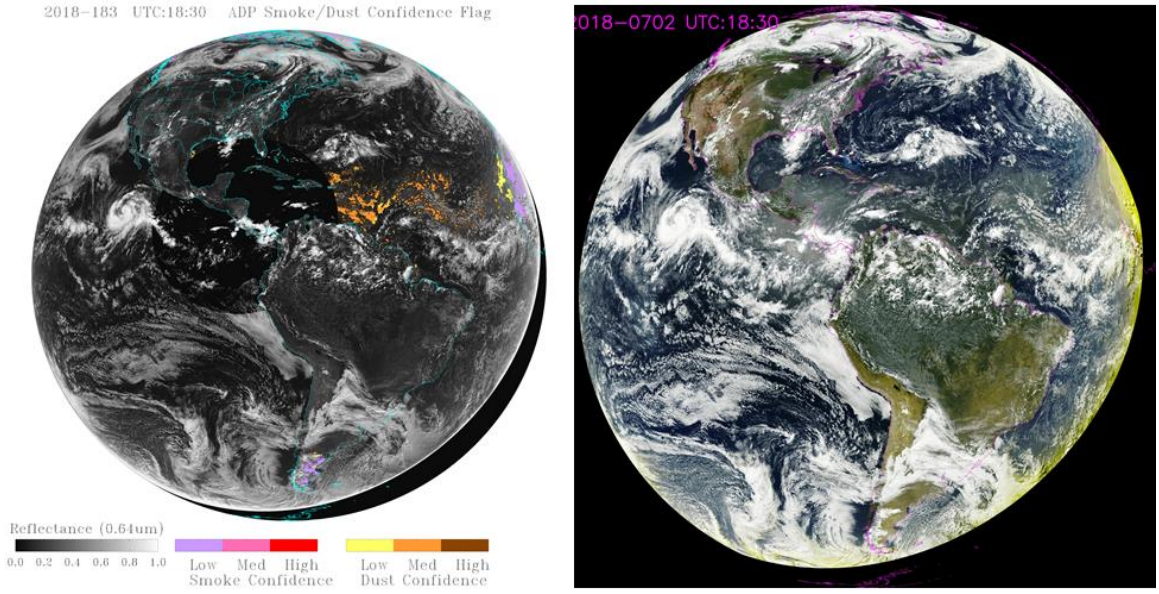

Figure 14. GOES-16 ABI ADP on June 02, 2018 at 18:30UTC showing dust pixels colored yellow (low confidence), orange (medium confidence) and brown (high confidence) (left) and GeoColor image (right).

3.5.2.9 **Thick Smoke Detection over Land**

Figure 15 is a detailed flow chart of the algorithm to detect the presence of smoke over land during daytime. Note that, the tests are not performed in the presence of snow/ice and ice clouds.

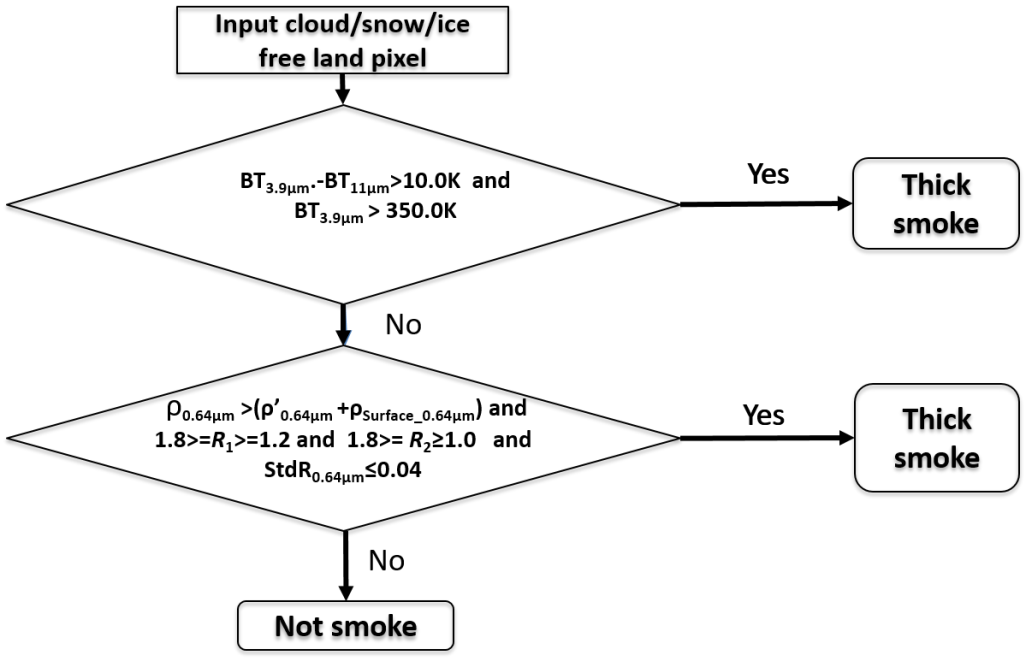

Figure 15: Detailed flow chart of thick smoke detection over land.

In Figure 15, $\rho'_{0.64\mu m}$ is the Rayleigh reflectance at 0.64 μm and it is defined as:

$$\rho'_{0.64\mu m} = 5.0 \cdot 0.75 \cdot (1 + (\cos(\omega))^2)$$

ω is the scattering angle. $\rho_{surface\_0.64\mu m}$ is the estimated surface reflectance at 0.64 μm, and it is calculated as:

$$\rho_{surface_{0.64\mu m}} = (c_1 + c_2 \cdot \theta_0) + (c_3 + c_4 \cdot \theta_0) \cdot \rho_{2.25\mu m}$$

Note that, θ_0 is the solar zenith angle, $\rho_{2.25\mu m}$ is the TOA reflectance at 2.25 μm. c_1, c_2, c_3 and c_4 are constants, their values are changing with four surface types, determined by the value of NDVI, i.e., NDVI=($\rho_{0.86\mu m}$ - $\rho_{0.64\mu m}$)/($\rho_{0.86\mu m}$ +$\rho_{0.64\mu m}$), as following:

NDVI>=0.55:

c_1=1.374160E-02, c_2=-5.128175E-05, c_3=2.761044E-01, c_4=1.034823E-03

NDVI <=0.3 and NDVI<0.55

c_1=2.990101E-02, c_2=-1.873911E-04, c_3=4.602174E-01, c_4=9.658934E-04

NDVI <=0.2 and NDVI<0.3:

c_1=5.179930E-02, c_2=-1.043257E-04, c_3=4.937035E-01, c_4=4.310074E-04

NDVI <0.2:

c_1=-3.397737E-02, c_2=1.640336E-03, c_3=1.087497E+00, c_4=-9.538776E-03

The specific tests as currently implemented sequentially are:

1) Test for the presence of snow/ice by using primary snow/ice mask, and if the primary is not available, then using secondary snow/ice mask. After that, internal snow ice test is applied. Test for the presence of clouds relies on the diagnostic tests in ABI cloud mask. Pixel is considered to be obscured by clouds if any of these five cloud mask tests in Table 13, i.e. pCiirus1, pCirrus2, pCirrus3, pFlag1 and, pFlag2, is true. Any pixel with the presence of snow/ice or cloud, as indicated by the snow/ice mask, internal snow/ice test or cloud mask, is not processed. And, the corresponding cloud or snow/ice flag is set as 1.

2) Test for the quality of the input radiance data

   - $\rho_{0.47\mu m}$, $\rho_{0.64\mu m}$, $\rho_{0.86\mu m}$, $\rho_{2.25\mu m} > 0$ &
   - $BT_{3.9\mu m}$, $BT_{11\mu m}$, > 0K
   - ABI quality flags for above channels equal to zero, indicating quality of the data is assured.

If good data test passed then the process precede, otherwise process is terminated and smoke quality flag is set as a value of 3, indicating bad data.

3) Fire detection (hot spot)

   - If $BT_{3.9\mu m} > 350K$ and $BT_{3.9\mu m} - BT_{11\mu m} \geq 10K$, then fire present and associated with thick smoke

4) Spectral and uniformity tests for thick smoke

- If $\rho_{0.64\mu m} > (\rho'_{0.64\mu m} + \rho_{surface_{0.64\mu m}})$ and $1.2 \leq R_1 \leq 1.8$ and $1.0 \leq R_2 \leq 1.8$ and $StdR_{0.64\mu m} \leq 0.04$ (3x3), then thick smoke

5) Set smoke flag

- If fire or thick smoke then smoke is present

3.5.2.10 Determination of quality and confidence flags

For pixels detected as smoke, their qualities are determined by three confidence levels. The approach to determine confidence value for each test is the same as that described in section 3.5.2.3.1. Details for determination confidence level for smoke over land are given as follow:

1. Smoke from fire as shown in section 3.5.2.4

   Test1: $BT_{3.9\mu m} > 350K$
   Test2: $BT_{3.9\mu m} - BT_{11\mu m} \geq 10K$

$$con\_value = \frac{\left[con_{value(Test1)} + con_{value(Test2)}\right]}{2.0}$$

   If con_value<=0.25 confidence level=low
   If con_value>0.25 &<0.75 confidence level=medium
   If con_value>=0.75 confidence level=high

2. Thick smoke as shown in section 3.5.2.4

   Test1: $\rho_{2.25\mu m} < 0.2$
   Test2: $\rho_{0.64\mu m} > (\rho'_{0.64\mu m} + \rho_{surface_{0.64\mu m}})$
   Test3: $1.2 \leq R_1 \leq 1.8$
   Test4: $1.0 \leq R_2 \leq 1.8$

$$con\_value = \frac{\left[con_{value(Test1)} + con_{value(Test2)} + con_{value(Test3)} + con_{value(Test4)}\right]}{4.0}$$

   If con_value<=0.25 confidence level=low
   If con_value>0.25 &<0.75 confidence level=medium
   If con_value>=0.75 confidence level=high

Note that, the confidence level is also determined by the solar/viewing geometry, i.e., for a pixel detected as smoke, its confidence level is as:

If SZA>60 or VZA>70 confidence level=low

For ADP derived from GOES-17 ABI data, the final pixel level confidence level is set as bad due to the FPM temperature anomaly if DQF for any one of these channels, i.e., Band 7, Band 14, has a value of 4.

3.5.2.11 Example result – smoke over land

The results of an application of the smoke test to MODIS Terra data on May 2, 2007 at 16:35 UTC is shown in Figure 16. Smoke over Florida is detected. Comparisons of smoke mask to RGB images show that both smoke over land and water were well captured. Another example for GOES-16 observations is given in Figure 17. It is indicated smoke plume shown in RGB is also identified as smoke in GOES-R ADP.

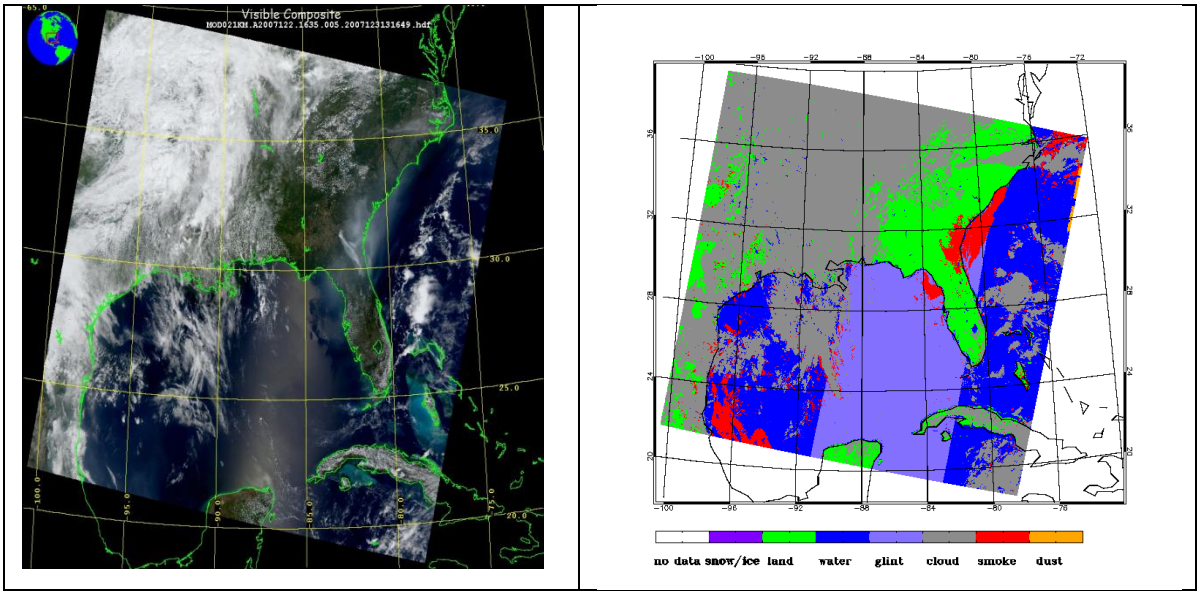

Figure 16. Terra MODIS true color image on May 2, 2007 at 16:35 UTC (left) and corresponding results of the ADP smoke test (right).

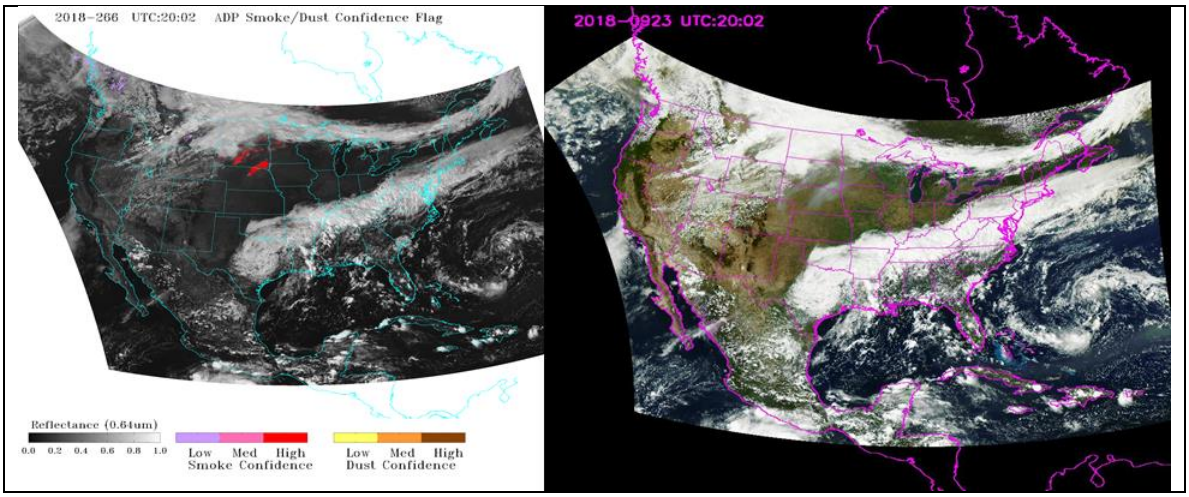

Figure 17. APD from GOES-16 ABI on Sep 23, 2018 at 20:02 UTC (left); smoke pixels are colored as red (high confidence), and corresponding GeoColor imagery (right).

3.5.2.12 **Smoke detection over water**

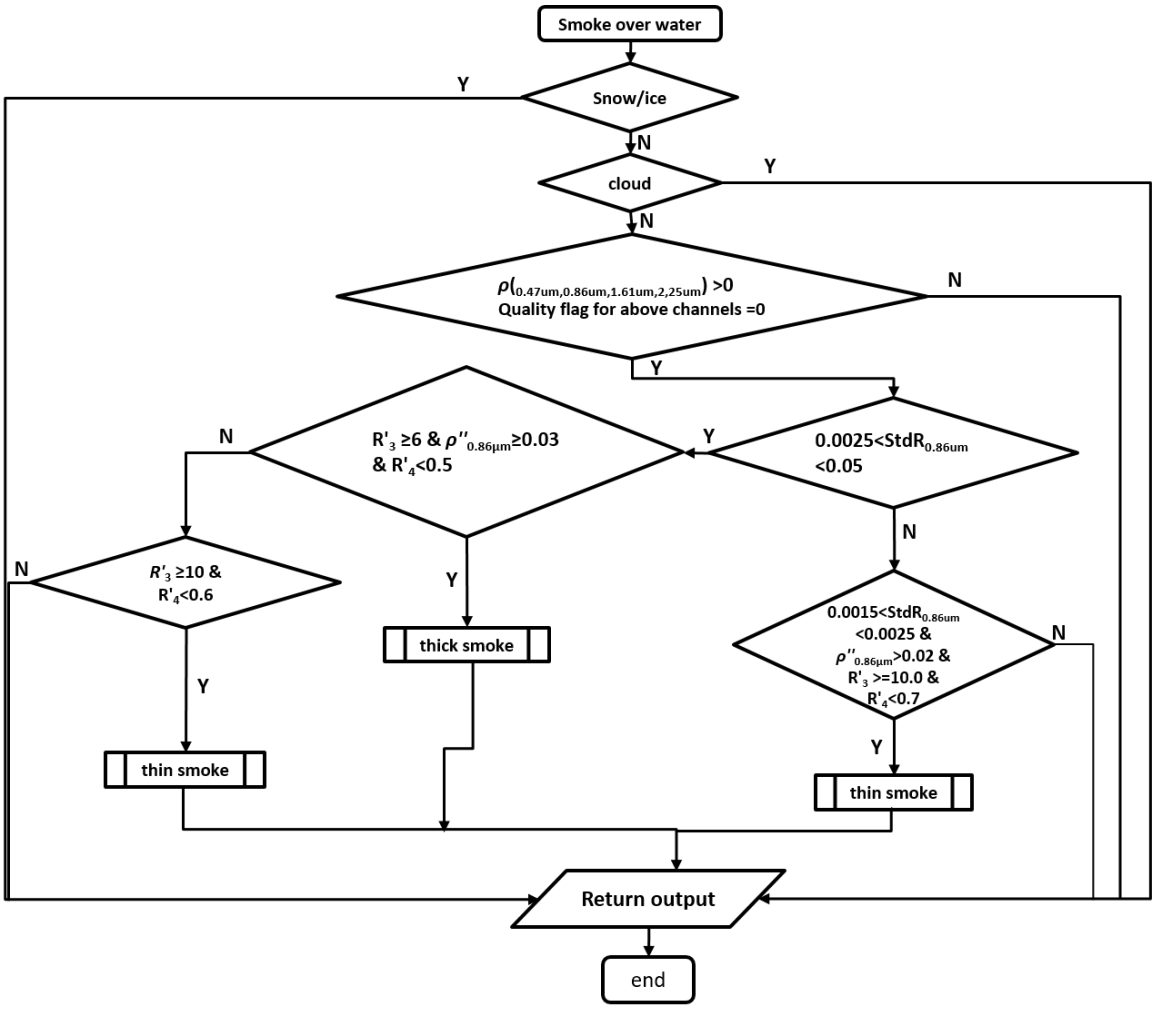

Figure 18: High level flow chart for smoke detection over water.

Figure 18 is a high level flow chart of the algorithm to detect the presence of smoke over water during daytime. The tests are not performed in the presence of ice clouds and sea/ice.

The specific tests as currently implemented sequentially are

1) Test for the presence of snow/ice by using primary snow/ice mask, and if the primary is not available, then using secondary snow/ice mask. After that, internal sea ice test is applied. Test for the presence of clouds relies on the diagnostic tests in ABI cloud mask. Pixel is considered to be obscured by clouds if any of these three cloud mask tests in Table 13, i.e. pCiirus1, pCirrus2 and pCirrus3, is true. Any pixel with positive snow/ice/cloud mask is not processed. And, cloud flag or snow/ice flag is set as 1, correspondingly.

2) Test for the quality of the input radiance data

- $\rho_{0.47\mu m}$, $\rho_{0.86\mu m}$, $\rho_{1.61\mu m}$, $\rho_{2.25\mu m} > 0$
- ABI quality flags for above channels equal to zero, indicating quality of the data is assured.

If good data test passed then the process precede, otherwise process is terminated and smoke quality flag is set as a value of 3, indicating bad data.

3) Uniformity test

- If $0.0025 \leq StdR_{0.86\mu m} \leq 0.05$, then thick smoke determination test
- If $0.0015 \leq StdR_{0.86\mu m} < 0.0025$, then thin smoke determination test

2.1). Thick smoke determination test

- If $R_3' \geq 10.0$ and $R_4' < 0.6$, then thin smoke (1)
- If $\rho''_{0.86\mu m} > 0.03$ and $R_3' \geq 6.0$ and $R_4' < 0.5$, then thick smoke

2.2). thin smoke determination test

- If $\rho''_{0.86\mu m} > 0.02$ and $R_3' \geq 10.0$ and $R_4' < 0.7$, then thin smoke (2)

4) Set smoke flag

$\rho''_{0.86\mu m}$ is the TOA reflectance at 0.86μm ($R_{0.86\mu m}$) corrected for Rayleigh scattering, i.e. $\rho''_{0.86\mu m} = \rho_{0.86\mu m} - \rho'_{0.86\mu m}$, with $\rho'_{0.86\mu m}$ as the reflectance from Rayleigh scattering at 0.86 μm. R_3' and R_4' are defined as follows:

$$R_3' = \frac{\rho_{0.47\mu m} - \rho'_{0.47\mu n}}{\rho_{1.61\mu m} - \rho'_{1.61\mu m}} \qquad R_4' = \frac{\rho_{2.25\mu m} - \rho'_{2.25\mu n}}{\rho_{1.61\mu m} - \rho'_{1.61\mu m}}$$

$\rho'_{1.61\mu m}$ is the reflectance from Rayleigh scattering at 1.61μm, $\rho'_{2.25\mu m}$ is the reflectance from Rayleigh scattering at 2.25μm

3.5.2.13 Determination of quality and confidence flags

For any pixel detected as smoke pixel, its quality flag is defined by three confidence levels. The approach to determine confidence value for each test is the same as that described in section 3.5.2.3.1. Details for determination confidence level for dust over land are given as follow:

1. Thick Smoke (1) as shown in section 3.4.2.5

Test1: $R_3' > 6.0$

$$con\_value = con_{value(Test1)}$$

If con_value<=0.25 confidence level=low
If con_value>0.25 &<0.75 confidence level=medium
If con_value>=0.75 confidence level=high

2. Thin Smoke (1) as shown in section 3.4.2.5

   Test1: $R_3' \geq 10.0$
   Test2: R_4' <0.6

$$con\_value = \frac{\left[con_{value(Test1)} + con_{value(Test2)}\right]}{2.0}$$

   If con_value <=0.25 confidence level=low
   If con_value >0.25 &<0.75 confidence level=medium
   If con_value>0.75 confidence level=high

3. Thin smoke (2) as shown in section 3.4.2.5

   Test1: $R_3' \geq 6.0$
   Test4: R_4'<0.5

$$con\_value = \frac{\left[con_{value(Test1)} + con_{value(Test4)}\right]}{2.0}$$

   If con_value<=0.25 confidence level=low
   If con_value>0.25 &<0.75 confidence level=medium
   If con_value>=0.75 confidence level=high

Note that, the confidence level is also determined by the solar/viewing geometry, i.e., for a pixel detected as smoke, its confidence level is as:

If SZA>60 or VZA>70 confidence level=low

For GOES-17, final pixel level confidence level is set as bad due to FPM temperature anomaly if DQF for any one of these channels, i.e., Band 7, Band 11 and Band 12 has a value of 4.

3.5.2.14 Example result – smoke over water

The results of applying the smoke test over water to Terra MODIS data on October 28, 2003 at 18:25 UTC is shown in Figure 19. Smoke over the coast of California, due to a fire in the dry season, is detected. The detected coverage of the smoke is very similar to the pattern in the RGB image, indicating the success of the EPS ADP algorithm. Another example is given in Figure 20, which shows the application of the EPS ADP algorithm to GOES-16 ABI observations on March 24, 2018 at 16:47 and 20:17 UTC. The detected smoke plumes in ADP for a smoke event over the Gulf of Mexico, close to Florida, are very similar to these shown in the RGB images.

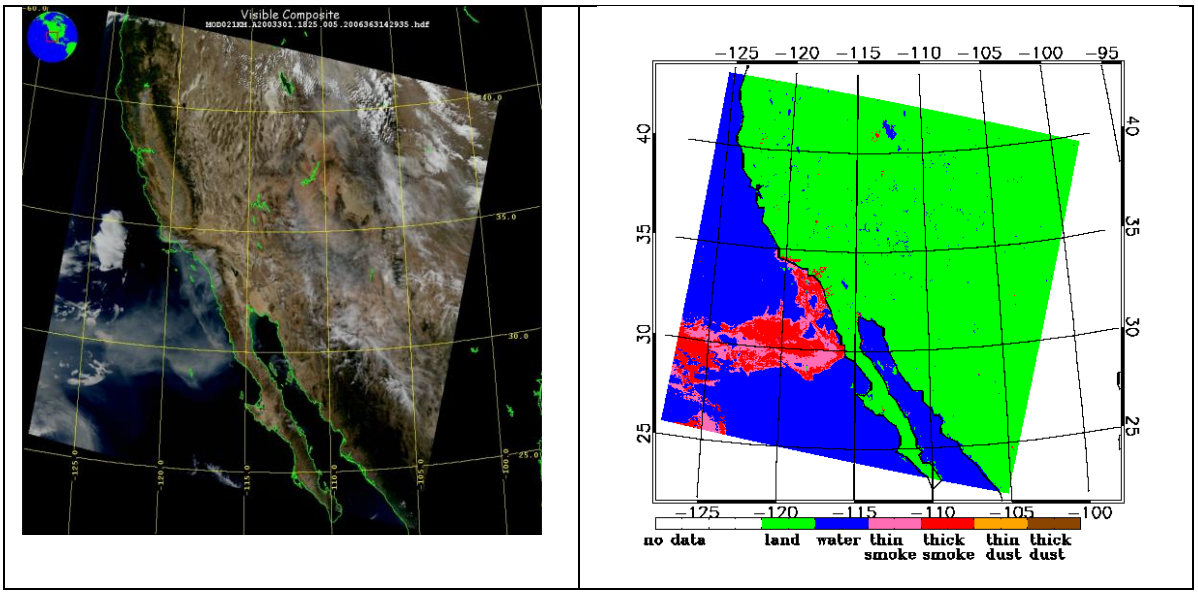

Figure 19. Terra MODIS Terra true color image on October 28, 2003 at 18:25 UTC (left) and the corresponding results of ADP smoke test (right).

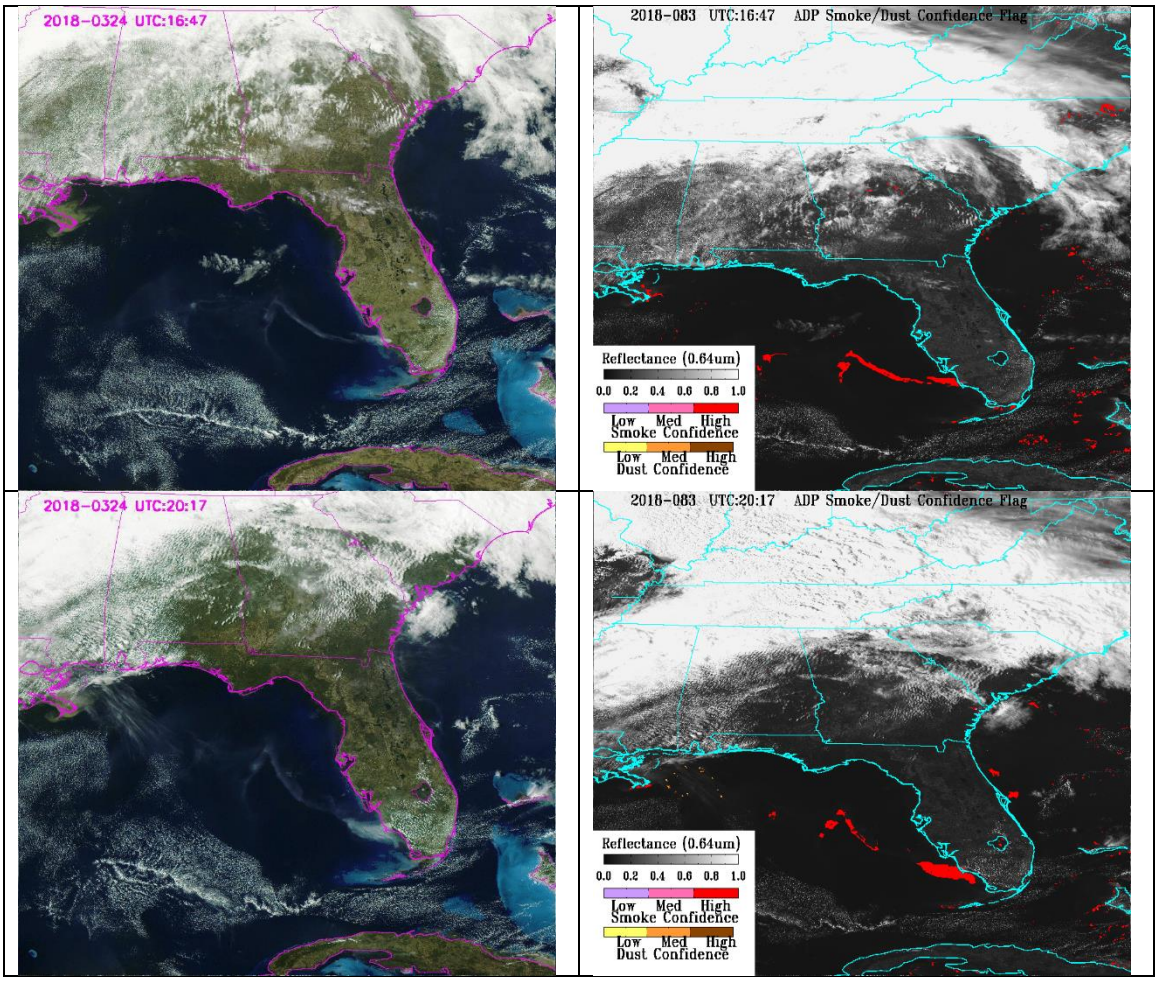

Figure 20. GOES-16 ABI GeoColor imagery on March 24, 2018 at 16:47 UTC and 20:17 UTC (left) and the corresponding results of ADP algorithm (right).

3.5.3 **Noise reduction in smoke/dust detection**

Smoke/dust events are usually larger than several ABI pixels. To reduce noise that can occur from detection of smoke or dust in a single pixel, buddy checks are applied after the steps described in the previous sections. For smoke pixels, the buddy check is performed for surrounding pixels in a 3 x 3 box. If the number of pixels detected as smoke in this box is < 5, then the detected smoke is considered noise, and the corresponding smoke flag is reversed from 1 to 0, and the corresponding confidence flag is changed to as a default value, i.e., 0. The same buddy check procedure is applied to dust pixels which is identified as dust.

In addition, to reduce the contamination from pixels which contain melting snow/ice or are covered partially by snow/ice, and are thus usually missed by the snow/ice mask, snow/ice adjacency tests are performed. These tests are performed for all pixels identified as snow/ice by the snow/ice mask. If a pixel is identified as snow/ice by the snow/ice mask, then the smoke/dust flag in all surrounding pixels in a 3 x 3 box is set to 0, and the corresponding confidence flags are set to the default value of 0.

3.5.4 **Algorithm Output**

The final output of EPS ADP algorithm includes a binary (yes/no) detection mask for smoke, dust, volcanic ash (currently is set as 0), clouds, snow/ice and none/unknown/clear (NUC). The full set of output variables are listed in Table 2, and the corresponding data quality flags as shown in Table 3.

4 PRELAUNCH TEST DATASETS AND OUTPUTS

4.1 Proxy Input Data Sets and Validation Data

4.1.1 **Input Datasets**

The MODIS sensor flying on NASA's Aqua and Terra satellites has 36 spectral bands measuring wavelengths from the visible to infrared with spatial resolution of 250 m to 1 km. The MODIS cloud mask is part of the MODIS Cloud Product [*Ackerman et al.*, 1998, 2008; *Frey et al.*, 2008; *King et al.*, 2003; *Platnick et al.*, 2003]. Because MODIS has nearly all of the same channels as ABI, MODIS provides an optimal source of data for testing the EPS ADP algorithm (Table 9).

The disadvantage of MODIS is its lack of temporal coverage compared to ABI. During the GOES-16 pre-launch period, a total of 146 cases (MODIS granules; 80 for dust and 66 for smoke) were used for testing the performance of EPS ADP algorithm (version 3.0). No simulated ABI data with aerosols were available during the pre-launch period.

MODIS Level 1b 1 km radiance data were obtained from NASA Level 1 and Atmosphere Archive and Distribution System (LAADS, http://ladsweb.nascom.nasa.gov/). Visible channel reflectances were normalized to the overhead sun position by dividing with the SZA. For the IR channels, radiances were converted to brightness temperatures. Viewing and illumination geometry and geo-location are from the MOD/MYD03 product. Various cloud tests used in the EPS ADP algorithm are extracted from the corresponding bits in the MODIS cloud mask product (MOD/MYD35). The snow/ice mask from MOD/MYD35 is used as the primary source of the snow/ice mask. The land/water mask is also from MOD/MYD35. Both the sun glint mask and the day/night flag are internally calculated as described in section 3.12.

4.1.2 **Verification data**

4.1.2.1 **Supervised MODIS RGB image and MODIS Aerosol optical depth product**

Both smoke and dust have a distinctive signature in RGB image, and NASA Natural Hazard system (http://earthobservatory.nasa.gov/NaturalHazards/) and MODIS rapid response system (http://rapidfire.sci.gsfc.nasa.gov/gallery/) routinely issues MODIS observations containing the smoke and dust outbreaks around the globe. By selecting granules which are dominated by either only smoke or only dust, a supervised truth dataset were obtained. Then the corresponding Aerosol Optical Depth (AOD) product is used to identify the smoke/dust laden (AOD>0.2) and smoke/dust free (0.2>AOD>0.0) pixels; Note that, the traditional MODIS AOD product over land only covers

dark dense vegetation surface. However, MODIS deep blue AOD product on AQUA provides AOD coverage on bright surface such as over desert. MODIS pixels with no AOD retrievals are considered as covered by clouds or snow/ice, bright surface over land and bad input data. These conditions are consistently unfavorable for detection of smoke/dust as well as discussed in Section 3. In addition, due to the difference in cloud screening procedures between MODIS AOD product and EPS ADP algorithm, only pixels with both MODIS AOD product and ADP indicating cloud-free conditions are used for quantitative analysis.

4.1.2.2 **CALIPSO VFM product**

With the launch of CALIPSO and CloudSat in the EOS A-Train formation in April 2006, the ability to conduct global satellite cloud product validation increased significantly. Besides cloud type, CALIPSO also identifies aerosol types including smoke and dust. The CALIPSO Vertical Feature Mask (VFM) is used for validating the ABI EPS ADP. The VFM provides the vertical distribution of aerosol layer and also six types of aerosol, including clean marine, dust, polluted dust, polluted continental, clean continental, polluted dust and smoke. However, the sparse spatial coverage and narrow swath of CALIPSO observations limits the amount of match-up overpasses with MODIS for smoke and dust cases. From 2006 to 2010, about 48 match-up cases were found with CALIPSO passing through the smoke/dust plumes. Among them there are 22 smoke cases and 26 dust cases.

4.2 Output from simulated/proxy data sets

4.2.1. Output for Dust Detection

4.2.1.1 **Comparison with RGB image and AOD product**

Supervised RGB images can capture dust events very well since dust plumes look brown in the image compared to white clouds. Thus, RGB imagery can be used to validate the dust detection in the EPS ADP algorithm by applying the algorithm to MODIS measurements of a dust event and comparing the detection result with the MODIS RGB image. One example is shown in Figure 21 for April 7, 2007 at 07:30 UTC. Qualitative comparison of dust detection shows good agreement with the MODIS RGB image.

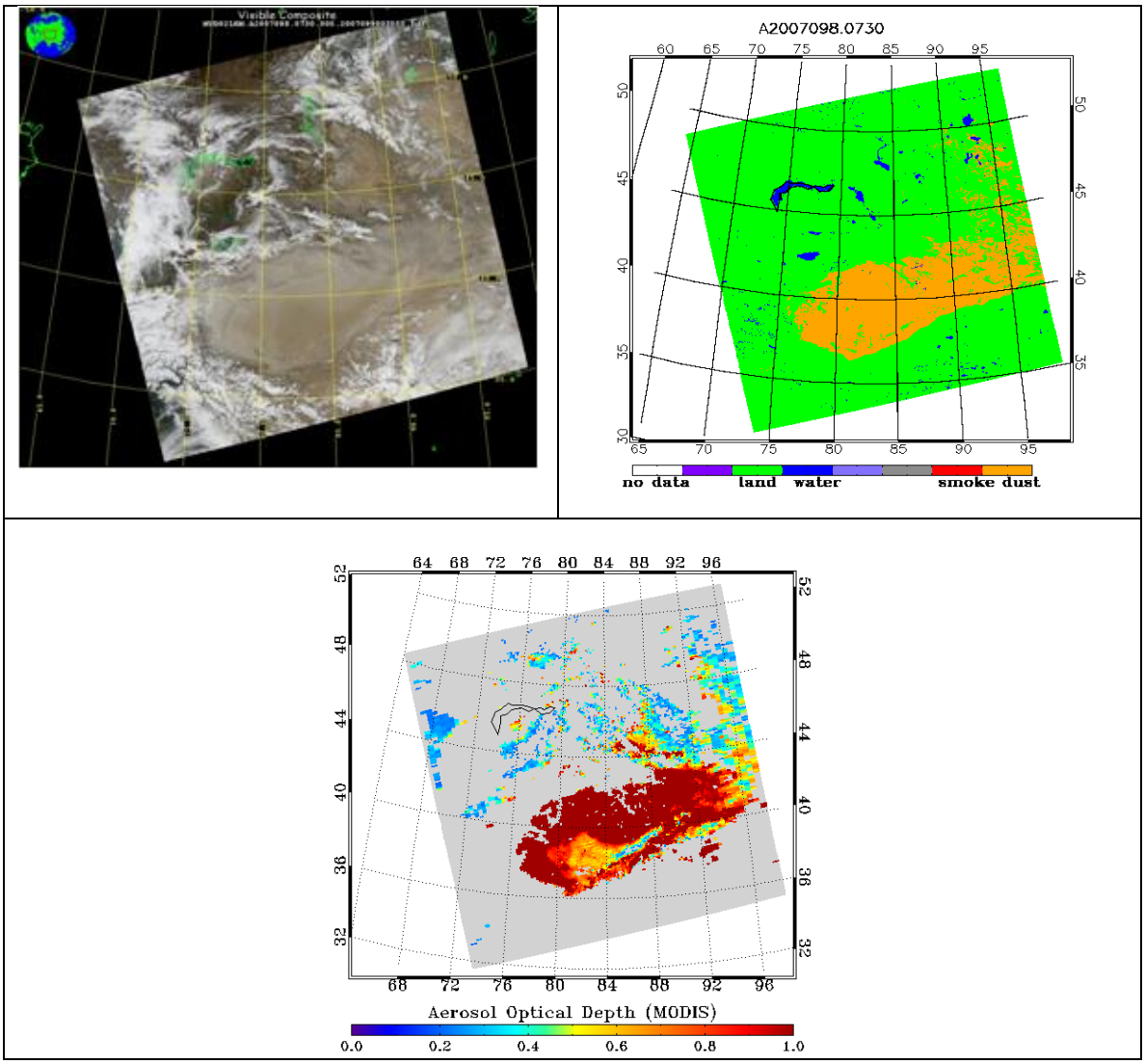

Figure 21. Terra MODIS RGB image on April 7, 2007 at 07:30 UTC (top left); the results of the dust detection (top right); MODIS AOD (only pixels with AOD > 0.2 are shown)(bottom).

Dust particles are mainly located near desert regions and downwind areas and a dust event is mainly associated with high aerosol optical depth (AOD) so that the AOD distribution retrieved from satellite observation can help us to qualitatively examine the ADP dust detection algorithm.

4.2.1.2 **Comparison with CALIPSO VFM**

CALIPSO is part of the same A-Train as MODIS Aqua and its VFM products provide vertical distribution of 6 aerosol types, including smoke and dust over its narrow (about 300 meters) track. Although the sparse spatial coverage of CALIPSO LIDAR observations limits the number of overpass matchups with MODIS Aqua granule, several cases containing dust outbreak were found. And the possibility of using the MODIS and CALIPSO overpass and the CALIPSO aerosol type data to validate the ADP dust detection is explored.

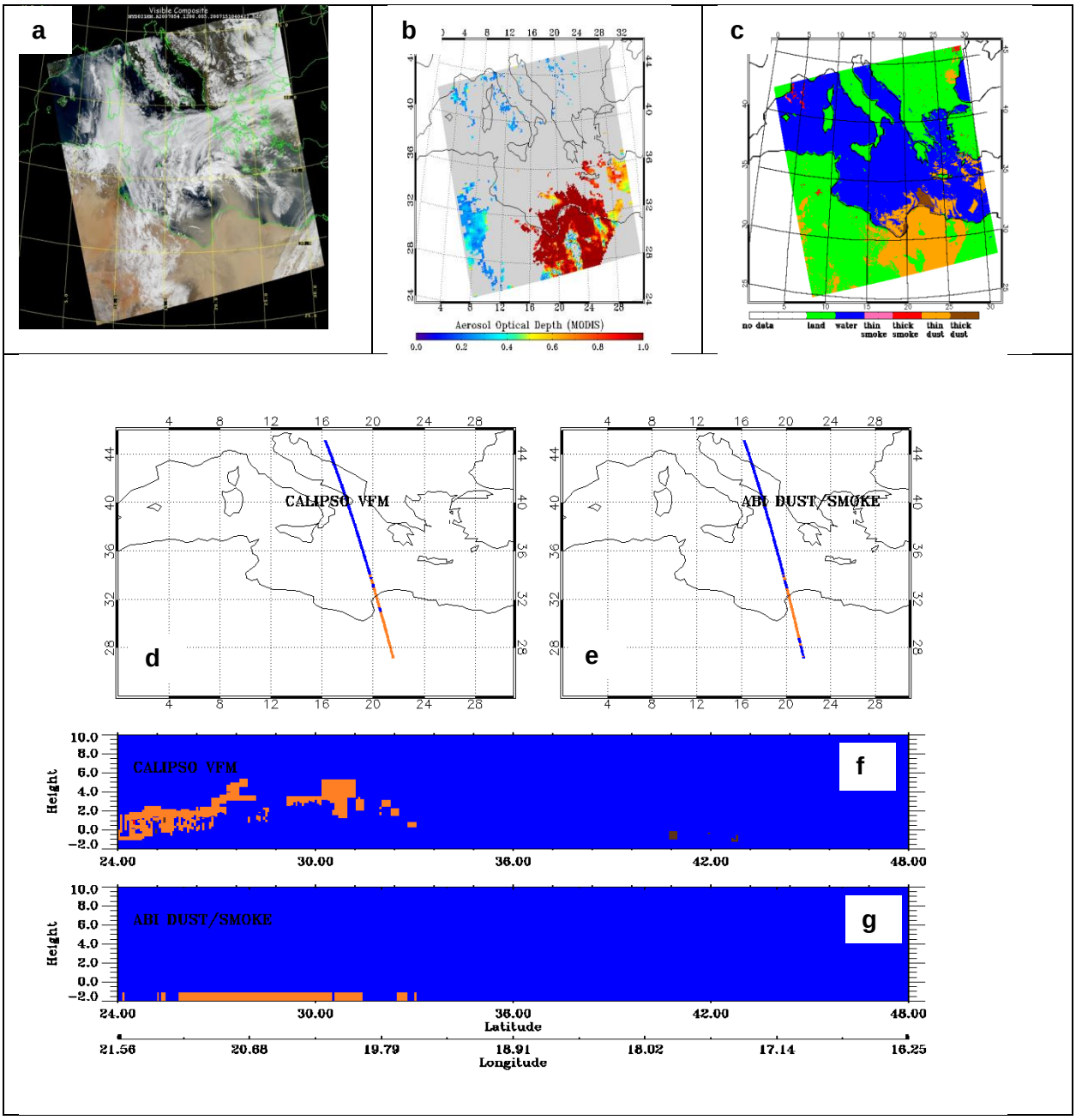

Figure 22. Comparison of dust detected (orange) using ABI ADP algorithm with CALIPSO Vertical Feature Mask (VFM) on February 23, 2007, at 12:00 UTC. a) RGB image, b) Aerosol Optical depth from MODIS C5 aerosol Product, c) Dust mask from ADP, d) Dust (orange) on CALIPSO track, e) Dust (orange) detected with ABI ADP algorithm on CALIPSO track, f) Dust vertical distribution on the part of CALIPSO track collocated with ABI ADP, g) Dust from ABI ADP on the same part of track as in b.

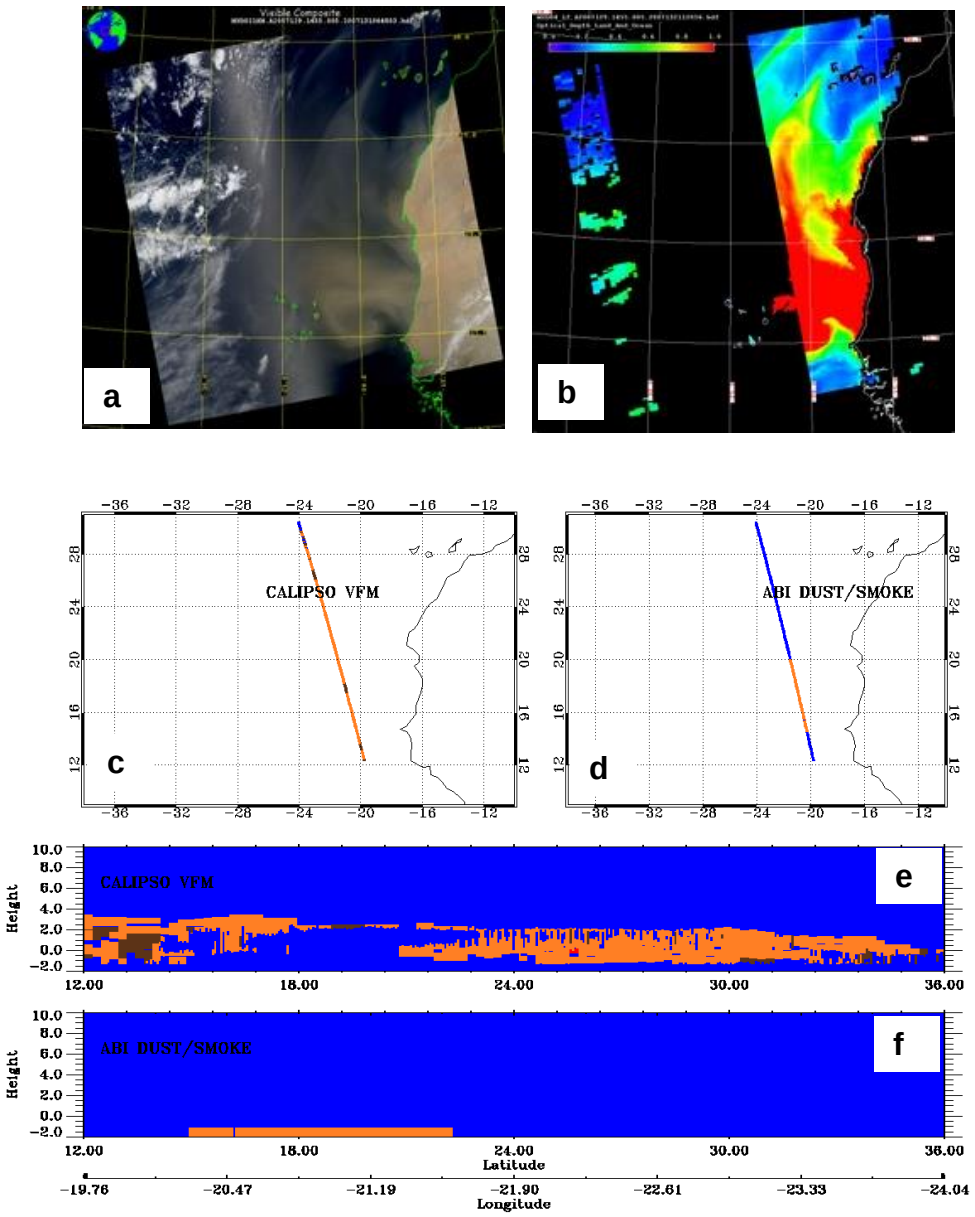

Figure 23. Comparison of dust detected (orange) using ABI ADP algorithm with dust (orange) and polluted dust (brown) in CALIPSO Vertical Feature Mask (VFM) on May 09, 2007 at UTC 14:55. a) RGB image, b) Aerosol Optical depth from MODIS C5 aerosol Product, c) Dust (orange) on CALIPSO track, d) Dust (orange) detected with ABI ADP algorithm on CALIPSO track, e) Dust vertical distribution on the part of CALIPSO track collocated with ABI ADP, f) Dust from ABI ADP on the same part of track as in b.

First example is shown in Figure 22 for CALIPSO VFM vs. ABI ADP for the Aqua MODIS image on February 23, 2007 at 12:00 UTC. The dust plume is clearly visible in the RGB image. As shown in Figure 22 (d) and (e), the CALIPSO VFM indicates the existence of dust over the initial part of the CALIPSO track, which has collocations with MODIS; the dust is seen starting from the surface of Libyan Desert and becoming elevated over the sea. The ABI ADP dust mask over the

co-located CALIPSO track is given in Figure 22c. The CALIPSO VFM shows that dust was dispersed between the surface and 2 km (Figure 22g). There is good agreement between the dust plume pattern detected by ADP and the pattern shown in MODIS RGB and AOD. Similar good agreement is seen with the CALIPSO VFM track. According to the definition of accuracy (correct aerosol detection) shown in equation in 4.31, the agreement between ABI ADP and CALIPSO VFM is 85%.

The co-located overpass shown in Figure 23 between CALIPSO and MODIS is over water. It is also on the edge of a sun glint region where ABI ADP data are not processed. Therefore, by excluding pixels in the overpass within sun glint and with MODIS AOD < 0.2, the agreement between ABI ADP and CALIPSO VFM is about 81 %. For a total of 26 match-up cases for dust, the average of agreement is ~81%.

4.2.2 Output for Smoke Detection

4.2.2.1 Comparison with RGB image

Smoke is associated with fire events and the spatial distribution of smoke plumes is uniform and looks gray to a human eye compared to a white cloud, which makes smoke easy to discern in RGB imagery. Thus, RGB imagery can be used to validate EPS ADP smoke detection. An example is shown in Figure 24 for a fire event in Australia observed by Aqua MODIS on August 25, 2006 at 17:15 UTC. Qualitative comparison with the MODIS RGB image shows good agreement for smoke detection, especially for the thick smoke plumes over vegetated areas.

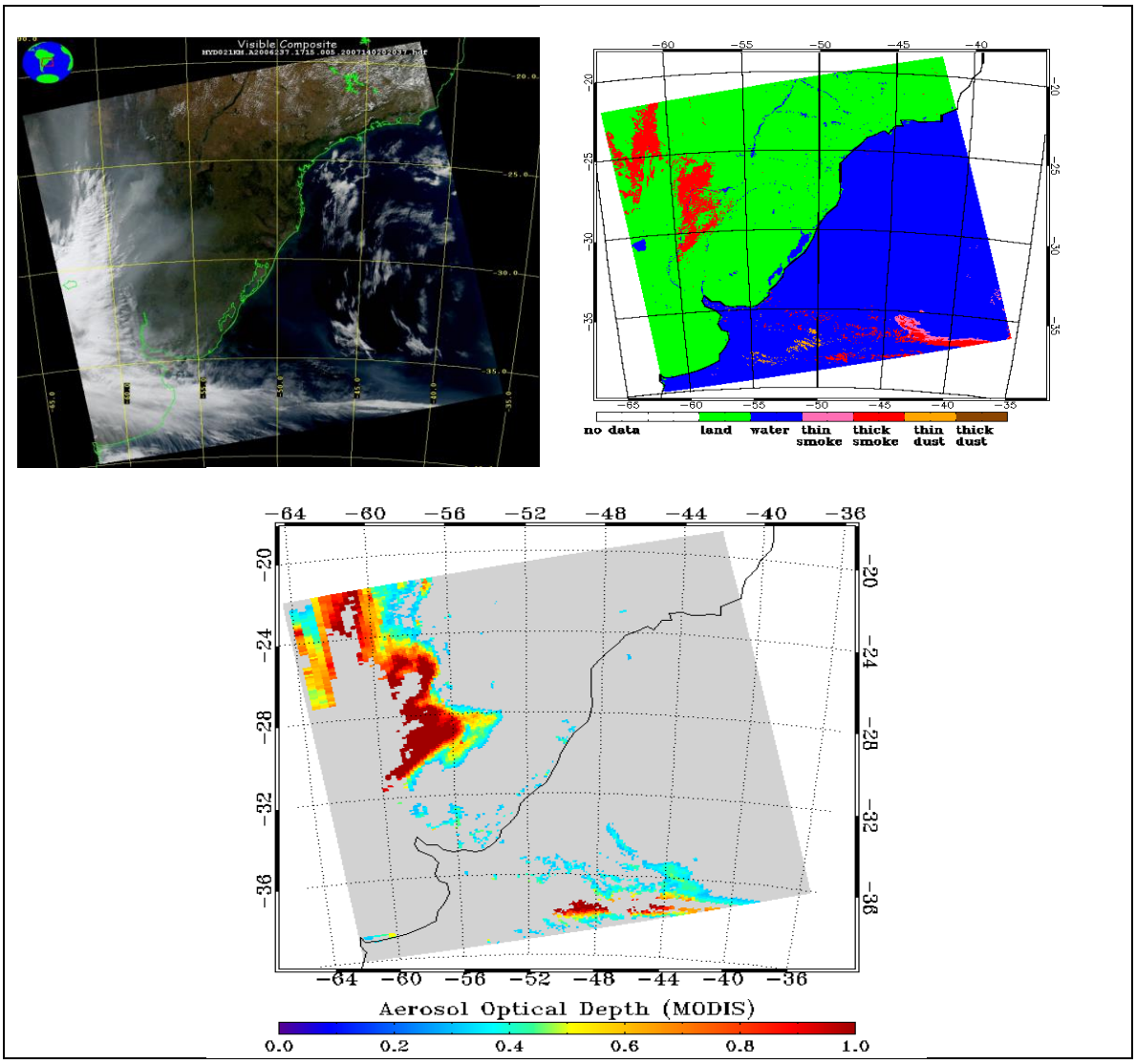

Figure 24. Aqua MODIS RGB Image on August 25, 2006 at 17:15UTC (upper left); the results of the smoke detection (pixels flagged as smoky are in colored red) (upper right); MODIS AOD (only larger than 0.2 are shown) (bottom).

In general, the AOD of the smoke plumes (shown in Figure 24) is high. Thus, AOD imagery can be used to quantitatively validate the EPS ADP smoke detection. As seen in Figure 22, AOD plumes compare well with the ADP smoke flags; the agreement is 84%.

4.2.2.2 **Comparison with CALIPSO VFM**

In Figure 25 and Figure 26, two cases of ABI ADP smoke detection are shown for two different days in different years. For both examples, the ABI smoke detection mask agrees well with MODIS RGB imagery and the matchups with CALIPSO. There are some parts of the CALIPSO track where the ABI ADP does not agree, however. The sensitivity of the ADP retrieval to the

height of the aerosol layer and aerosol amount has not been tested, and this may be the cause of the discrepancies with the CALIPSO VFM. For a total of 22 smoke cases, the agreement between ABI ADP and CALIPSO VFM is about 80%.

For smoke detection, two CALIPSO VFM vs. ABI ADP cases are presented. They are both over land on July 23, 2006 at 05:15 UTC and October 2, 2007 at 17:50 UTC (Figure 24 and Figure 25). The agreement between the ABI ADP and CALIPSO VFM is 75% and 80% respectively.

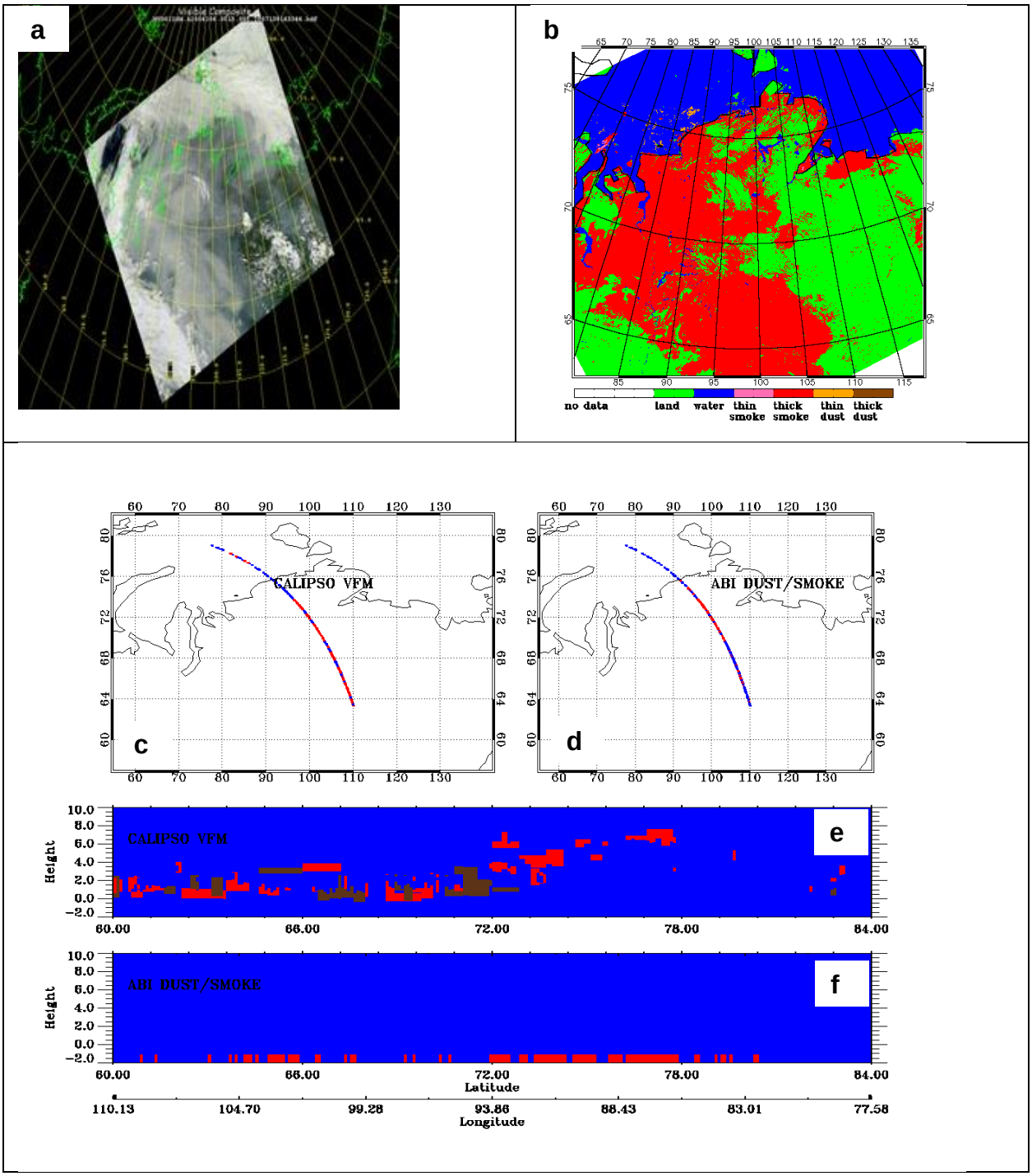

Figure 25. Comparison of smoke detected (red)) using ABI ADP algorithm with smoke in CALIPSO VFM on July 25, 2006 at 05:15 UTC. a. RGB image b. Aerosol Optical depth from MODIS C5 aerosol Product. C. Smoke (red) on CALIPSO track. d. Smoke detected with ABI ADP algorithm on CALIPSO track. e. Smoke vertical distribution on the part of CALIPSO track collocated with ABI ADP d. smoke from ABI ADP on the same part of track as in b.

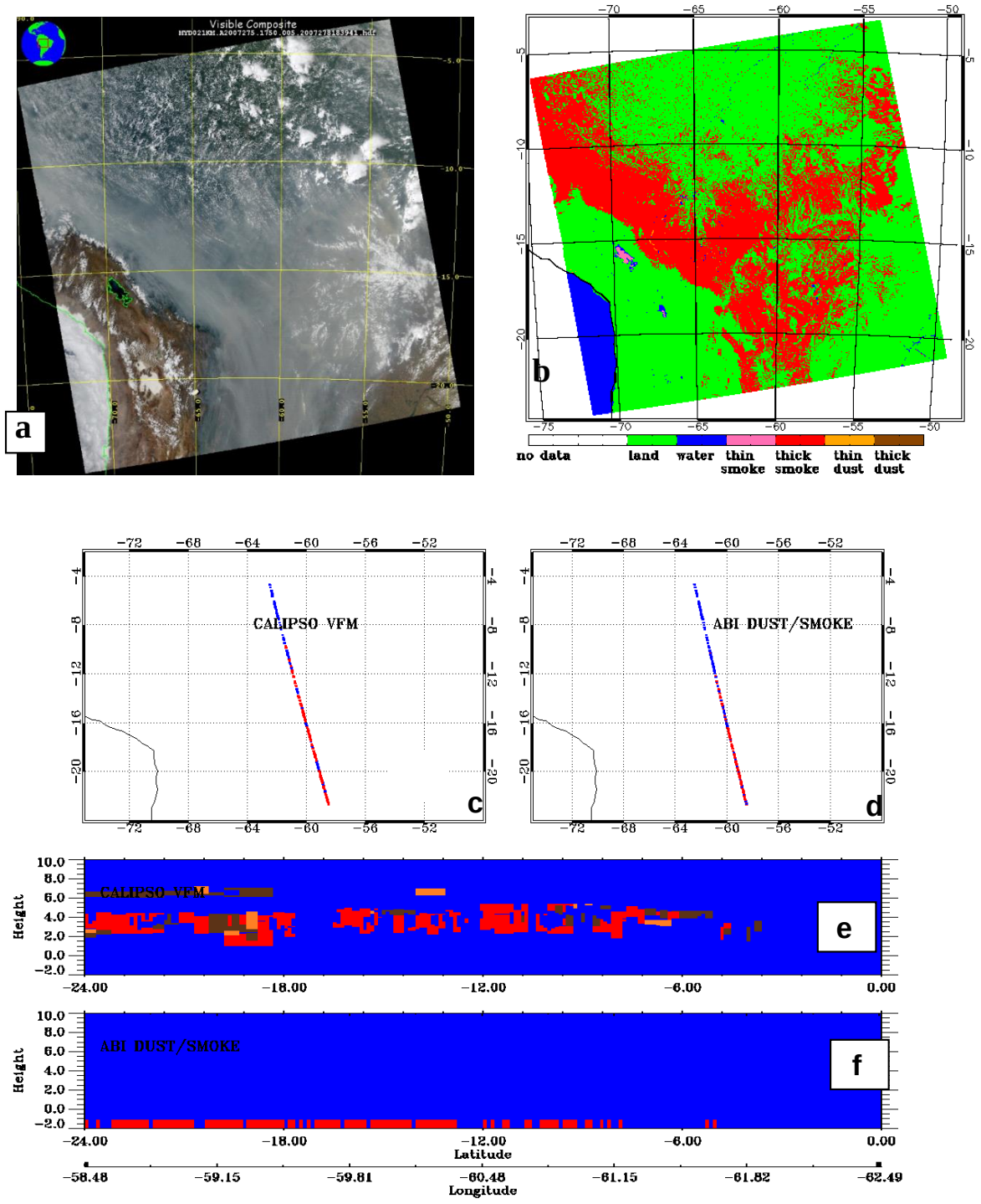

Figure 26. Comparison of smoke detected (red) using ABI ADP algorithm with smoke in CALIPSO Vertical Feature Mask (VFM) on October 2, 2007 at 17:50 UTC. a) RGB image, b) Aerosol Optical depth from MODIS C5 aerosol Product, c) Smoke (red) on CALIPSO track, d) Smoke detected with ABI ADP algorithm on

CALIPSO track, e) Smoke vertical distribution on the part of CALIPSO track collocated with ABI ADP, d) smoke from ABI ADP on the same part of track as in b.

4.2.3. Correct Detection (Accuracy) Estimates

Due to lack of ground truth for the accuracy estimate, the evaluation of ADPs is mainly based on the inter-comparison to other satellite based smoke and dust products (such as RGB image, HMS smoke analysis, and CALIPSO VFM product). As mentioned before, the correct detection (Accuracy) estimates are semi-quantitative.

Correct detection = (TPD + TND) / (TPD+FPD+TND+FND) (4.3.1)

In equation 4.3.1, TPD is true positive detection, TND is true negative detection, FPD is false positive detection, and FND is false negative detection. The primary validation approach will provide an overall performance of the algorithm but will not provide information on performance of the algorithm over different geographic regions. Therefore, additional spot checks and statistics will be carried out.

Because accuracy of aerosol detection calculated using equation 4.3.1 will include true negative detects (clear sky pixels), it will not provide information on the true positive detects which a user might be interested in. Therefore, probability of correct positive) detection (POCD and false alarm ratio probability of false positive detection (POFD) are computed using equations 4.3.2 and 4.3.3:

$$POCD = \frac{\text{TPD}}{(\text{TPD}+\text{FND})} * 100.0 \quad (4.3.2)$$

$$POFD = \frac{\text{FPD}}{(\text{FPD}+\text{TPD})} * 100.0 \quad (4.3.3)$$

As discussed in section 4.2, two types of validation data are used: supervised MODIS RGB/AOD and CALIPSO VFM. By collocating outputs from the ABI ADP algorithm run with MODIS measured radiances used as proxy with these two types of validation data, statistics on correct detection, POCD, and POFD are calculated (see Table 14)

Table 14. Validation statistics for ABI EPS ADP data.

Aerosol Type	Verification Dataset	Number of Matchups	Number of Satellite Tracks	Correct Detection	POCD	POFD
Dust	CALIPSO VCM	2,031	26	81.3%	70.6%	29.4%
Smoke		5,192	22	80.5%	71.9%	28.1%
Dust over land	Supervised MODIS AOD product	688,911	54	84.5%	63.6%	36.3%
Dust over water		353,723	45	83.2%	78.5%	21.5%
Smoke over land		639,637	60	80.1%	77.3%	22.7%
Smoke over water		459,803	57	82.2%	86.4 %	13.5%

Based on these validation studies, the ABI EPS ADP algorithm meets the F&PS requirements (80% correct detection for dust over land and water, 80% correct detection for smoke over land, and 70% correct detection for smoke over water).

However, EPS ADP validation efforts are being expanded by compiling large amount of AOD and extinction data from ground-based networks such as the AERosol Robotic NETwork (AERONET) and Interagency Monitoring of Protected Visual Environments (IMPROVE). The presence of dust and smoke can be indirectly inferred from these measurements and used in the validation of the ABI EPS ADP. This work is currently ongoing and will be presented in subsequent validation documents.

4.3 Error Budget

To examine the sensitivity of the detection algorithm to the radiometric bias/noise, we perturbed the reflectances at all detection channels with a bias of -5% and a random noise of 5% and compared the results with those without the radiometric perturbation. An example of a dust case for the MODIS Aqua data on April 15, 2003 at 20:20 UTC is shown in Figure 27. After adding the radiometric noise/bias, the number of dust pixels detected is reduced by about 9.3%.

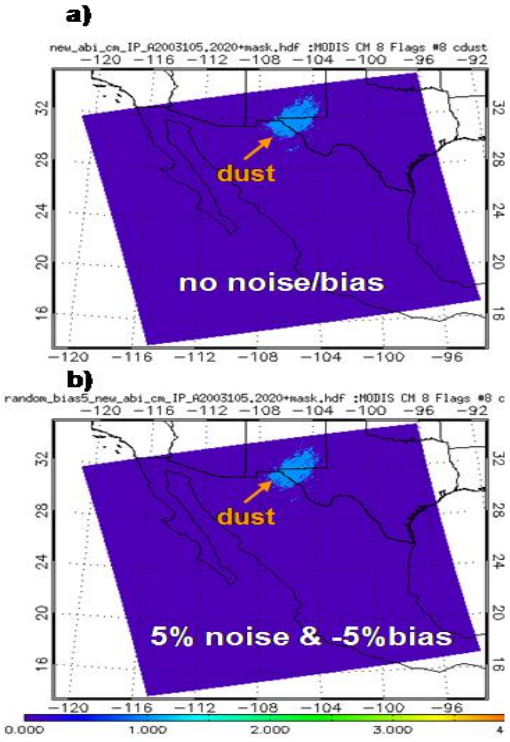

Figure 27. Comparison of dust detection before (a) and after (b) perturbation of the reflectance of the detection channels for a dust case.

An example of a smoke case for the MODIS Aqua data on August 19, 2003 at 19:00 UTC is shown in Figure 28. After adding the radiometric noise/bias, the number of dust pixels detected is reduced by about 7.6%. The impact mainly comes from the bias rather than the noise. These sensitivity tests suggest that algorithm modifications may be needed after the ABI instrument launches or instrument behavior changes from pre-launch to post-launch.

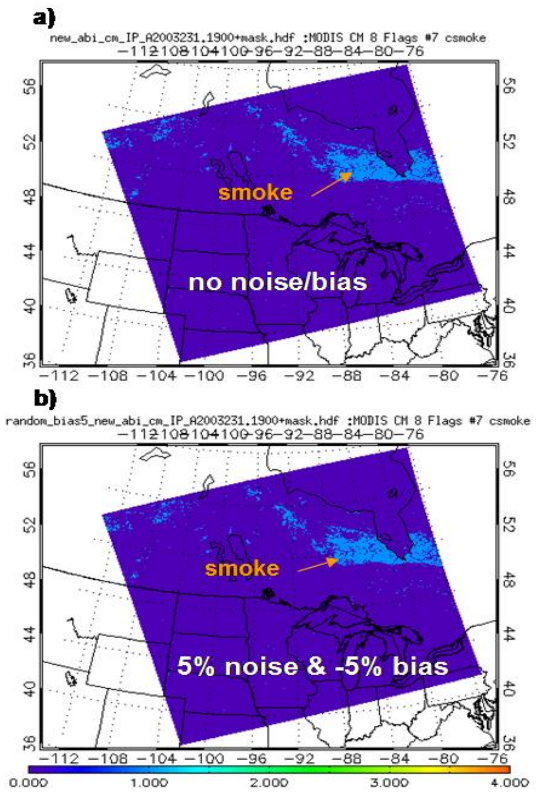

Figure 28. Similar to Figure 27 but for a smoke case of MODIS Aqua data on August 19, 2003 at 19:00 UTC.

4.3. Framework run and validation

4.4.1. Framework run

As shown in section 4.1, the EPS ADP algorithm was validated extensively. However, this validation work was done with offline runs, i.e., running the algorithm without integrating it into the GOES-R ABI product framework. In an operational environment, the EPS ADP algorithm will be running in this framework. In general, the procedure for running the algorithm in the framework is as follows: first, common input radiance data are generated from proxy data; the common dataset includes both the required input and ancillary data in a common data format, i.e., netCDF. Second, the algorithm is called according to the order of precedence. Finally, results from each product are written to an output file in netCDF format.

4.4.2. Consistency tests with MODIS granules

To test the offline runs with runs through integration of ADP algorithm into the framework, comparisons were made between outputs from offline run with outputs from framework run with common input data and using the V3 algorithm. For tests shown below, MODIS observations from two granules were used as proxy for GOES-R ABI, i.e., 1 km radiances from MODIS bands corresponding to ABI channels required by ADP algorithm and cloud mask from MODIS cloud mask product. Figure 29 and Figure 30 show the comparisons of offline smoke/dust mask with those from framework run for two MODIS granules. Framework run was able to

reproduce exactly the same results as from offline run for one granule and another one except one pixel. The difference in that one pixel is caused by the difference of precision in one of the threshold values used in the algorithm, i.e., brightness temperature of MODIS band 31 (11μm, BT11). The value of BT11 is 284.99874 in offline run and 285.000122 in framework run, while the threshold used in the smoke detection is set as 285.0.

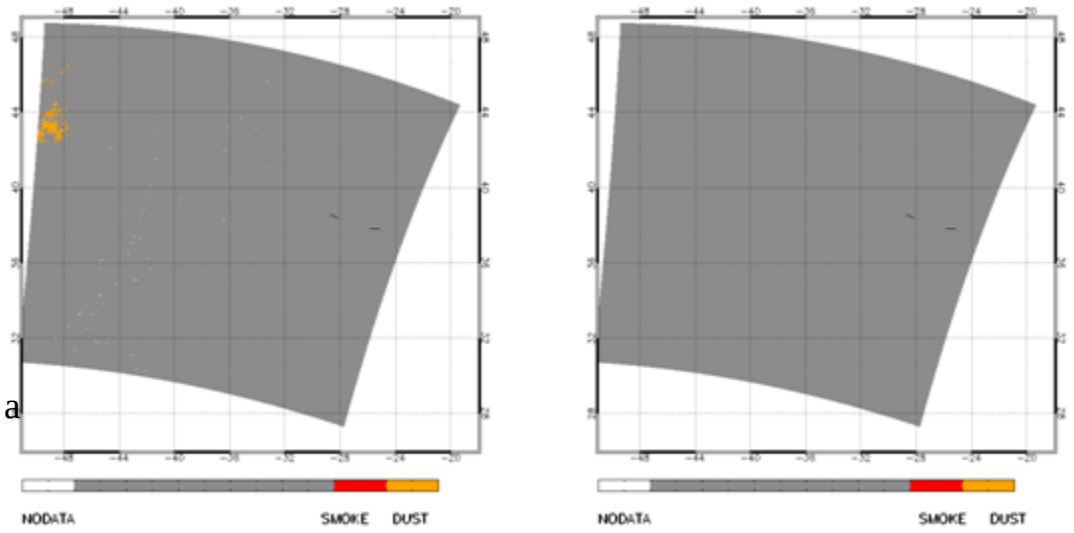

Figure 29. Comparison of the framework run (left) with the offline run (right) for Terra MODIS observations on June 4, 2005 at 13:20 UTC.

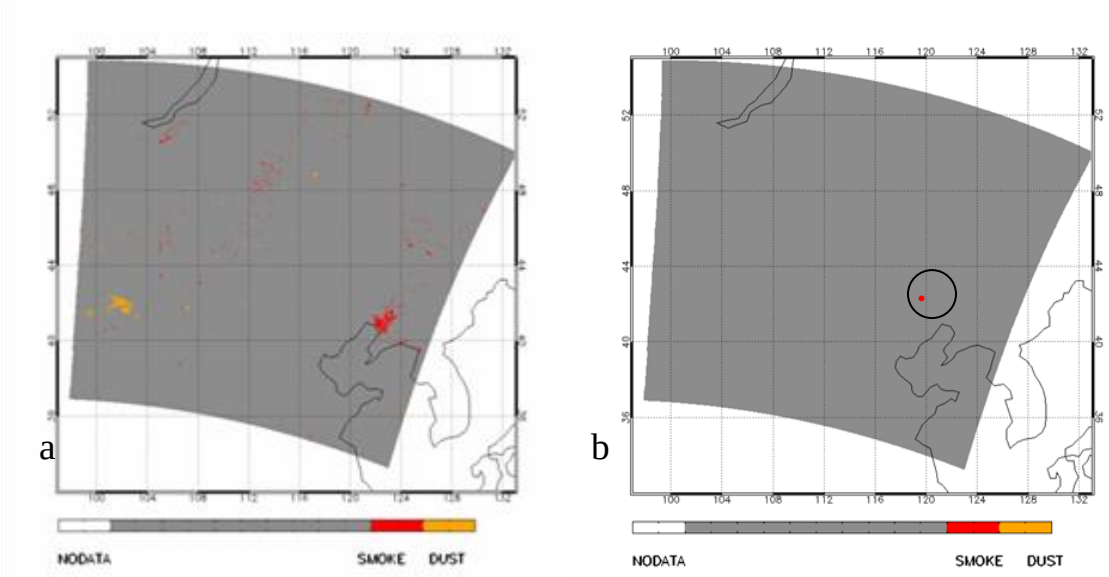

Figure 30. Comparison of the framework run (left) with the offline run (right) for Terra MODIS observations on June 4, 2005 at 03:25 UTC.

4.4.3. Results from Framework run with global MODIS observation

To further test the framework run, global MODIS (both Terra and Aqua) observations for August 24 and 25, 2006 were selected as proxy input to the ADP algorithm. Figure 31 shows global ADP from the framework run of the EPS ADP algorithm. The white shaded region is due to missing MODIS granule data. In general, the framework run produced no abnormal smoke or dust patterns for each of these two days, and consistency is seen between results from these two consecutive days. Furthermore, a large smoke plume resulting from biomass burning was identified over South America, and blowing dust is shown over the Sahara desert. Although the location of the dust and smoke plumes are consistent between the two days, there are differences in the amount of smoke and dust present. This is very typical because while old fires die out, new fires form and dust transport occurs in the free troposphere, moving it long distance over short time periods. In fact, with the current operational GOES fire and aerosol products, we know that substantial diurnal variation exists for fire duration. In addition, as shown in Figure 32 and Figure 33, ADP from the framework run has a pattern of smoke/dust that is very similar to that identified in the MODIS RGB images. These framework runs were not compared to offline runs. It should also be noted that these runs are based on the Version 3 of the EPS ADP algorithm. Framework runs using Version 5 of the algorithm for a longer time period covering several seasons are underway.

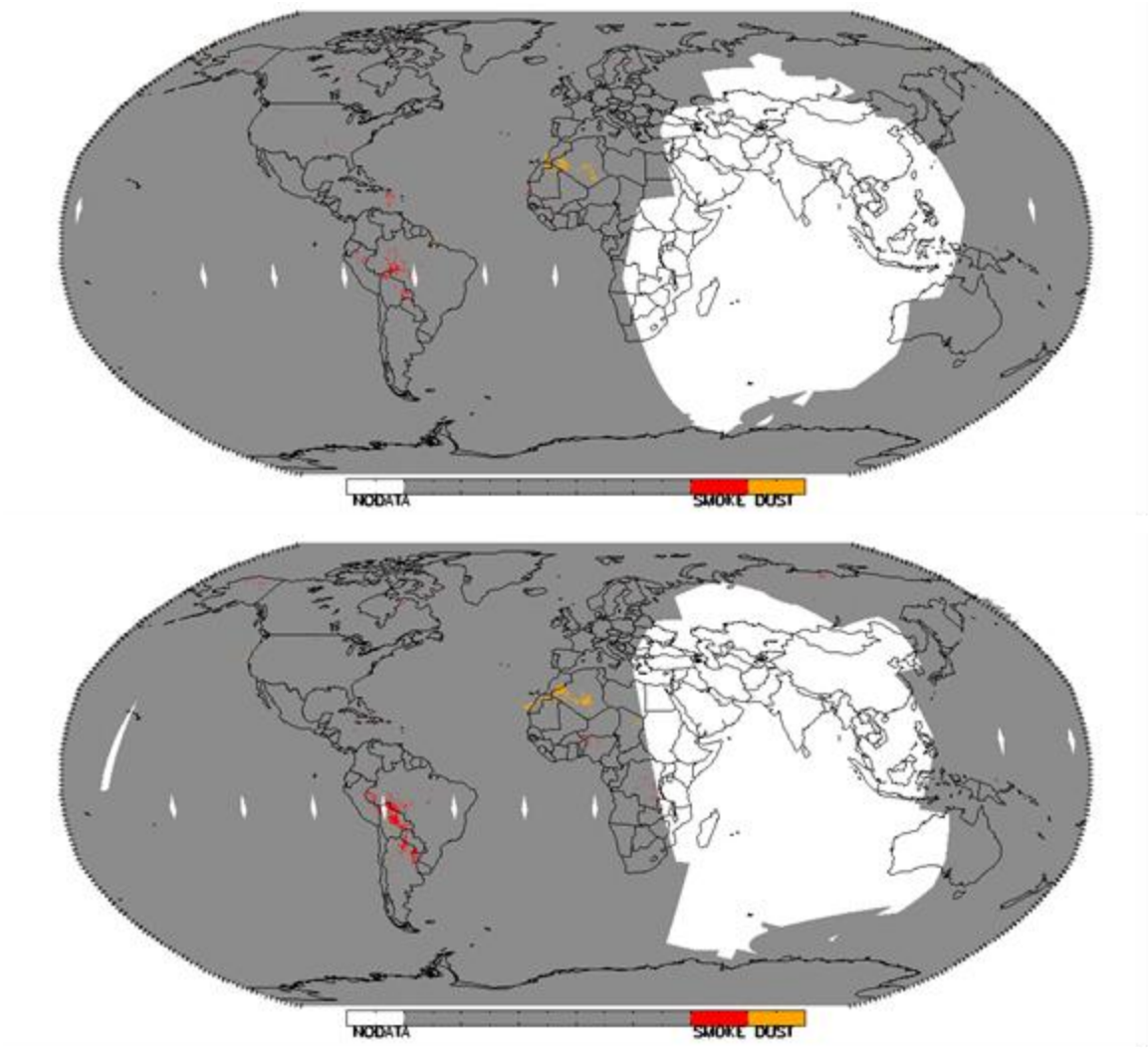

Figure 31. Global smoke/dust mask from the EPS ADP algorithm run in the framework for Aqua MODIS observations for August 24, 2006 (top) and August 25, 2006 (bottom).

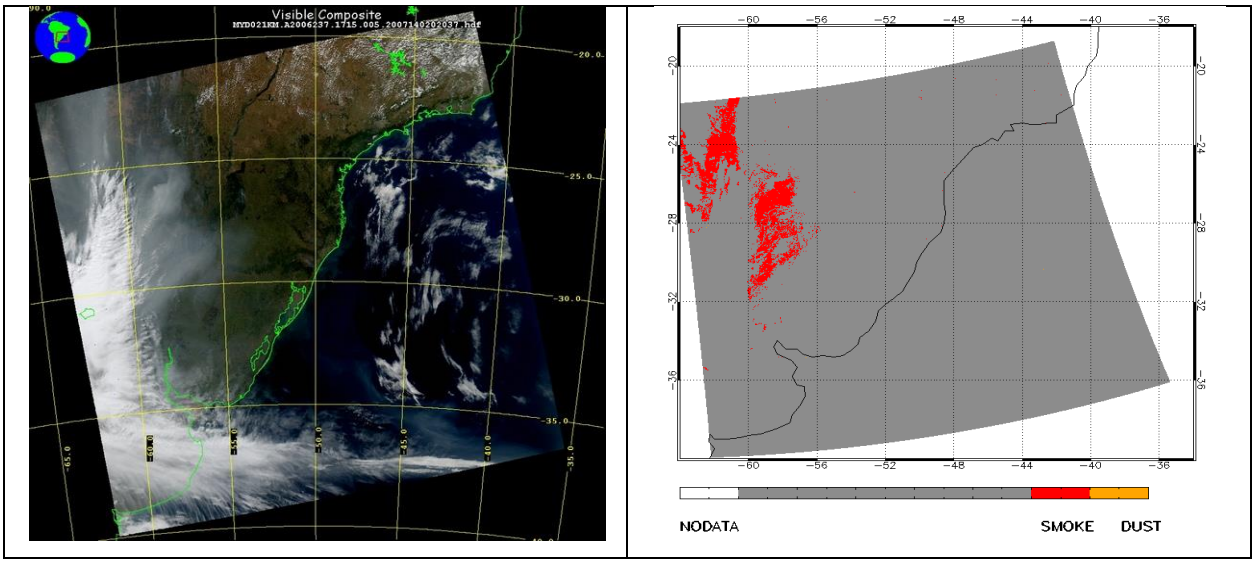

Figure 32. Smoke/dust mask from the EPS ADP algorithm run in the framework for Aqua MODIS on August 27, 2006 at 17:15 UTC. Left: MODIS RGB image; Right: ADP smoke/dust mask.

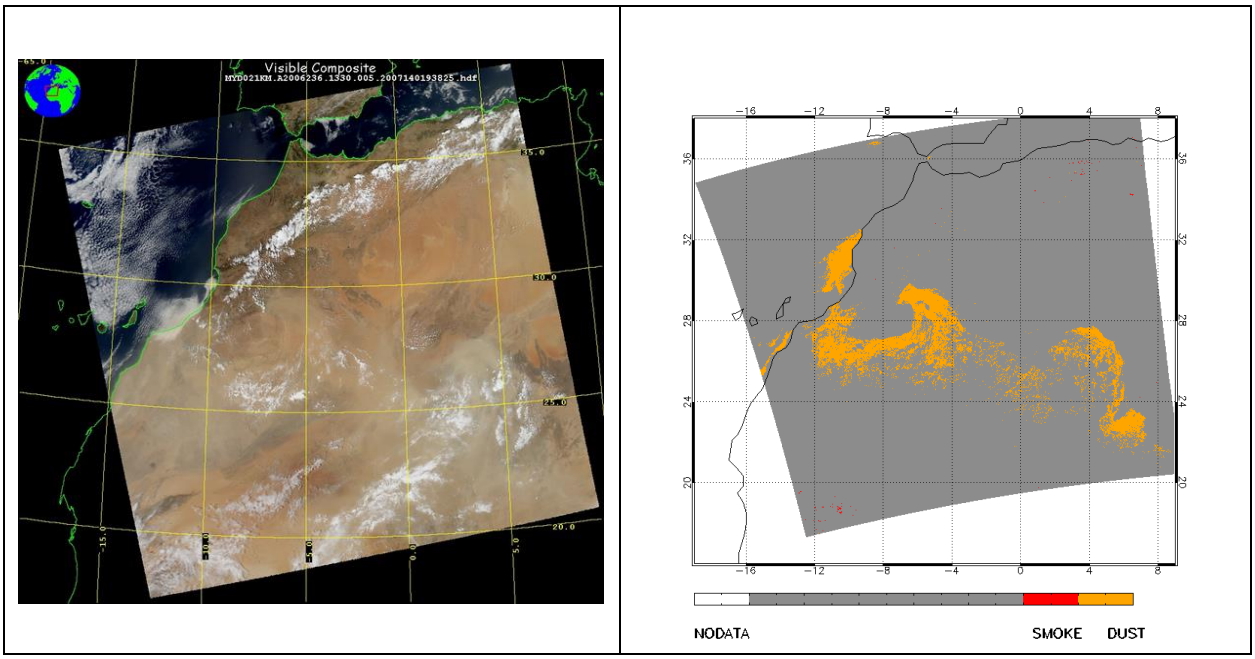

Figure 33. Smoke/dust mask from the EPS ADP algorithm run in the framework for Aqua MODIS on August 24, 2006 at 13:20 UTC. Left: MODIS RGB image; Right: ADP smoke/dust mask.

5 POST-LAUNCH TEST DATASETS AND OUTPUTS

5.1 Input Data Sets and Validation Data

5.1.1 Input data set

GOES-R was launched on November 19, 2016, and renamed GOES-16 after launch. It was positioned at 89.0 °W until December 18, 2017, when it moved to its final operational position, of 75.2 °W. GOES-16 ABI observations used in post-launch validation of the EPS ADP algorithm cover the time period from December 10, 2017 to October 31, 2018. The algorithm used to generate ADP from GOES-16 observations is the latest version as descried in this ATBD and it is the same as in ground system.

5.1.2 Truth data

The truth data and validation strategies used in post-launch validation are the same as in pre-launch validation as described in Section 4. In addition, AERONET measurements were added as another truth data for post-launch validation.

5.1.2.1 Aerosol Robotic Network (AERONET) observations

The ground-based remote sensing network, AEROsol Robotic Network (AERONET), equipped with well-calibrated sunphotometers over more than 100 sites throughout the world, measures and derives quality-assured aerosol optical properties for a wide diversity of aerosol regimes, for up to the last 10 years [Holben et al., 1998; 2001; Dubovik et al., 2002]. These high quality data have been widely used as ground "truth" for evaluation and validation of satellite remote sensing of aerosols [Yu et al., 2003; Remer et al., 2005]. As for primary source of *in situ* observations, observations from AERONET will be the primary source, since the stratification of Angstrom Exponent data from AERONET indicates the presence of smoke or dust particles in the atmosphere.

The matchup strategies are as following:

- Collocated AERONET and GOES-R ADP smoke/dust detection results
  - Spatial coverage: a circle with a radius of 25 km and centered on AERONET stations are chosen to determine the dominant aerosol type from GOES-R ADP.
  - Temporal average: AERONET measurements within a 30minutes window centered on the NPP VIIRS overpass time, at least three measurements are available.
- Dominant aerosol type from EPS ADP
  - 80% of pixels in the circle are cloud, snow/ice and glint-free (for over water)
  - The type of more than half the valid retrievals was chosen as the dominant type from EPS ADP.
- Classification of Aerosol Type over AERONET:
  - Smoke:

    AOD>0.2 and AE>1.0
  - Non-Smoke:

    AOD>0.2 and AE<0.5
  - Dust:

AOD>0.3 and AE<0.5

- Non-Dust:

AOD>0.3 and AE>1.0

5.2 Output from GOES-16 ADP

5.2.1 **Output for dust detection**

5.2.2 **Comparisons with RGB and GOES-16 AOD product**

Examples of three dust events over the U.S. are given in Figure 34, comparing the ABI synthetic RGB and ADP. The dust plume is uniform and appears yellowish in RGB compared to clouds and smoke plumes. Thus, the RGB image can be used to validate qualitatively the ADP dust detection. As all three dust example show, the spatial coverage of dust plumes, indicated in ABI ADP as yellow-orange-brown color, agree with the dust plumes shown in RGB images very well.

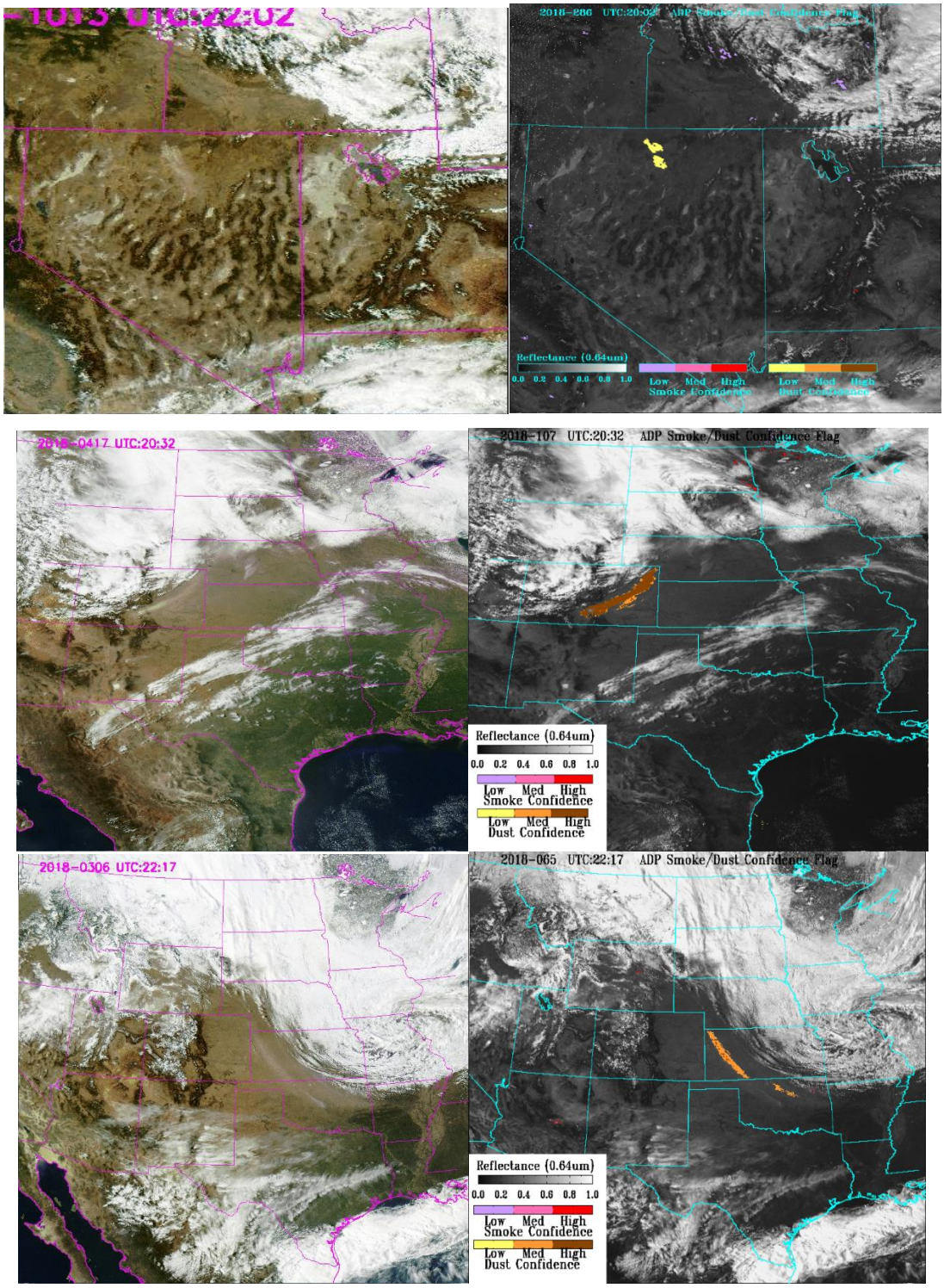

Figure 34. Comparison of ABI ADP dust detection (right) with synthetic RGB (left) from GOES-16 observations. Top row: October 13, 2018 at 23:02 UTC. Middle row: April 17, 2018 at 20:32 UTC. Bottom row: March 06, 2018 at 22:17 UTC.

5.2.3 **Comparisons with CALIPSO VFM product**

Figure 35 shows an example of ABI ADP compared to the CALIPSO VFM track for a Saharan dust transport event. The dust detected by ABI ADP is coincident with the dust shown by VFM over the part of track where there are no clouds.

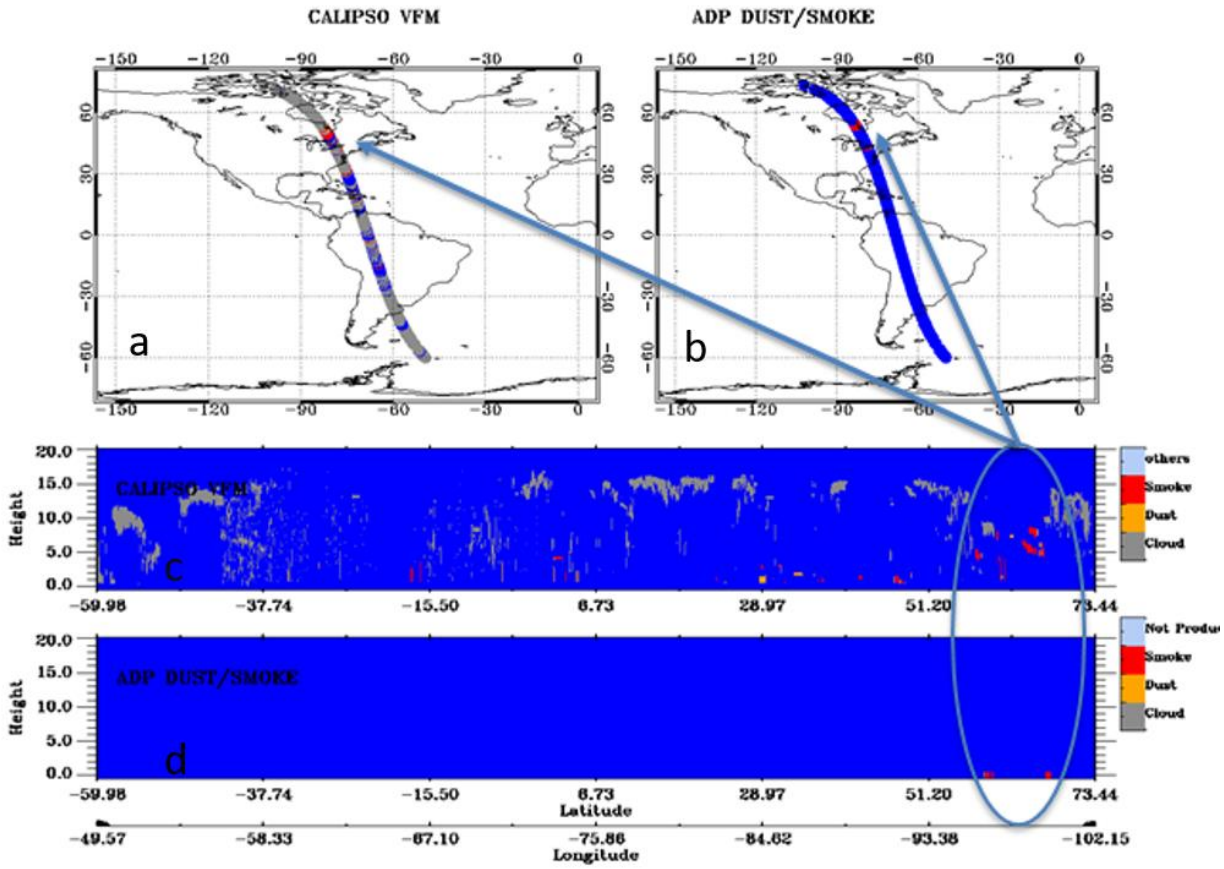

Figure 35. Comparison of dust detected (orange) using ABI ADP algorithm over GOES-16 observations on July 13, 2018 at UTC: 18:45 with dust in CALIPSO Vertical Feature Mask (VFM). a) Dust (orange) from VFM on CALIPSO track, b) Dust detected with ABI ADP algorithm over GOES-16 observations collocated on CALIPSO track, c) Dust vertical distribution from VFM on the part of CALIPSO track collocated with ABI ADP, d) dust from ABI ADP on the same part of track as in c.

To qualitatively evaluate ABI ADP, matching-ups with the CALIPSO VFM were conducted for the time period from December 14, 2017 to October 13, 2018. The corresponding statistics matrix, including accuracy, POCD and POFD, are given in Table 15. Based on the validation with CALIPSO VFM, smoke detection from ABI ADP can have an accuracy of ~99%, POCD of ~84% and POFD of ~24%.

Table 15. Verification statistics for EPS ADP.

Verification Dataset	Time Period	True Positive	False Positive	False Negative	True Negative	Accuracy	POCD	POFD
CALIPSO VFM	12/14/17-10/13/18	4612	1476	667	488,749	99.4%	87.4%	24.2%
AERONET		6540	173	883	57,439	98.5%	88.4%	2.6%

5.2.4 **Comparisons against AERONET measurements**

Dust detections by the EPS ADP algorithm run on GOES-16 ABI observations were validated with AERONET observations according to the strategies described in section 5.1.2.1 for the time periods from December 14, 2017 to October 13, 2018. The derived statistics are given in Table 15. As shown in Table 15, dust detection with ABI ADP on GOES-16 observation can have an accuracy of ~98%, POCD off~88% and POFD of 2.6%.

In addition, to evaluate how dust detection in the EPS ADP algorithm performs over time, a time series of dust detection over AERONET stations located at dust dominated regions were examined. Figure 36 shows the examples for three stations, i.e., Cape Verde, Ragged Point and Cape San Juan. ADP dust (red diamond) always corresponds to the times when AODs are elevated due to passing dust storms, and for times when AODs are low, ADP shows no dust (pink triangle), indicating high correct detection rate. In addition, very few false detections (blue star) were seen, indicating a low false detection rate for ADP. These results are further indicated in the statistics shown for each station in Figure 36.

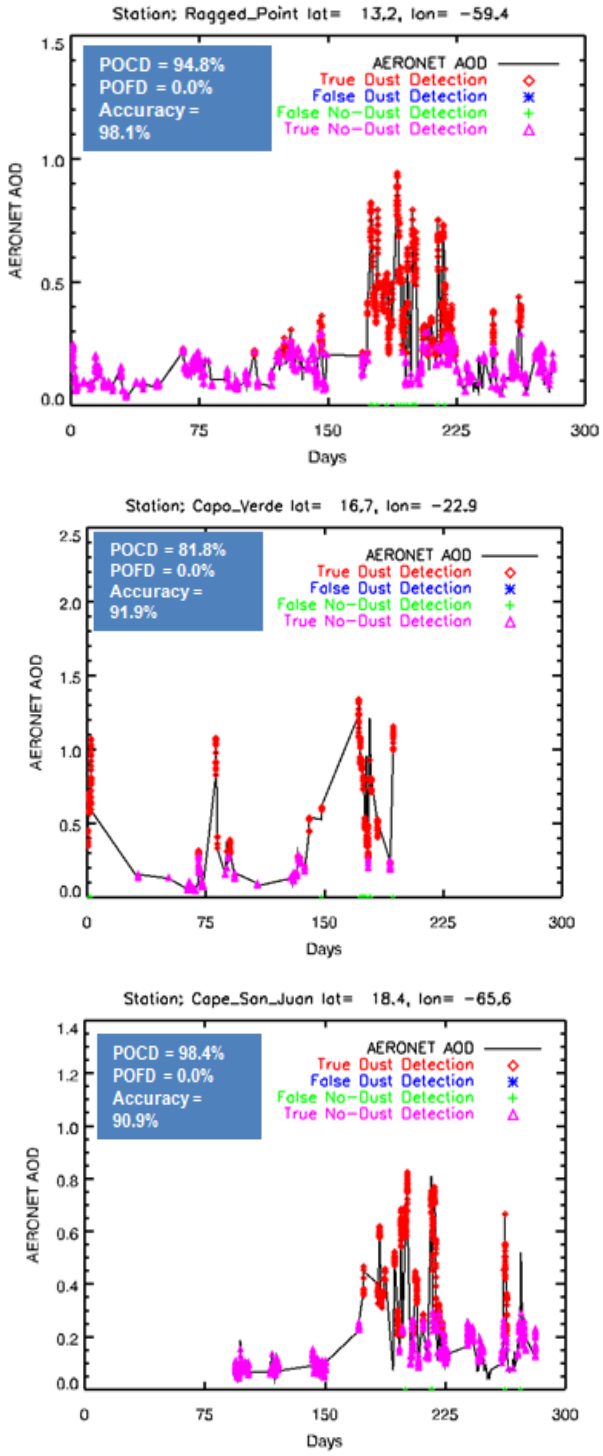

Figure 36. Time Series of dust detection from ABI ADP overlaid on AERONET AOD from three dust dominant stations. a: Ragged point. b: Cape Verde. c: Cape San Juan.

5.2.5 Output of smoke detection

5.2.5.1 Comparisons with GOES-16 synthetic RGB images

Figure 37 shows three examples where smoke detection from ABI ADP is compared to synthetic RGB generated from GOES-16 ABI observations. Pixels where smoke is detected in ABI ADP are colored light-purple, pink, and red, respectively for low, medium and high confidence level of smoke detection. The three examples cover smoke from small-scale agriculture burning, smoke from forest fires, and transported smoke plumes.

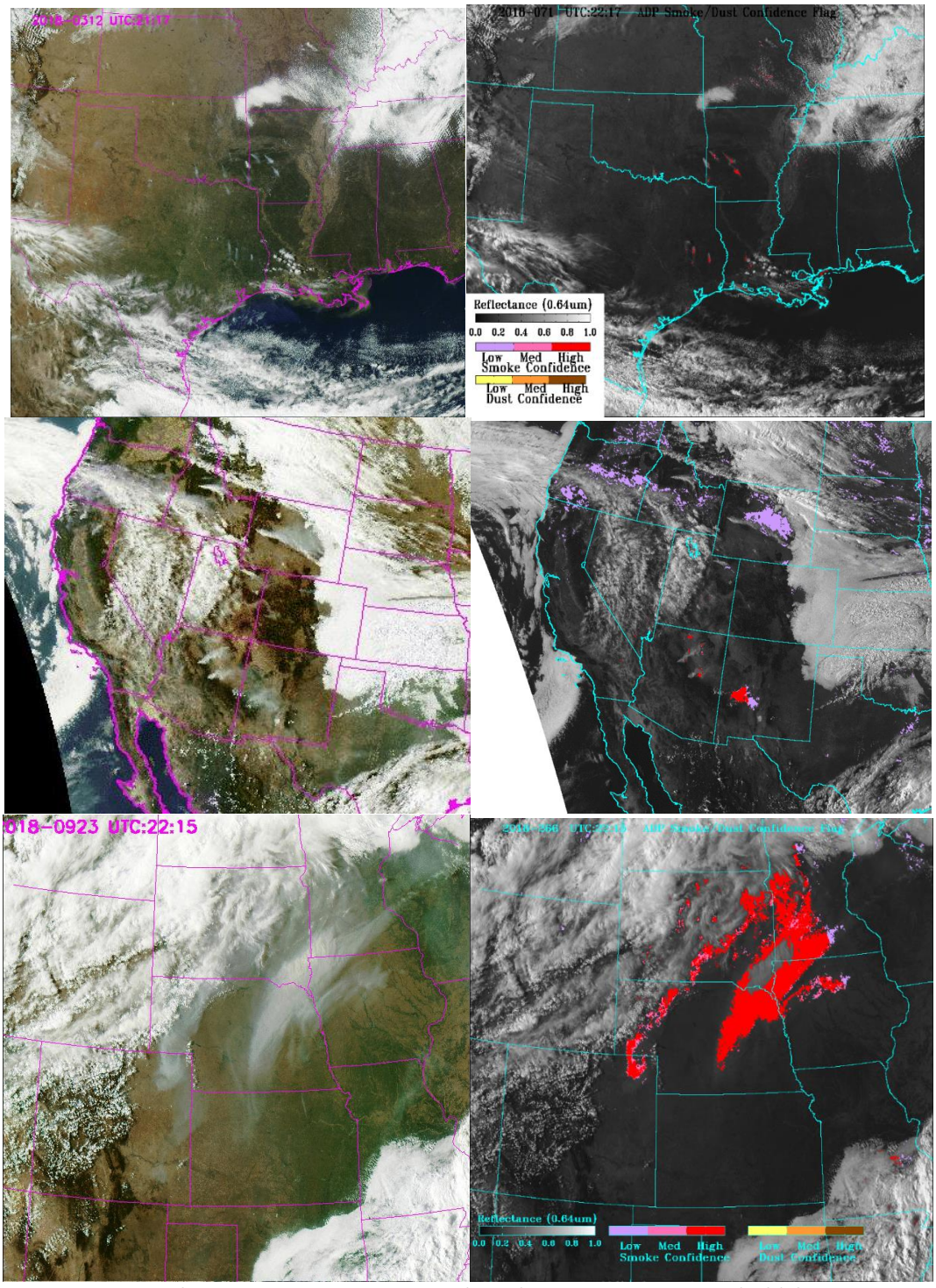

Figure 37: Comparison of ABI ADP smoke detection (right) with synthetic RGB (left) from GOES-16 observations. Top row: March 06, 2018 at 22:17 UTC. Middle row: September 25, 2018 at 20:32 UTC. Bottom row: September 23, 2018 at 22:15 UTC.

5.2.5.2 **Comparisons with CALIPSO VFM product**

ABI ADP smoke detection was qualitatively compared to CALIPSO VFM for the time period from December 14, 2017 to October 13, 2018. The corresponding statistics matrix, including accuracy, POCD and POFD, are given in Table 16. Based on validation with the CALIPSO VFM, smoke detection from the EPS ADP with GOES-16 ABI observations can have an accuracy of ~99%, POCD of ~94% and POFD of ~18%.

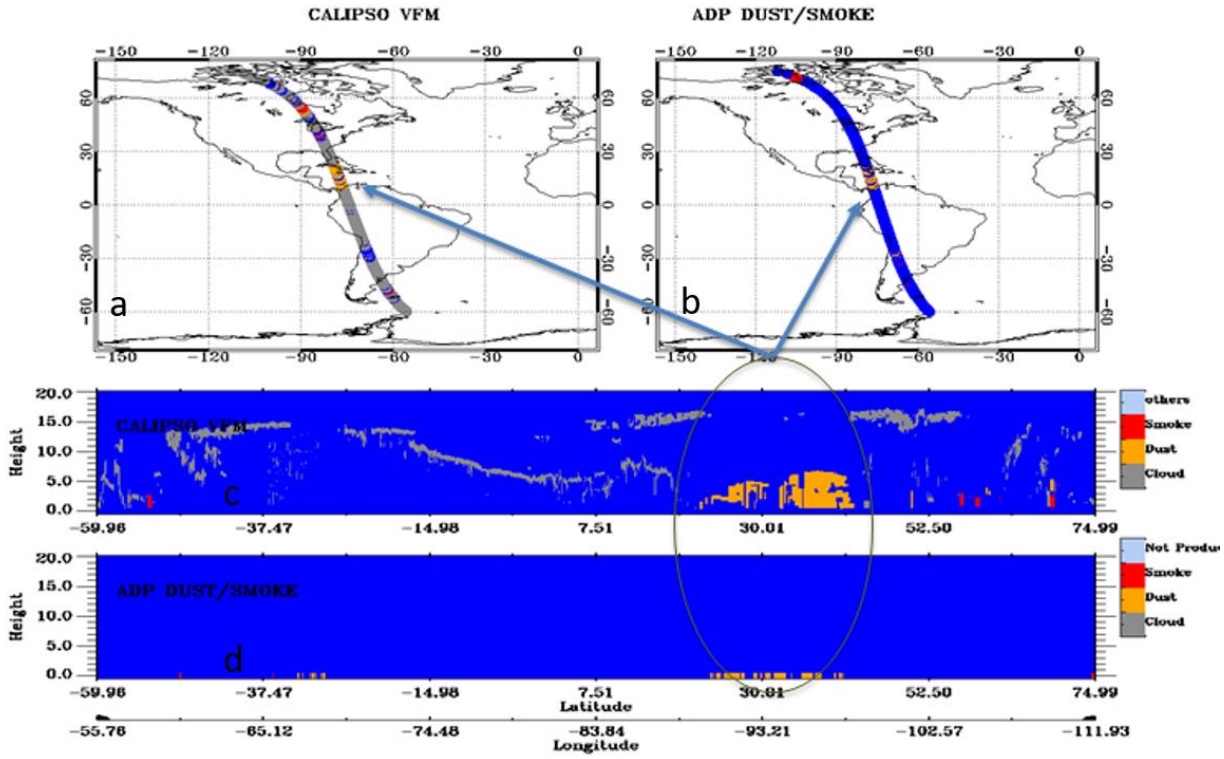

Figure 38. Comparison of smoke detected (red) using ABI ADP algorithm over GOES-16 observations on July 13, 2018 at UTC: 18:45 with smoke in CALIPSO Vertical Feature Mask (VFM). a) Smoke (red) from VFM on CALIPSO track, b) Smoke detected with ABI ADP algorithm over GOES-16 observations collocated on CALIPSO track, c) Smoke vertical distribution from VFM on the part of CALIPSO track collocated with ABI ADP, d) Smoke from ABI ADP on the same part of track as in c.

Table 16. Validation statistics for ABI EPS ADP.

Verification Dataset	Time Period	True Positive	False Positive	False Negative	True Negative	Accuracy	POCD	POFD
CALIPSO VFM	12/14/17-10/13/18	794	176	46	1,034,572	99.6%	94.5%	18.1%
AERONET		2,205	6,371	3,202	289,476	95.4%	87.4%	22.4%

5.2.5.3 **Comparisons against AERONET measurements**

Smoke detections by the EPS ADP algorithm run on GOES-16 ABI observations were validated with AERONET observations according to the strategies described in section 5.1.2.1.for the time period from December 14, 2017 to October 13, 2018. The derived statistics matrix is given in Table 16. As shown in Table 26, smoke detection with ABI ADP on GOES-16 observations can have an accuracy of ~95%, POCD pf ~87% and POFD of ~22%.

In addition, to evaluate how smoke detection in EPS ADP algorithm perform over time, a time series of smoke detection over AERONET stations located at smoke dominated regions were examined. Figure 39 shows the examples for three stations, i.e., ARM_SGP, MD_Science_Center and Rimrock. ADP smoke (red diamond) always corresponds to the times when AODs are elevated due to passing smoke plumes, and for times when AODs are low, ADP shows no smoke (pink triangle), indicating a high correct detection rate. In addition, very few false detections (blue star) were seen, indicating a low false smoke detection rate for ADP. These results are further indicated in the statistics shown for each station in Figure 39.

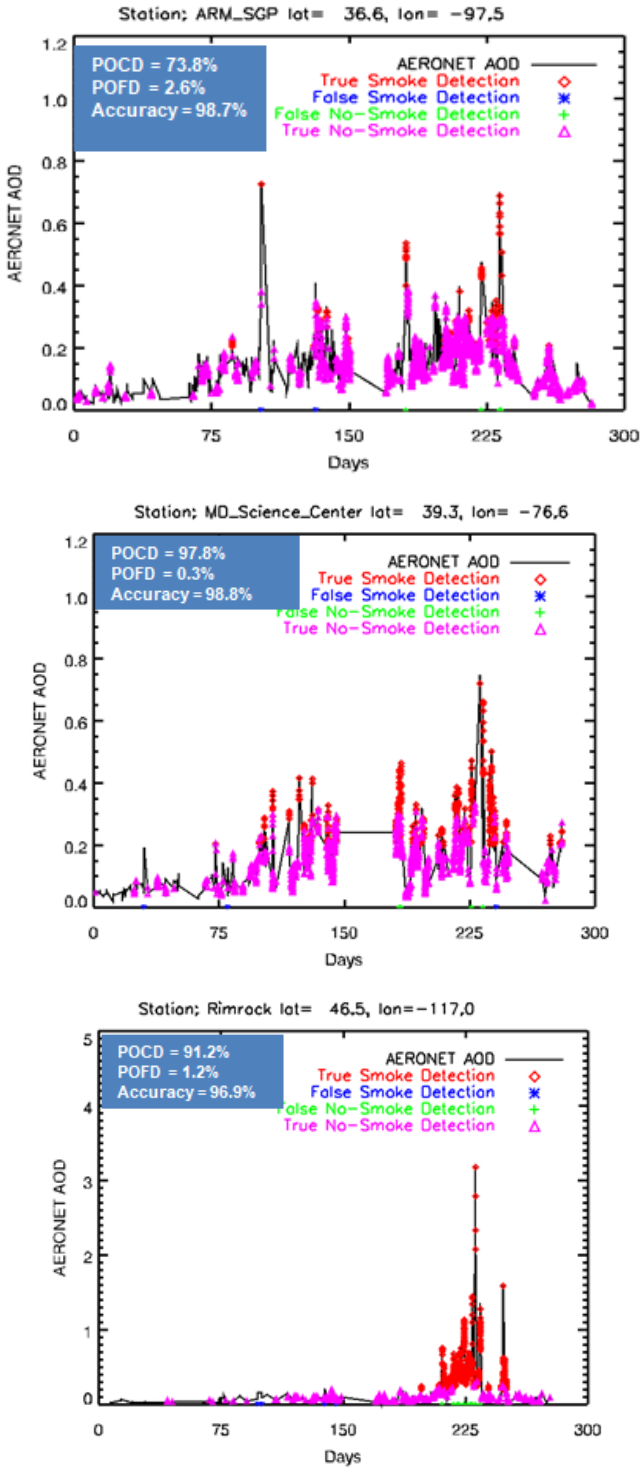

Figure 39. Time Series of smoke detection from ABI ADP overlaid on AERONET AOD from three smoke dominant stations. a: ARM_SGP. b: MD_Science_Center. C. Rimrock.

6 PRACTICAL CONSIDERATIONS

6.1 Numerical Computation Considerations

The ADP algorithm is implemented sequentially. Because some tests require ancillary data, the ancillary data (e.g., day/night, snow/ice, sun glint, and cloud/clear) need to be input first. To balance the efficiency and memory requirement for the full disk processing, a block of scanning pixels are read into a RAM buffer together instead of reading data pixel by pixel.

6.2 Programming and Procedural Considerations

The ADP requires knowledge of spatial uniformity metrics that are computed for each pixel using pixels that surround it. Detection is performed separately for land and water. In addition, future temporal tests require information from the previous image. Beyond this reliance, the ADP is a pixel by pixel algorithm.

6.3 Quality Assessment and Diagnostics

The following procedures are recommended for diagnosing the performance of the ADP.

- Monitor the percentage of pixels falling into each ADP aerosol bin values. These values should be quasi-constant over a large area.
- Monitor frequency of false positives of regions to assess need to have region specific thresholds developed and implemented.
- Periodically image the individual test results to look for artifacts or non-physical behaviors.
- Monitor retrievals over different surface (geographic) type for dependency of errors on surface brightness
- Monitor spectral threshold values and provide a quality flag depending on how close the spectral BT differences are to specified thresholds
- Monitor retrievals for temporal consistency. Are retrievals consistent from image to image?

Qualify flag with value of 0/1/2 representing lower/medium/high confidence is generated according to how far the actual value for each test is from the predefined threshold.

6.4 Exception Handling

The quality control flags for ABI ADP will be checked and inherited from the flagged Level 1b sensor input data, including bad sensor input data, missing sensor input data and validity of each channel used; and will also be checked and inherited from the ABI cloud mask at each pixel.

The ADP also expects the Level 1b processing to flag any pixels with missing geolocation or viewing geometry information.

The ADP does check for conditions where the ADP cannot be performed and generates quality control flags for snow/ice pixel, pixels with saturated channels; pixels missed geolocation or viewing geometry information.

6.5 Algorithm Validation

For pre-launch validation, ADP algorithm will be extensively validated by using MODIS RGB images, MODIS aerosol product and Vertical Feature Mask from CALIPSO. The new analysis in the development to validate the ADP using AERONET and IMPROVE data will be presented in the next release of the ATBD as well as the ADP validation report. For post-launch validation, besides above-mentioned approach, field campaigns will also be carried out. Details on Algorithm Validation are given separately in the ABI ADP algorithm testing and validation plan document.

7 ASSUMPTIONS AND LIMITATIONS

The following assumptions have been made in the current algorithm:

- Calibrated and geo-located radiances in ABI channels as required by ABI ADP algorithm as shown in Table 2 are available;
- ABI cloud mask is available and adequate for the purpose of DP algorithm
- All the ancillary data are available.

Limitations applying to current algorithm are:

- Only for daytime
- Smoke detection over land is limited to dark surface
- Not optimal for optically thin smoke and dust
- No testing has been done to determine algorithm limitations if smoke and dust or other types of aerosols co-exist in the same pixel

7.1 Performance

The following assumptions are made in estimating the performance of ADP algorithm:

- smoke/dust mask from CALIPSO VFM represents the truth;
- visual separation of smoke, dust and clear pixels from MODIS RGB image introduces negligible error;
- Thresholds used in the current algorithm are tailored for MODIS channel specifications. Post –launch tuning of these thresholds will not affect the estimate of algorithm performance.
- In case of ABI sensor degradation, product production might squeeze but studies will be carried out prior to the launch on the extent of the effect any changes to instrument characteristics will have on product quality.

7.2 Assumed Sensor Performance

The EPS ADP algorithm assumes the ABI sensor will meet its current specifications and produce calibrated quality radiance in the required channels (see Table 9). As shown in section 3.4.1., impacts from instrument noise and calibration error can be mitigated by adjusting thresholds accordingly. However, the EPS ADP algorithm has low tolerance for missing channels. As discussed in above sections, the EPS ADP algorithm selects the optimal channels or combination of channels to best separate signal of smoke/dust from others. Therefore, any missing channels will definitely downgrade the performance of the algorithm and eventually will lead to failure if crucial channels are missing.

Although the current version of the EPS ADP algorithm is not designed to mitigate for missing channels, the impacts of missing specific channels was estimated using three MODIS granules (i.e., Aqua 2010209.0920, Terra 2003301.1825 and Terra 2002007.1125) for smoke and dust detection. The relative changes (%) of the total number of smoke or dust pixels are summarized in Table 17.

Table 17. Relative change (%) from smoke/dust pixel to clear pixel and from clear to smoke/dust pixel (parentheses) under an assumption that one specific channel is missing.

Aerosol		ABI Channel								
		1	2	3	4	5	6	7	14	15
Smoke	Land	0.0 (0.1)	-100.0 (0.0)	0.0 (0.05)	----	----	0.0 (73.3)	0.0 (0.1)	----	----
	Water	0.0 (0.54)	---	0.0 (90.2)	0.0 (50.6)	----	0.0 (0.52)	----	----	----
Dust	Land	0.0 (0.1)	0.0 (15.8)	0.0 (15.8)	0.0 (0.32)	----	----	-0.12 (17.1)	-0.12 (28.8)	0.0 (4.63)
	Water	-18.8 (2.4)	-100.0 (0.0)	0.0 (3.3)	----	0.0 (0.33)	----	0.0 (0.14)	0.0 (2.4)	0.0 (1.8)

In addition, ADP algorithm will be dependent on the following instrumental characteristics.

- The spatial uniformity tests in ADP will be critically dependent on the amount of striping in the data.
- Errors in navigation from image to image will affect the performance of the temporal tests.

7.3 Pre-Planned Product Improvement

7.3.1 **Improvement 1**

Smoke detection over water is not optimal and will need improvements. We already improved the algorithm for the Version 5 release associated for the 100% delivery. Current algorithm has not been able to take advantage of temporal variability information that is unique for Geostationary Platform. We plan to utilize the rapid refresh rate of GOES-R ABI and improve the algorithm.

7.3.2 **Improvement 2**

The spectral screening thresholds are currently not a function of viewing and solar geometry. Testing will be carried out to understand the dependencies of some of the smoke/dust tests on viewing and solar geometries. Additional testing will also be done using simulated proxy data to determine ABI spectral thresholds and how robust these spectral thresholds are under different scenarios. Based on these tests, algorithm could be improved.

7.3.3 **Improvement 3**

There are other algorithms based on spectral threshold tests that have been recently developed for SEVIRI. We will try to adapt those tests to improve smoke detection over water, dust detection over land and water, and also find a way to detect dust in the night time. Algorithm would have to be substantially altered for night time dust detection because visible channels will not be available.

7.3.4 **Improvement 4**

Validation of smoke/dust detection still remains a challenge at this stage. Besides the validation exercises that have already been completed, additional validation will be carried out. They include comparisons with the ground-based measurements and other satellite products. Validation with ground-based measurement will take advantage of measurements from aerosol sampler in IMPROVE network and Angstrom exponent information from AERONET for any indications of smoke/dust particle over some local and regional event. This, however, is not a direct comparison but an indirect subjective evaluation of smoke/dust detection product. For comparisons with other satellite products, Aerosol Index from OMI/TROPOMI will be fully used to quantify the accuracy of smoke/dust products.

8 REFERENCES

Ackerman, S. A., Using the radiative temperature difference at 3.7 and 11mm to track dust outbreaks, *Remote Sensing of Environment*, **27**: (2) 129-133, 1989.

Ackerman, S. A., and K. I. Strabala, Satellite remote sensing of H_2SO_4 aerosol using the 8-12μm window region: Application to Mount Pinatubo. *J. Geophys. Res.*, **99**, 18,639-18,649, 1994.

Ackerman, S. A., Remote sensing aerosols using satellite infrared observations. *J. Geophys., Res.*, **102**, 17069–17079, 1997.

Ackerman, Steven A.; Strabala, Kathleen I.; Menzel, W. Paul; Frey, Richard A.; Moeller, Christopher C. and Gumley, Liam E., Discriminating clear sky from clouds with MODIS, *J. Geophys. Res.*, **103**, 32,141-32,157, 1998.

Ackerman, S. A., R. E. Holz, R. Frey, E. W. Eloranta, B. Maddux, and M. McGill, Cloud Detection with MODIS: Part II Validation. Accepted with revision to *J. Tech.*, 2008.

Barton, I. J., A. J. Prata, I. G. Watterson and S. A. Young, Identification of the Mount Hudson volcanic cloud over SE Australia. *Geophy. Res. Lett.*, **19**(12), June 19, 1992, 1211-1214, 1992.

Bohren, C. F. and D. R. Huffman, "Absorption and scattering of light by small particles", Wiley, New York, 1983.

Darmenovm A. and I. N. Sokolik, Identifying the regional thermal-IR radiative signature of mineral dust with MODIS, *Geophy. Res. Lett.*, **32**, doi:10.1029/2005GL023092, 2005.

Dubovik, O., Holben, B., Eck, T., Smirnov, A., Kaufman, Y., King, M., Tanré , D. and Slutsker, I., Variability of absorption and optical properties of key aerosol types observed in worldwide locations, *J. of Atmos. Sci.*, **59**, 590–608, 2002.

Dunion, J.P. and Velden, C.S., The Impact of the Saharan Air Layer on Atlantic Tropical Cyclone Activity, *Bulletin of the American Meteorological Society*, **90**, 353–365, 2004.

Evan, A. T., A. K. Heidinger, and M. J. Pavolonis, Development of a new over–water advanced very high resolution radiometer dust detection algorithm, *Int. J. Remote Sens*, **27**(18), 3903-3924, 2006.

Frey, R. A., S. A. Ackerman, Y. Liu, K. I. Strabala, H. Zhang, J. R. Key, and X. Wang, Cloud detection with MODIS, Part I: Improvements in the MODIS cloud mask for collection 5. *Journal of Atmospheric and Wateric Technology*, **25**, 7, 1057-1072, 2008.

Hansen, M., R. DeFries, J.R.G. Townshend, and R. Sohlberg, UMD Global Land Cover Classification, 1 Kilometer, 1.0, Department of Geography, University of Maryland, College Park, Maryland, 1981-1994, 1998.

IPCC, *Climate Change 2007*: The Physical Science Basis, Cambridge Univ. Press, New York, 996pp, 2007.

Kaufman, Y. J., et al., Operational remote sensing of tropospheric aerosol over land from EOS moderate resolution imaging spectroradiometer, *J. Geophys. Res.*, **102**, 16,971-16,988, 1997.

King, M. D., Menzel, W. Paul, Y. Kaufmann, Didier T., B.-C. Gao, S. Platnick, S. Ackerman, L. Remer, R. Pincus, and P. A. Hubanks, Cloud and aerosol properties, precipitable water, and profiles of temperature and water vapor from MODIS. *IEEE Transactions on Geoscience and Remote Sensing*, **41**, 442-458, 2003.

Legrand, M., G. Cautenet, and J.-C. Buriez, Thermal impact of Saharan dust over land, Part II: application to satellite IR remote sensing, *J. Appl. Meteorol.*, **31**, 181-193, 1992.

Legrand, M., A. Plana-Fattori, and C. N'Doume, Satellite detection of dust using IR imagery of Meteosat 1. Infrared difference dust index, *J. Geophys. Res.*, **106**, 18,251-18,274, 2001.

Platnick, S., M. King, S. A. Ackerman, P. W. Menzel, B. A. Baum, J. C. Riédi, R. A. Frey, The MODIS Cloud Products: Algorithms and Examples from Terra, *IEEE Transactions on Geoscience and Remote Sensing*, **41**, 459-???, 2003

Prata, A. J., Observations of volcanic ash clouds in the 10-12-MU-M window using AVHRR/2 data. *International Journal of Remote Sensing* **10**(4-5), 751-761, 1989.

Rember, L., Y. J. Kaufman, D. Tanré, D., S. Mattoo, D. A. Chu, J. V. Martins, R-R. Li, C. Ichoku, R. C. Levy, R. G. Kleidman, T. F. Eck, E. Vermote, and B. N. Holben, The MODIS aerosol algorithm, products, and validation. *J. Atmos. Sci.*, **62**, 947–973, 2005.

Tanre, D., and M. Legrand, On the Satellite Retrieval of Saharan Dust Optical Thickness Over Land: Two Different Approaches, *J. Geophys. Res.*, **96**, 5221–5227, 1991.

Verge-Depre, G., M. Legrand, C. Moulin, A. Alias, and P. Francois, Improvement of the detection of desert dust over the Sahel using METEOSAT IR imagery, *Ann. Geophys.*, **24**, 2065-2073, 2006.